TECHNISCHE UNIVERSITÄT DARMSTADT

Institut für Elektrische Energiewandlung

Planning and application of electrical drives (PAED)
- Drives for electric vehicles

Hybrid and electrical vehicles
Text book

(Source: Tesla roadster)

Issue SS 2016   **Prof. Dr.-Ing. habil. Dr. h.c. Andreas Binder**

LECTURE NOTES TO:

Planning and application of electrical drives:

Electric drives for ZEV

1. Overview

In Chapter 3 an overview of the components of the electric drive train is given and Chapter 4 deals with the technology of E-motors. In Chapter 5 the inverter is discussed, while in Chapter 6 the accumulators and in Chapter 7 the storage capacitors are explained. In Chapter 8 the battery management is explained and Chapter 9 presents some realized ZEVs. Chapter 10 gives the list of some used hybrid cars and further literature. The lecture notes were written by Prof. Andreas Binder and Mr. Stefan Dewenter with the aid of documents by Ms. Katja Heiling and Mr. Ullrich Georgi. The English translation was done by Mr. Nam Anh Dinh Ngoc.

2. Aim of the lecture notes

Based on published specialized literature following questions for the electric drive system of a zero emission vehicle (ZEV) shall be answered:
- What drive motors are suitable?
- What inverter concepts (ECU) are possible?
- What are common controlling concepts of motors?
- What types of energy storage are available?
- What are the influences of the drive variants on cooling system and vibration excitation?

The state of the art of current accumulators is discussed

3. Overview – Electric drive train

A purely electrically driven automobile has in the simplest case following components:
- (Electric) energy Storage
- Charging device for storage
- Converter for electric energy
- E-motor
- Drive control
- Overriding control
- Gear between E-motor and wheels
- Sensors/encoders
- Cooling system

a) Energy storage:
The energy storage can store energy directly electrically (super capacitors in Farad range) or in another form, e. g. mechanic energy in a flywheel storage, chemical binding energy in an accumulator (lead battery, nickel metal hydride battery, lithium ion battery). Characteristic values for the storage are the stored energy/volume (energy density) and the possible power/volume (power density). Magnetic storages need very strong magnetic fields (about 8 T) and are therefore realized by superconducting coils, in order to limit the losses. Due to the cooling demand effort those do not come into consideration. Alternatively the energy can be stored in form of chemical binding energy in e. g. liquid (cold) hydrogen

or gasous hydrogen under high pressure, in order to be afterwards burnt together with oxygen from air in a fuel cell to steam to provide a DC-voltage for the drive system. „Zero emission" then refers to the C-H-, NOx and CO/CO_2-exhaust gases.

b) Charging device:
For accumulators and capacitors DC-voltage sources are necessary, in order to charge the storage electrically or chemically. Depending on the height of the DC-voltage generally pulsed power electronic circuits provide the needed DC-voltage from the public 3-phase grid. In case of a flywheel storage a 3-phase system is needed in order drive the motor generator as a motor and get the required speed.

c) Converters for electric energy (inverter, ECU):
For accumulators and capacitors DC/AC-converters are required (inverter), which power electronically generate a 3-phase board grid with variable voltage amplitude and frequency out of the DC-voltage, for running the rotating field machine with variable speed. For DC-drives pulsed DC/DC-converters are necessary, in order to provide a variable DC-voltage for variable speed. When using flywheel storages normally the 3-phase system provided by the motor generator is rectified and the required AC- or DC-system is generated by power electronics.

d) E-motor:
Generally electric machines are being distinguished between DC- and AC-machines. DC-machines as unipolar machines with pure DC-current in stator and rotor are only available for low voltages and hence rarely used. DC-machines with AC-current in the rotor need a mechanic rectifier (commutator) and brushes for current transmission. Due to the maintenance effort and additional mass those motors probably will not be applied in ZEV. AC-machines as rotating field machines are available as asynchronous- and synchronous machines. They are compact and robust, so that they will find application in main drive variants for future ZEV.

e) Drive control:
In order to change the speed of DC-machines the armature voltage or the main flux have to be changed, apart from the loss intensive resistance control of old DC-tram concepts. By changing the armature voltage speed changes due to the low armature inductance much faster (in the range of tens of ms) than by changing the main flux, which can be changed only 100-times slowlier. For excitation with permanent magnets the main flux cannot be changed. The speed of AC-drives is changed by the frequency of the supplying voltage. If the magnetic flux in the machine is supposed to remain constant, the voltage amplitude has to be changed proportional to the frequency. In order to achieve fast speed changes similar to DC-drives, the main flux has to be kept constant. Only the torque generating part of the current is allowed to change. Therefore a field oriented control is required, which is implemented in the control processor of the ECU e. g. a 32 bit-processor.

f) System control:
While the speed of the E-Motors and hence the vehicle speed is controlled in cruise-control, the adjustment of vehicle speed is decided by the driver in torque control ("gas pedal") by demanding more or less torque from the motor. Thus only torque of the motor is being controlled. In order to achieve high speed, without increasing the voltage too much (= without dimensioning the ECU for too high electric power), above a "corner speed" the magnetic flux inside the machine is reduced. The machine runs field weakened and produces less torque, than it could according to its specification. But it can be operated at high speed, which allows high vehicle speed e. g. on highway. The driving resistance has a limiting effect. Additional torque for acceleration when overtaking at high speed is then not possible anymore. When using accumulators in parallel with super capacitors the battery can be run gently (less discharge depth, less cycles), if discharging/-charging peaks are withdrawn from the super capacitors (battery management).

g) Gear between E-Motor and wheels:

As the E-motor can be run with high efficiency in a wide speed range a switching gear for adjustment of speed to the vehicle speed is not necessary. Because torque determines size of the machine and the machine is dimensioned for much higher speed than wheel speed to save construction volume. In order to keep a single stage gear, and in order to limit the maximum speed of the machine (bearing!, centrifugal force!, smooth running!), gear transmission ratios below 10 are sensible. Depending on the construction principle simple spur gears (skewed teeth) can be used.

h) Encoder sensors:

For the monitoring of E-motor for speed control either encoders are necessary or the speed is calculated via „sensorless" speed monitoring from measurings of electric quantities. Such encoderless processes have to be customized to the different motor types (induction/synchronous machines etc.) and adjusted by storing the correct parameters of the machine (inductances, resistances) in the microprocessor of the ECU. For synchronous machines a rotor position capturing is necessary for torque control, which can also be realized encoderless. Furthermore for torque control a current measuring in the ECU is needed; due to the symmetry of the current system often only two of the three phase currents are measured. Temperature sensors inside the motor windings and inside the bearings serve as security monitoring. In the ECU the temperature of the junction of the power semiconductors are monitored for instance indirectly via electric parameters (collector-emitter voltage versus collector current) or directly by temperature sensors on the heat sink with additional temperature models inside the ECU. In the same way temperature sensors and current/voltage measurings monitor the accumulators and super capacitors and serve – together with e. g. battery models inside the monitoring processor – as input for the overriding battery management.

i) Cooling system:

The cooling system for compact drives is mostly based on liquid coolants, which has a higher heat capacity than air. The indirect liquid cooling has come out on top (e. g. 50% water, 50% glycol due to freezing protection), which carries heats away from power electronics and housing of the machine. Due to economic reasons a circuit is used, in which at first the more sensitive power electronics are cooled, their junction temperature is not supposed to exceed a temperature of approx. 125°C … 135°C in Si-based insulated gate bipolar transistors (IGBT). Hence the entering temperature of the coolant in the series connected machine is much higher, e. g. 50°C (and higher). Depending on machine and inverter size 8 … 15 l/min coolant flow is used. The thermal time constant of the inverter is determined by the size of the heat sink and lies in the order of few minutes. For machines up to approx. 50 … 70 kW also for induction machines the water jacket cooling is still possible without any problems. The heat flow from the rotor (cage losses!) happens at internal air circulation on the end shields and the stator. For bigger induction machines a direct rotor cooling e. g. by forced air cooling must be provided, in order to carry the rotor losses away. Otherwise the temperature difference between internal and external bearing ring becomes too high (more than 30 K) and leads - especially at high speed of the machines of approx. max. 10000/min … 12000/min in spite of higher bearing air - to bearing problems due to the expansion of the rotor. For PM-machines with their low-loss rotors that limit does not exist.

The thermal time constants of the machine are due to the higher mass of copper and iron generally much higher than those of the inverter. The smaller time constant (e. g. 10 min.) represent the winding and the longer time constant (e.g. ca. 30 min) is the one of the iron, which mass is much bigger that the mass of copper, because of the flux conducting parts and iron saturation above approx. 1.8 T the cross section of iron cannot be made too small.

4. Electric machines for electric vehicles

There is a vast variety of electric drives for vehicles. Usually traction drives lie in the power range 20 … 80 kW depending on vehicle size. Generally these electric machines have to be assembled close to the axle for the wheels like the internal combustion engine, where they drive the wheels via a gear. In special cases the electric machine can also be on the axis as a direct drive or drive the wheels as a hub motor, but then has due to the higher torque bigger dimensions, as the electromagnetic tangential force in the air gap – referred to the rotor surface – in spite of highest machine utilization is with 0.5 … 1 bar (specific thrust τ) relatively low, so that torque has to be generated by a big rotor diameter.

Thereby an electric drive for vehicles shall fulfill the following requirements:
- High power density (ratio of power to mass $\Leftrightarrow$ W/kg)
- High torque density (ratio of torque per machine volume $\Leftrightarrow$ Nm/m³)
- High efficiency at part load and rated load
- Recuperation of braking energy with high total efficiency
- High robustness against accelerating forces
- Liquid cooling
- Reliability
- Low manufacturing costs
- Simple manufacturing
- Highly sophisticated
- Automobile suitability

4.1   Machine types

Electric machines, which find application in automobiles as traction drives, are
- **DC-machine** with series- and shunt-wound winding,
- Induction machine,
- **P**ermanent magnet excited **s**ynchronous **m**achine (PSM),
- **S**witched **R**eluctance **M**achine (SRM),
- **T**ransversal **f**lux **m**achine (TFM)

Each of these machines (Fig. 4.1-1) is based on the principle that torque is generated, by

a) a current-carrying conductor e. g. of the rotor in a magnetic field inside the stator, which experiences a tangential force in in rotational direction (*Lorentz*-force) or

b) dragging the rotor by the rotating field in the stator, due to the existing differences in the magnetic conductance (reluctance difference) along the rotor circumference.

The current I is provided by a supplying source (inverter) by an applied voltage U. The current adjusts itself such that the applied voltage equals the sum of the voltage U_i, which is induced by the magnetic field into the windings, and the voltage drop at the armature resistance. The generated torque M is proportional to current I while the required voltage U ($U \approx U_i$) is proportional to the speed n due to Faraday's induction law. Both current and voltage are proportional to the magnetic flux Φ. The flux $\Phi = B \cdot A_p$ is proportional to the flux density B in the air gap and the rotor surface per magnet pole A_p. In the range of constant power $P = 2\pi n M$ resp. $P \sim 3 \cdot U \cdot I$ (Fig. 4.1.1-2) the increase of speed is done by a weakening of the magnetic field, as the voltage U is limited due to the maximum inverter output voltage, which cannot be higher than the battery voltage of the vehicle. Below that limit the battery DC-voltage is chopped into blocks of different widths by the inverter pulse-width-modulation, so that the voltage is decreased. Hence below the corner speed n_N, where the voltage reaches its maximum value, the voltage follows the law (4-2) at constant flux, above corner speed n_N the flux has to be weakened, which has to be done for each motor type in a different way.

$$M = k_1 \cdot \varPhi \cdot I \tag{4-1}$$

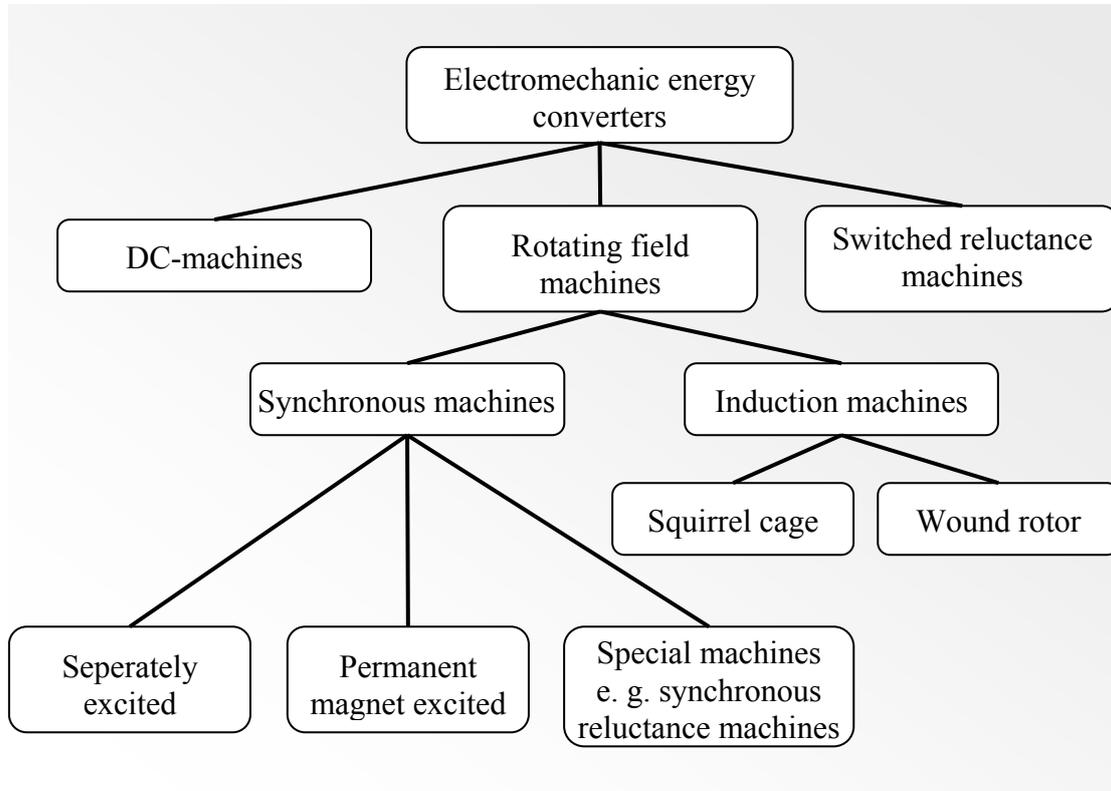$$U = k_2 \cdot \varPhi \cdot n \tag{4-2}$$

Fig. 4.1-1: Overview of E-drives

Because in field weakening range flux decreases, torque also decreases, even if the machine conducts the maximum possible current, which is limited by the maximum inverter current. $M \sim \varPhi \cdot I \sim A_{\mathrm{p}} B \cdot I$ concludes for a machine with $2p$ poles, that torque is proportional to the machine volume V and $M = F \cdot r = 2p \cdot \tau \cdot A_{\mathrm{p}} \cdot r \sim \tau \cdot V$ to the specific thrust τ. The rotor radius r and the number of conductors z on the circumference, which conduct current I and give a contribution to the torque of the machine, yield with the current loading on the circumference $A = z \cdot I /(2\pi \cdot r)$ to the specific thrust by comparison of the expressions above.

$$\tau = k \cdot A \cdot B \tag{4-3}$$

In (4-3) k is a machine specific factor; the magnetic flux density B cannot be increased very much due to iron saturation, so that only current loading A can be increased by more intensive cooling, in order to increase the thrust. Thereby E-machines for vehicles are designed for continuous operation for S2-1h (1 hour continuous operation, then turn-off), the overload capability is designed for about 200% for short time acceleration. At current densities inside the copper conductors up to approx. 12 A/mm^2 the current layer and hence the electromagnetic thrust is, for water jacket cooling, limited to the values from above.

In **hybrid vehicles** the permanent magnet excited synchronous machine, the induction machine and the switched reluctance machine are used in the first place. The DC-machine does not find application in latest models due to the commutator, brush abrasion and the limited speed. Company *Voith* focuses on the application of the transversal flux machine (PM-synchronous machine with transverse flux guiding), because it has the highest specific thrust at low speed (about factor 2 higher), but at high pole count. The

TFM is recommended for direct drive without a gear. The PM-synchronous machine with axial flux guiding is almost coequal, but it can also be applied at higher speed without any problems. Compared with the induction machine it has lower losses and higher power densities. The switched reluctance machine also has higher power densities and lower losses than the induction machine, but it is noise susceptible and sensitive rotor eccentricities.
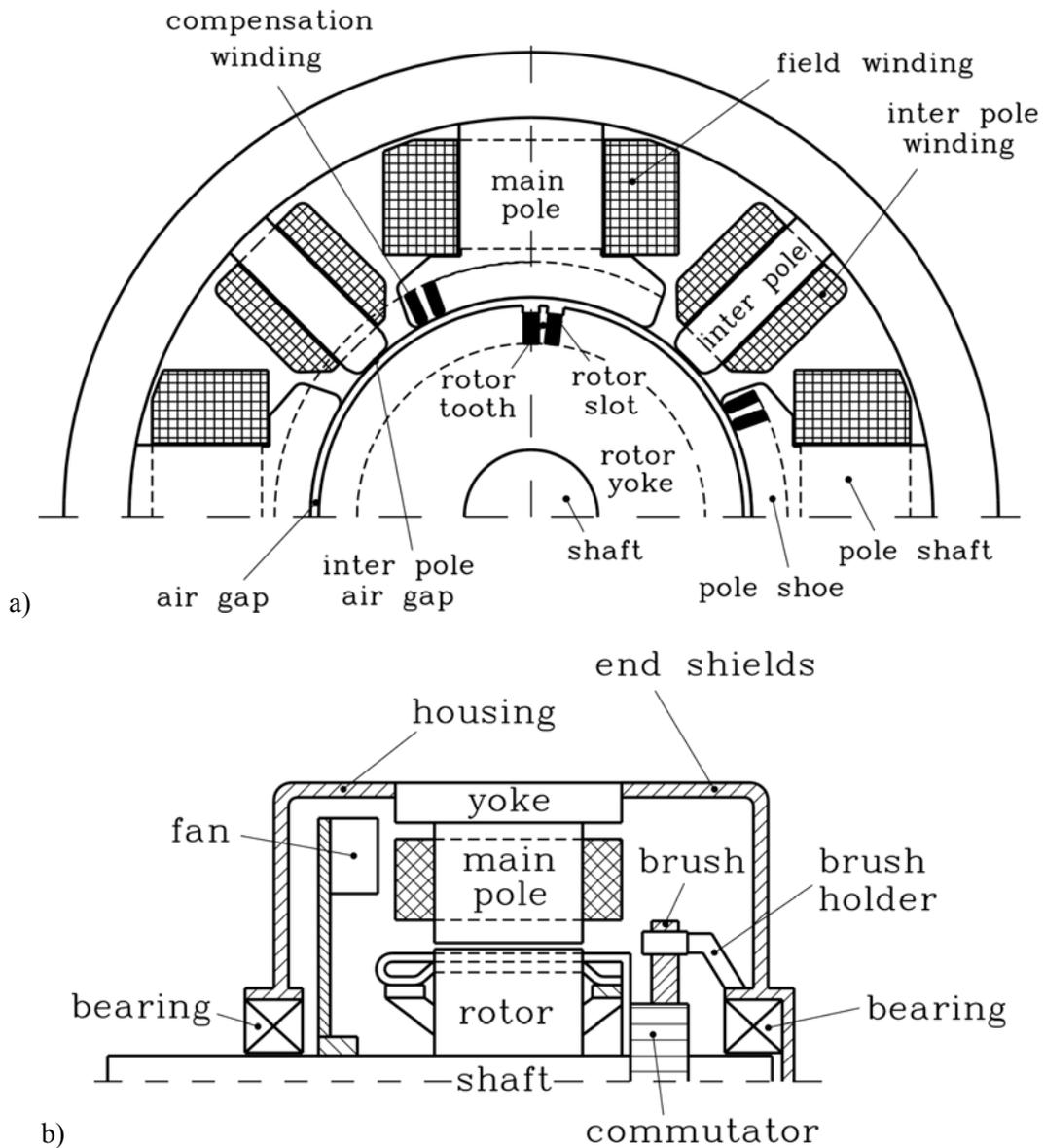
4.1.1 DC-machine

Fig. 4.1.1-1: Principal assembly of a DC-machine:
a) Cross section of the machine, b) lengthwise cut of the machine

The DC-machine exists as series- and shunt-wound version. It was especially applied for the first purely electrically driven vehicles and is well suited for vehicles as series-wound machine with high start-up. As shunt-wound machine it is preferably used with converter supply. By that the above-mentioned characteristic curves and field weakening are well feasible (Fig. 4.1.1-2).
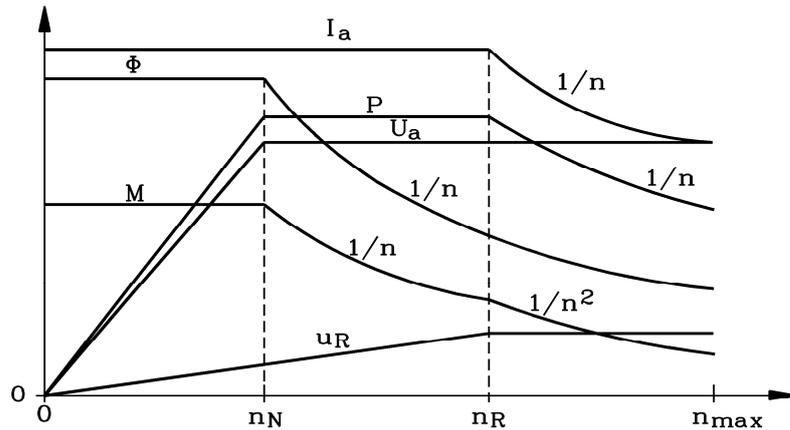
Fig. 4.1.1-2: Characteristic field of the separately excited compensated) DC-machine with variable voltage supply U_a and variable flux Φ. Maximum values of armature voltage, armature current, torque, flux, power and reactance voltage.

The advantages of the DC-machines:
- Cheap converter (e. g. IGBT-Converter: 4 transistors, 4 freewheeling diode the)
- Simple controlability
- Low torque ripple
- Good cooling possibilities
- Low converter losses

Drawbacks of the DC-machine:
- Wear due to mechanic commutation
- Mechanically limited maximum speed especially by the commutator
- High inertia of mass due to the heavy commutator
- Lower efficiency (inter pole winding, brush losses), especially at part load

The recent developments in the domain of inverter technology lead to the fact, that the DC-machine is almost fully replaced by the induction machine and the synchronous machine. In spite of being easy controllable the disadvantages due to the weight of the DC-current converter is more grievous, especially as power semi-conductors are becoming more and more cheaper.

4.1.2 Induction machine

Rotating field machines have a distributed 2p-pole winding in the stator e. g. consisting of three each by one third pole pair pitch displaced winding phases on the circumference, which are e. g. star connected. When those three phases are supplied with DC-currents (frequency f), which are each displaced in time by one third of one period $T = 1/f$, a rotating air gap magnetic field comes up, which rotates with synchronous speed n_{syn} (Fig. 4.1.2-1 and Fig. 4.1.2-2).

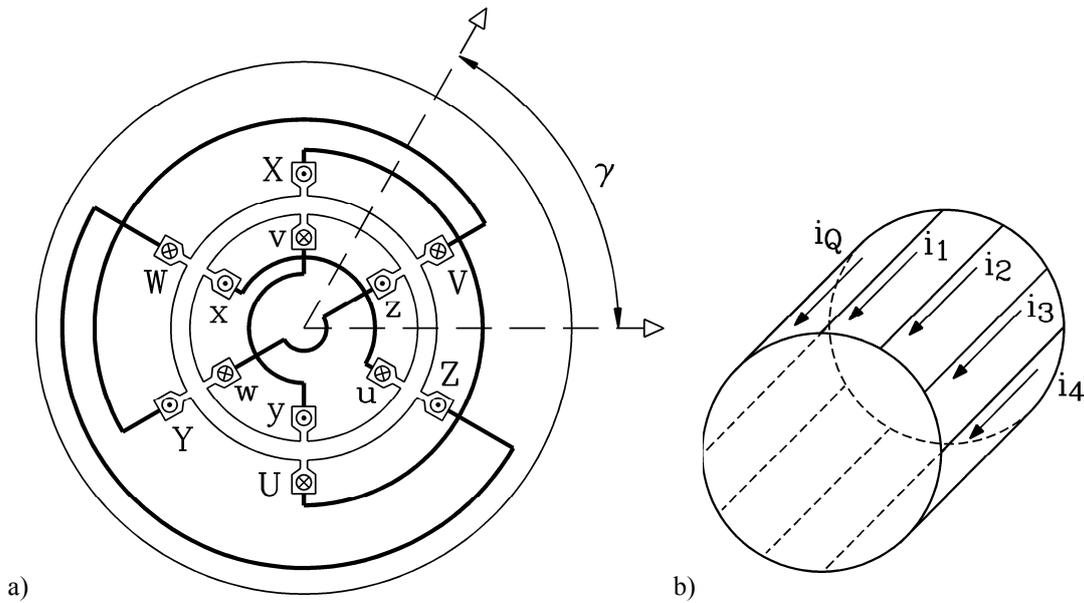$$n_{syn} = f \, / \, p \qquad\qquad\qquad\qquad (4.1.2-1)$$

Fig. 4.1.2-1: a) 3-phase rotating field winding in stator of an electric machine with constant air gap (depiction of cross section $2p = 2$). The rotor is here constructed similarly. For squirrel cage machines the rotor is replaced by a squirrel cage b).
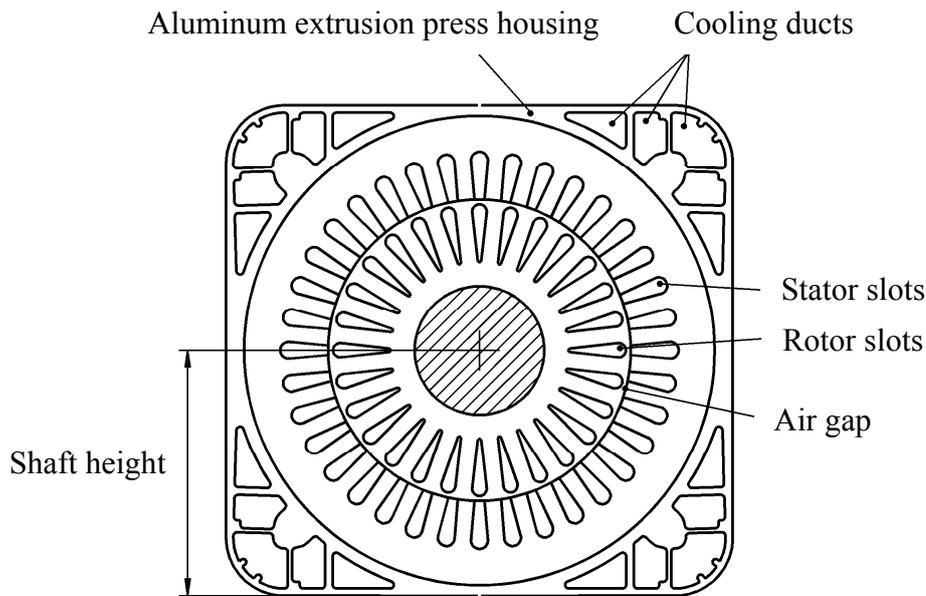

Fig. 4.1.2-2: Cross section of a four pole, surface cooled squirrel cage induction machine with aluminum cage ($n_{max} = 15000$/min, shaft height 112 mm), fed by frequency converter, closed pear shaped rotor slots, externally air cooled, main-spindle drive in a tooling machine

Rotating field machines are distinguished between synchronous machines and induction machines, in case of induction machines it can be distinguished between squirrel cage and wound cage induction machines. The latter have no importance for vehicles, so that only the squirrel cage machine will be treated here. The rotating field induces voltages into the slowlier rotating rotor (speed $n < n_{syn}$), which drive currents in the squirrel cage, which again together with the stator field generate a torque. The speed-torque-characteristic (*Kloss´* function) shows a significant maximum torque (break down torque), whereas torque is zero if the rotor rotates with the same speed of the rotating field $n = n_{syn}$. This no-load point can be shifted in inverter operation, as the inverter supplies the machine with variable voltage U and frequency f. If U is increased proportional to f ($U \sim f$), the breakdown torque remains constant with increasing frequency $M_b \sim (U/f)^2$. When the maximum voltage is reached, the break down torque decreases according to $\sim 1/f^2$. Flux decreases due to (4-2) proportional to $1/n$ resp. $1/f$, so that field

weakening is active and torque at rated current I_N decreases because of (4-1) proportional to $1/n$ resp. $1/f$. From the crossing point of this torque boundary the breakdown torque boundary has to decrease with $1/f^2$.
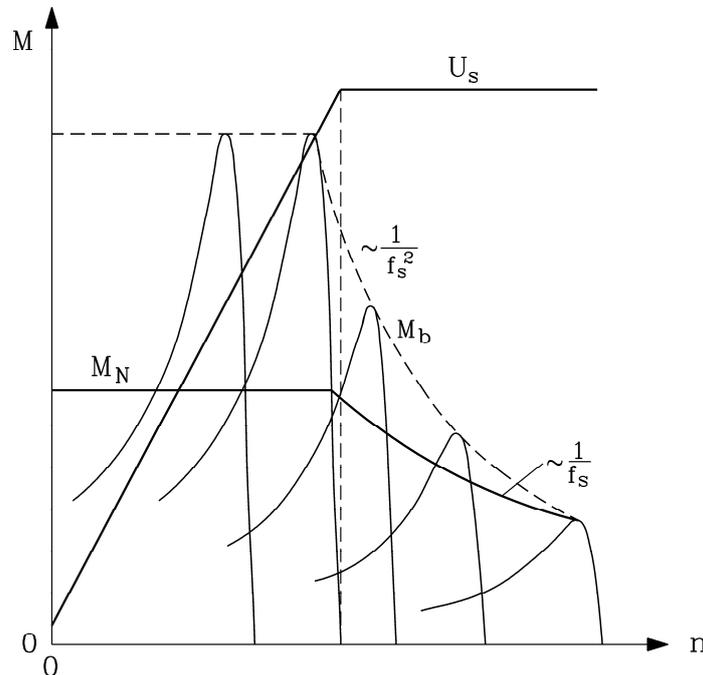

Fig. 4.1.2-3: By inverter parallelly shifted *Kloss-M(n)*-functions and their envelope as boundary lines of an induction machine (simplified depiction) for inverter supply at power limit, given by the inverter maximum voltage and current

The loss balance of the induction machine for a fixed operation point (speed, torque):
Electric input power $P_{e,in}$
Ohmic losses in **stator winding** $P_{Cu,s}$
Iron losses (eddy current and hysteresis losses) in stator iron stack $P_{Fe,s}$
Additional losses in stator winding and iron stack
   a)   By deviation of the magnetic field from sinusoidal shape (harmonics) for sinus commutation
   b)   By deviation of the voltage from sinusoidal shape when inverter fed, what generates harmonic currents
Ohmic losses in **rotor winding** $P_{Cu,r}$
Due to the low rotor frequency in rated operation the iron losses in the rotor stack are negligible small
Friction and ventilation losses P_{fr}
Additional losses P_{add} due to harmonics, which appear as eddy currents in the rotor, and thus brake the rotor
Output power at the shaft $P_{m,out}$
Hence the **shaft torque (clutch torque)** M_s is by the **rotor loss torque** M_d smaller than the electromagnetic torque in the air gap.

The conchoids in Fig. 4.1.2-4 show operation points of same efficiencies in form of contour lines. As motor-output quantities speed and torque determine the operation point. The high efficiencies lie in higher speed range. For inverter operation it is possible, to start-up with breakdown torque, what makes high startup torque with relatively low starting current (approx. 2 times rated current) possible.

Advantages of the induction machine:
- High development level
- Speed sensor for speed controlled operation necessary, but no position sensor is necessary
- Robust construction

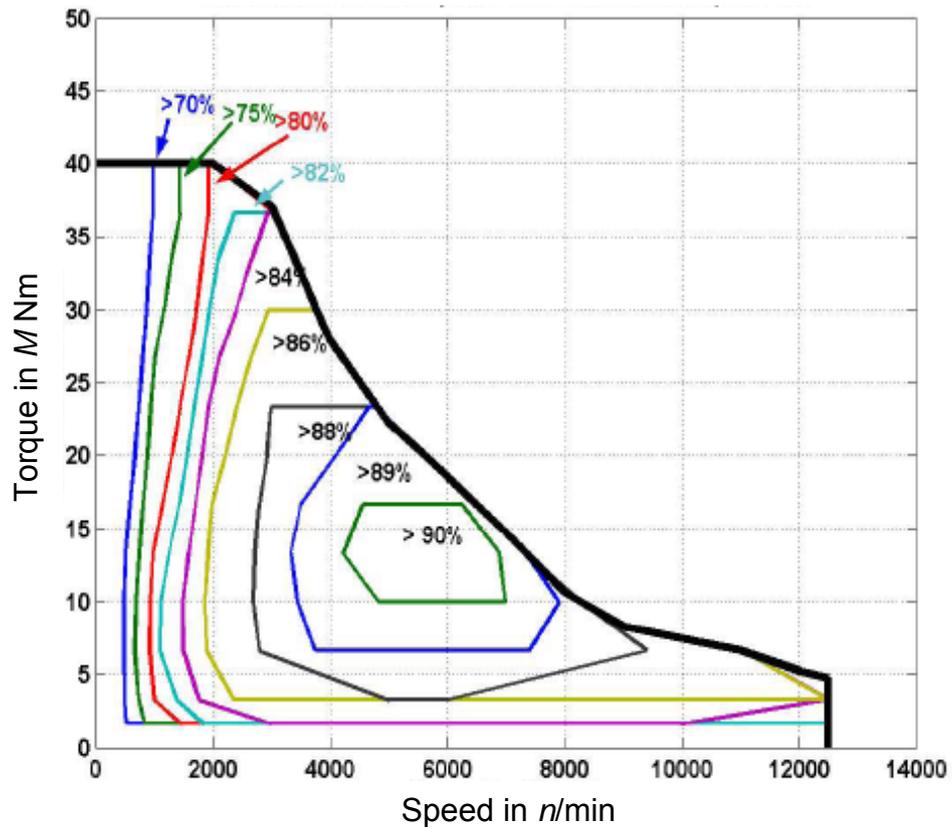- Short time loading until break-down possible

Fig. 4.1.2-4: Lines of constant efficiencies for speed variable operation of a four pole induction machine at inverter operation (conchoids). The machine was constructed for a hybrid vehicle and has a water jacket cooling. The boundary line of the machine for short time operation according to Fig. 4.1.2-3 results due to the maximum inverter output voltage and current.

Drawbacks:
- Low efficiency in low speed range and part load due to magnetizing current
- Rotor losses inevitable

4.1.3   Permanent magnet excited synchronous machine

In **p**ermanent magnet excited **s**ynchronous - **m**achines (PSM) the magnetic field is generated without energy effort by permanent magnets in the rotor. The synchronous machine is like the induction machine a rotating field machine. The stator winding generates a rotating field, which drags the permanent magnets of the rotor synchronously with the same speed $n = n_{syn}$. Hence the PSM needs like the induction machine an inverter for variable speed operation.
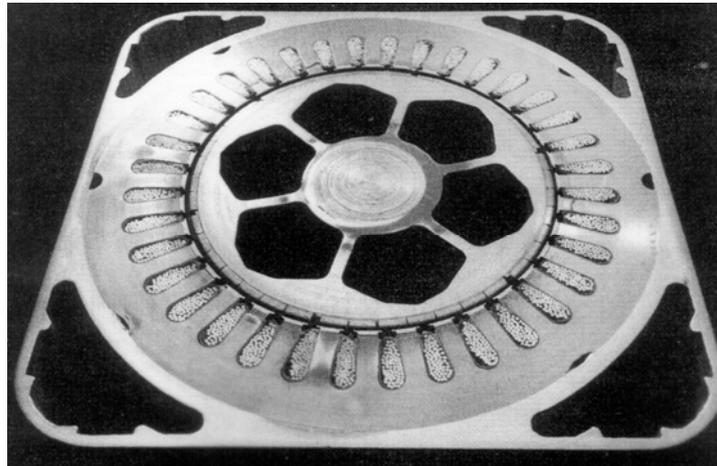

Fig. 4.1.3-1: Cut view of a 6-pole permanent magnet-machine with surface mounted magnets of neodymium-iron-boron (fixed with a glass fiber bandage) in the rotor (Source: *Siemens AG*)
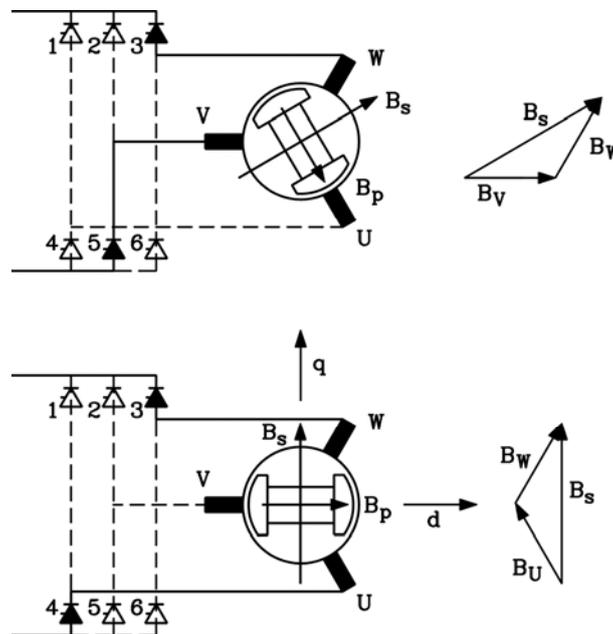

Fig. 4.1.3-2: Rotor position sensor-control: by a switching of stator current („q-current") of phase V and W to phase U and W for 2 different rotor position in time step of 1/6 period the angle between rotor and stator field is kept constant and hence e. g. the maximum possible torque is reached. For inter position between the two depicted rotor positions the stator field is impressed by switching of power switch 4 and 5 such that the angle between rotor and stator field remains constant The required freewheeling diodes the which antiparallel to the power switches 1…6 are not depicted.

The angle between the position of the north pole of the stator field and the south pole of the rotor field is zero at no-load. No torque is generated. At load of the rotor this angle becomes bigger. The rotor is tensed like a spring by the force generating part of the field. If a maximum angle of 90° is exceeded, the rotor "falls out of step" and stops. The maximum torque (synchronous breakdown torque) limits for given

voltage and hence impressed current the overload capability of the machine. Hence torque can be considered proportional to the rotor field (flux density B_p, generated by the permanent magnets), to stator field (flux density B_s, generated by stator current I) and to the enclosed angle between rotor and stator field. If rotor position is measured by a rotor position sensor, the voltage can be adjusted by the inverter in case of an increase of the load and hence of the rotor angle relatively to the stator field, so that torque can be kept constant via the increased current, as B_s is increased (Fig. 4.1.3-2). By this procedure the maximum angle of 90° between stator and rotor field and hence for a given current maximum torque can be generated, which is a loss optimal operation. The stator field is perpendicular to the rotor field, which is why the stator current is called „quadrature current" I_q. The position sensor can also be used as a speed sensor, so that a speed control can be realized by frequency adjustment of the inverter.

Table 4.1.3-1: Comparison of different magnet materials

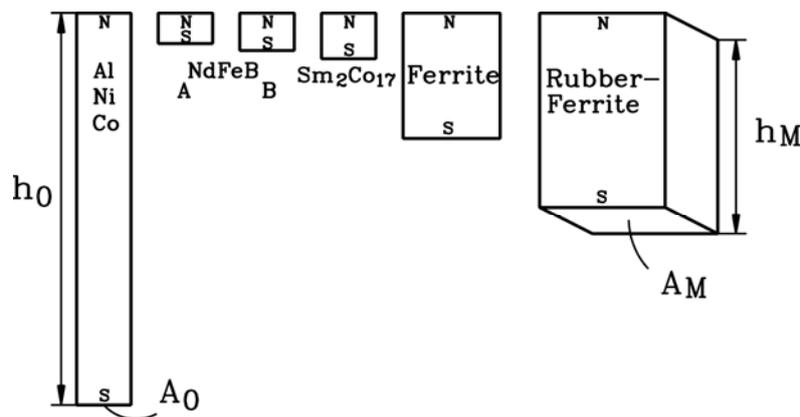| At 20°C	AlNiCo	NdFeB (A)	NdFeB (B)	Sm_2Co_{17}	Ba-Ferrite	Rubber - Ferrite
B_R / T	1.3	1.4	1.2	0.95	0.4	0.24
H_{CB} / kA/m	90	1100	900	710	270	175
A_M/A_0	*1*	*0.93*	*1.08*	*1.36*	*3.25*	*5.4*
h_M/h_0	*1*	*0.08*	*0.1*	*0.13*	*0.33*	*0.51*
V_M/V_0	*1*	*0.076*	*0.11*	*0.18*	*1.08*	*2.8*

Fig. 4.1.3-3: Comparison of different magnet materials (1) AlNiCo, (2) rare-earth-magnet NdFeB, type A for continuous operation temperature 70°C, (3) NdFeB, type B for continuous operation temperature 180°C, (4) Sm_2Co_{17}, (5) Ba-Ferrite, (6) composite of rubber and Ba-Ferrite

The remanence flux density B_R specifies what maximum flux density can be generated by the rotor (for zero air gap between stator and rotor). It decreases with increasing temperature with approx. 0.1 %/K for NdFeB. The higher B_R, the smaller the pole surface can be for the same flux. The coercive field strength H_{CB} specifies what externally applied magnetic field contrary to the magnetizing direction of the magnets is necessary, to push the flux density of the rotor magnets to zero. The higher H_{CB}, the smaller the magnet height can be chosen. Thanks to the high energy density of rare earth magnets NdFeB and SmCo, depicted as the product of remanence flux density B_R and coercive field H_{CB}, the rotor magnets are very small (Fig. 4.1.3-3) and therefore the rotor very compact.

NdFeB has the smallest volume at the same flux and same demagnetization strength, but a higher decrease of characteristic quantities with rising temperature than SmCo. Only lower energy densities are possible for materials suited for higher continuous temperatures. Continuous rotor temperatures up to approx. 180 °C are currently sensibly realizable with NdFeB, with SmCo also temperatures well above 200 °C. With increasing speed the induced voltage increases according to (4-1) $U_i = U_p$ with n, as the PM-flux of the rotor is constant (Fig. 4.1.3-4). When the inverter voltage $U_{s,max}$ is reached and equals U_p, no current can flow into the stator windings anymore, and torque would be zero, unless an additional

stator magnetic field is generated by an additional stator current component (I_d) which is oriented directly contrary to the rotor field, and thus weakens it, so that the resulting induced voltage $U_i < U_p$ in the stator winding is again smaller than $U_{s,max}$. As the current component I_d generates a stator field, which is antiparallel to the rotor field, and appears lengthwise to the rotor field, this current is called d-current. As the total current inside the stator windings has to remain constant („current limit" of the inverter, loss limit of the inverter), this field weakening operation by I_d is only possible, if the torque generating current component I_q is decreased. Because the sinusoidal current $i_d(t)$ is displaced to the sinusoidal current $i_q(t)$ by one quarter of period in each winding phase, for the superposition to the resulting stator current for each phase:

$$I_s = \sqrt{I_d^2 + I_q^2} \qquad\qquad (4.1.3\text{-}1)$$

is valid.

According to Fig. 4.1.3-4 this is possible, if for $n > n_N$ power is supposed to remain constant, so M decreases with $1/n$, as according to (4-1) $I_q \sim 1/n$ decreases also.
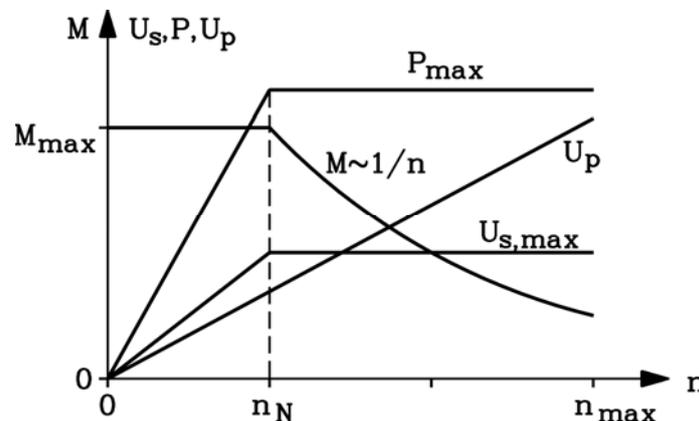

<u>Fig. 4.1.3-4:</u> PM-motor for speed variable operation, corner speed n_N and motor output power P_{max} remain constant. Maximum torque of the motor, back-EMF, voltage supplied by the inverter and motor output power are depicted.

The stator counterfield is directly proportional to the current I_d and to the stator inductance L, so a bigger L allows a smaller I_d, hence lower ohmic losses and a wide field weakening range are possible. The design of the PM-machine is decisive for its operation properties. An example for the operation of the PM-synchronous motor with field weakening is explained for the inverter voltage limit $U_{s,max} = U_N$ (= 100%) and the inverter current limit $I_{s,max} = 2I_N$ (= 200% of rated current). The reactance of the stator per phase (product of stator frequency and stator inductance: $X_d = 2\pi f_N \cdot L$) is – referred on $Z_N = U_N / I_N$: $x_d = X_d/Z_N = 0.33$ p. u.. The back-EMF at rated speed is $U_p/U_N = 0.7$. Operation points a) to d) are depicted.

 a) Rated speed, rated torque,
 b) Rated speed, twice rated torque,
 c) 170% rated speed, reduced torque by field weakening due to reduced q-current and a counter field due to a negative I_d-current,
 d) 400% rated speed at strong field weakening.

<u>Table 4.1.3-2:</u> Electric operating specifications of a PM-motor at speed variable operation with field weakening (p.u.-values: $u_s = U_s/U_N$, $i_s = I_s/I_N$)

	Voltage u_s	Current i_s	i_{sd}	i_{sq}	Power	Speed n
a)	0.8	1.0	0	1.0	P_N	n_N
b)	1.0	2.0	0	2.0	$2P_N$	n_N
c)	1.0	1.5	**-0.8**	1.27	$2P_N$	$1.7n_N$
d)	1.0	1.7	**-1.6**	0.5	$2P_N$	$4n_N$

Advantages of the PM-machine:
- Highly sophisticated
- Low-maintenance and robust, as no brushes are needed
- Compact thanks to high energy magnets (NdFeB or SmCo), hence low weight
- High speeds possible, if rotor magnets are well fixed (e. g. carbon fiber bandage)
- Higher efficiency than DC- or induction machines
- High torque density
- Low noise

Drawbacks:
- Higher control effort
- Speed- and position sensors required

In modern hybrid vehicles the PM-machine is the most commonly applied electric machine, as it has also high torque at high speed density in spite of the required field weakening current in that case. This is especially possible if the magnets are buried in the rotor. A difference of reluctances between the flux paths in d- and q-axis comes up, so that the rotor iron without the permanent magnets generates a torque (reluctance torque). This reluctance torque supports the PM-torque, so that q- current for the PM-torque can be reduced, which gives room for sufficient d-field weakening current, without letting the losses increase too much. In Fig. 4.1.3-5 the q-current can also - in case of dismounted magnets - generate a stator field, which builds up well in the rotor, as the flux paths over stator, air gap and rotor can close between the magnets. This field has its maximum in the air gap at the locations, where the PM-magnet field has its slots, so in vertical and horizontal direction. Exactly there the d-current flows with maximum amplitude and generates with the field of the q-current a torque (reluctance torque), which points for negative (so field weakening d-current) into the same direction as the PM-synchronous torque generated by the rotor magnets and q-current.
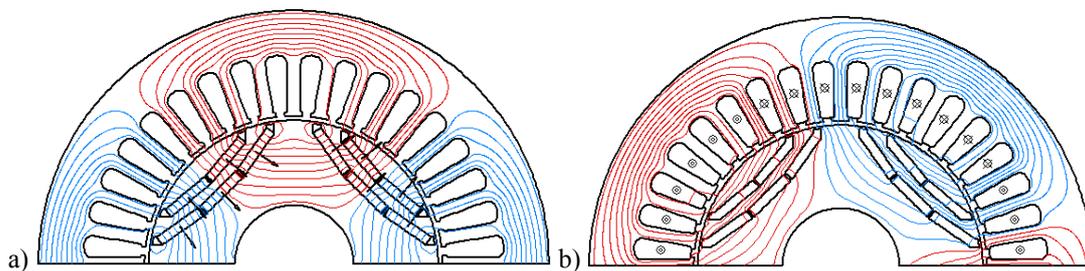

Fig. 4.1.3-5: Four-pole PM-motor with buried magnets in several layers, upper half depicted: a) No-load field, magnetizing direction of rotor magnets are depicted with arrows, stator current is zero, b) Field at rated torque, current direction in stator are depicted (positive or negative), program *FEMAG*. The stator phase current consists of a q- and a negative d-current component to utilize the reluctance torque.

4.1.4 Switched reluctance machine

Reluctance machines do only work with the difference of reluctances between d- and q-axis, in order to generate torque. In switched reluctance machines this difference is formed in stator AND rotor by distinct gaps between rotor and stator teeth for high torque generation. The switched reluctance machine stands out by its easy construction, especially concerning the rotor, and is thus inexpensively manufacturable.

Stator and rotor have <u>different</u> number of slots, e. g.: stator 8 teeth and slots, rotor: 6 teeth and slots (Fig. 4.1.4-1). The stator teeth carry coils (tooth coils), which are - according to the designed number of phases *m* - connected to different phases. In contrast to the distributed rotating field winding this is an easily manufacturable tooth coil winding (concentric winding). In Fig. 4.1.4-1 four phases 1, 2, 3, 4 are depicted with each 2 coils for a two pole machine. Each of the phases is being controlled by positive (unipolar) DC-pulses from different independent transistor half-bridges. That phase whose stator teeth are the closest to the rotor teeth is energized. The tangential magnetic pull of the field lines generates the reluctance torque. When stator and rotor teeth of the considered phase are aligned with each other, the tangential pull disappears. Successively this phase is turned-off and the next phase is energized. The rotation direction is achieved by changed energizing sequence of the four phases. In order to have the correct energizing sequence also at start-up a rotor position measuring is done like for PM-machines. As the magnetic pull is given as force per area by:

$$\sigma = B^2 /(2\mu_0) \qquad \mu_0 = 4\pi \cdot 10^{-7}\,\text{Vs}/(\text{Am}) \qquad\qquad (4.1.4\text{-}1)$$

The magnetic tangential force and hence the torque is proportional to square of the current due to $B \sim I$. At overload the iron in the stator and rotor teeth is saturated, so that the flux density in the iron only increases with $B \sim \sqrt{I}$. That is why for high current torque is proportional to *I* (Fig. 4.1.4-4a). In order to minimize the amount of power semiconductors normally the three phase switched reluctance machine is preferred (Fig. 4.1.4-2).
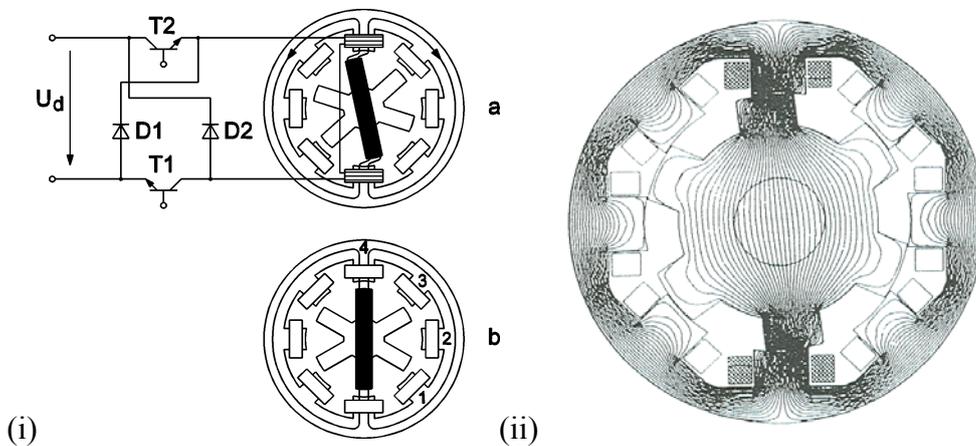

<u>Fig. 4.1.4-1:</u> Two-pole, four-phase switched reluctance machine (axial cut): (i) Phase "4" is energized by the transistor-H-bridge, which adjusts the desired DC-current amplitude out of the DC-link voltage U_d by pulse-width-modulation. The tangential magnetic pull drags the closest rotor teeth into aligned position under phase "4", (ii) Numeric field calculation, phase "1" (motor data: stator outer diameter: 320 mm, air gap: 1 mm, iron stack length: 320 mm, shaft diameter: 70 mm, number of turns per tooth coil: 10, DC-current per coil: 10 A DC)
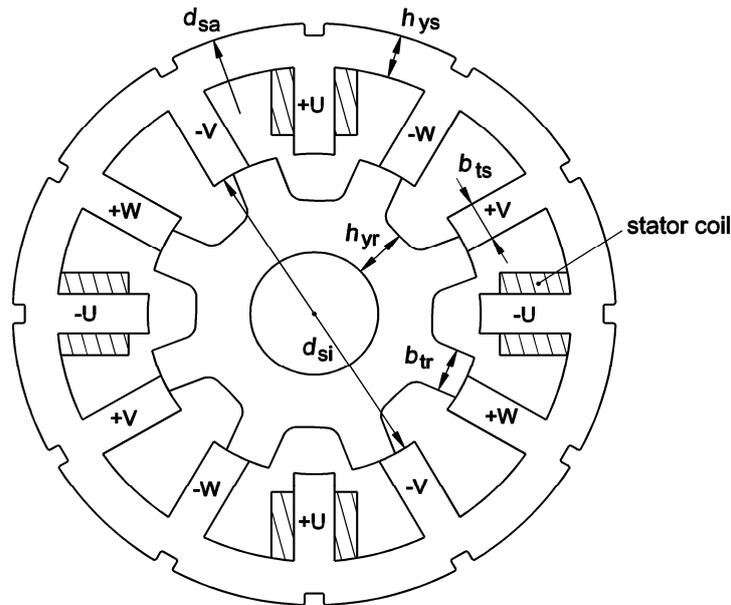
Fig. 4.1.4.2: Cross section of a four pole, three phase switched reluctance machine

In order to design a high difference of reluctance between slot-tooth and tooth-tooth position the air gap between rotor and stator teeth is chosen as small as possible – similar to the induction machine. The energization with ideal rectangular shaped DC current is performed with pulse-width-modulation almost correctly at low speed (Fig. 4.1.4-3a), at high speed not much time remains for the pulse-width-modulation due to the short current flow durations, so that the current shape is being deformed. Even for ideal rectangular shaped current the torque is, due to the air gap field, not constant (Fig. 4.1.4-3b). Torque pulsations increase for non-ideal current. This also results in non-ideal radial forces, so that magnetic noise generation is possible, because the oscillating stator iron stack acts like a phone. Due to the deformed current pulses at high speed torque is – for the same current amplitude - much lower than at low speed, because the mean value of current is significantly smaller. For high speed the ratio of current mean value and current amplitude decreases with $1/n$. The iron is unsaturated and torque (proportional to the square of current) decreases with $1/n^2$ (Fig. 4.1.4-4b). At no-load and part-load current is small due to the small torque and hence the flux of the machine and therefore also the magnetic pull, so that at no-load force-excitation of noises is small. At no-load the machine is generally unnoticeable concerning magnetic noises, but at load it can reach formidable noise levels L due to excitation of resonance oscillations (Fig. 4.1.4-5).
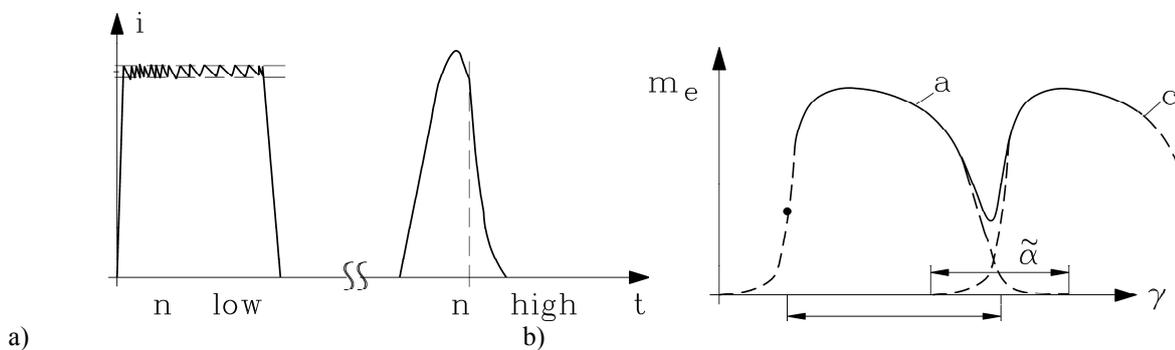

Fig. 4.1.4-3: a) Current in one phase at low (left) and high speed (right). The time scaling in the right Fig. is expanded compared to the left Fig. B) Torque ripple at ideal rectangular shaped current.
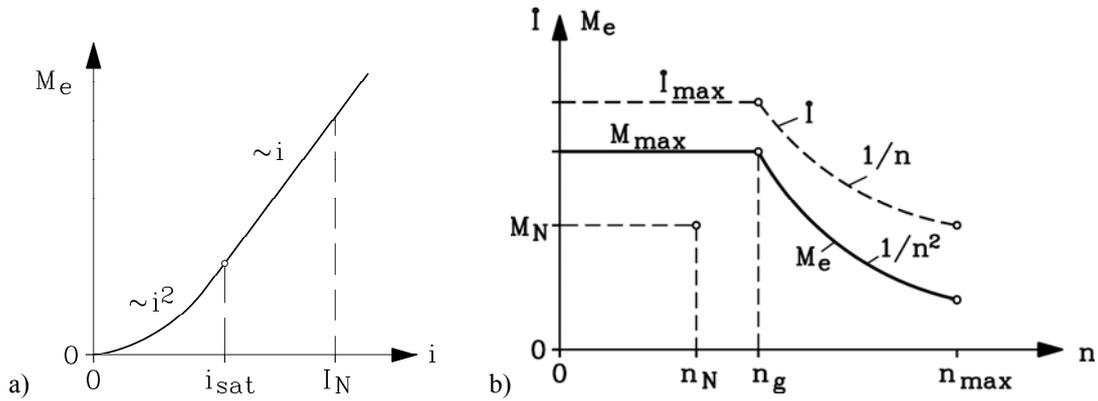
Fig. 4.1.4-4: a) Torque as a function of current for constant speed: unsaturated: $i < i_{sat}$: $M \sim i^2$, saturated $i > i_{sat}$: $M \sim i$, (I_N: rated current), b) Boundary line of torque as a function of speed for a current limit I_{max} given by the inverter. Above corner speed mean value of current decreases rapidly due to the deformed current pulse, so that torque also decreases
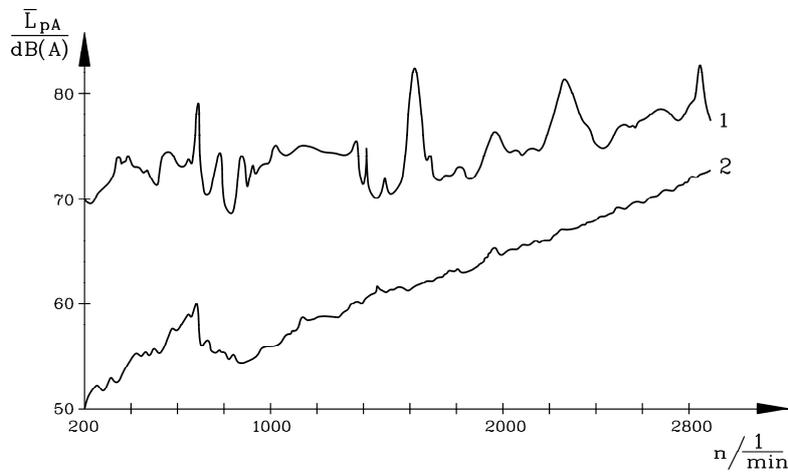

Fig. 4.1.4-5: Measured sound pressure level of a shaft ventilated 7.5 kW 12/8-switched reluctance machine (Fig. 4.1.4-2) in sound measuring room (1: operation with rated current, 2: operation at no-load). At no-load torque and current are very small, so that due to $B \sim i$ the exciting radial force per area $f_r \sim B^2 \sim i^2$ is also small, thus low noise is being excited. At rated operation higher noise peaks are measured due to resonance excitation.

Table 4.4.4-1: Measured loss balance data from heating runs in continuous operation at 1500/min, 54 Nm and $U_d = 540$ V DC-link voltage of a four pole standard induction machine and a switched reluctance machine of the same size and rated power (shaft mounted fan for ventilation, air cooling, surface cooling with cooling fins at the stator housing and a ventilation hood).

	Switched-reluctance-machine	Induction machine
Input- / output power P_{in} / P_{out}	9440 W/ 8480 W	9950 W/ 8480 W
Phase current (RMS/peak) $I / \hat{I}$	13.3 A/ 27.5 A	17.45 A/ 30 A
Stator frequency f_s	200 Hz	52 Hz ($U_{s,k=1} = 225.5$V)
Stator winding heating	110 K	101 K
Iron- / friction losses	200 W/ 165 W	265 W/ 55 W
Ohmic losses stator / rotor	595 W/ 0 W	650 W/ 350 W
Additional losses	0 W	150 W
Stator current density J_s	5.25 A/mm^2	8.23 A/mm^2
Current load $A = 2mN_sI_s/(d_{si}\pi)$	513 A/cm	305 A/cm
Motor efficiency η_{mot}	**89.8 %**	**85.2 %**
Inverter efficiency η_{inv}	96.6 %	97.0%
Drive efficiency η	**86.7 %**	**82.6 %**

Compared to the induction machine the cage losses as well as the additional losses are smaller for inverter feeding. Due to the compact tooth coils generally a good het flow results and thus lower heating of the windings for the same current densities, so that the ohmic losses in the stator are smaller than the ones of the induction machine. In total a higher efficiency is achieved for SRM compared to the induction machine for the same machine size. The induction machine with the specifications from Table 4.1.4-1 is designed for grid operation and not for inverter feeding, where low current displacement squirrel cages are used.

Advantages of the switched reluctance machine:
- Simple, cheap structure
- Robust rotor
- Low maintenance
- No distributed rotating field winding, but tooth coil winding
- High speeds
- Low rotor inertia
- Failure safety due to separated feeding of the phases (2-phase startup also possible)
- High torque density and start-up torque
- High motor utilization thanks to compact tooth coils and iron flux densities
- High efficiency (low rotor losses only due to hysteresis)
- High overload capability
- High continuous torque
- Low heating at low speed

Drawbacks:
- High torque ripple
- Big noise
- Speed dependent control
- Speed/position sensor necessary

Fig. 4.1.4-6: Rotor and stator stack of a 3-phase, two-pole 6/4-switched reluctance motor

4.1.5 Transversal flux machine (TFM)

The TFM is a rotor position-controlled PM-synchronous machine with the special property, that the flux is guided transversal to the rotational direction (Fig. 4.1.5-1). This results in the need to assemble two magnet rows with alternating polarity beneath the ring coil of the stator winding phase, where laminated U-iron yokes with a displacement of double pole pitch guide the flux of either N-poles or S-poles (further motion of the rotor of one pole pitch) around the ring coils. As only p U-yokes exist only e. g. the p N-poles of one magnet row and the opposite S-poles of the second row can generate a flux, so that flux linkage is directed only clock-wise in Fig. 4.1.5-1. After rotation of the rotor by one pole pitch the flux linkage inverses, so that an alternating flux linkage of the stator ring coil comes up and hence – like in the conventional PM-machine - a back-EMF is being induced (Fig. 4.1.5-2). If the magnets are imaginarily replaced by ampere turns (Fig. 4.1.5-3), one can recognize, that for AC-current supply a tangential force comes up, when pole gaps of the magnets are under the U-yokes. So via a rotor position sensor the inverter is controlled such that maximum current flows in the described case.
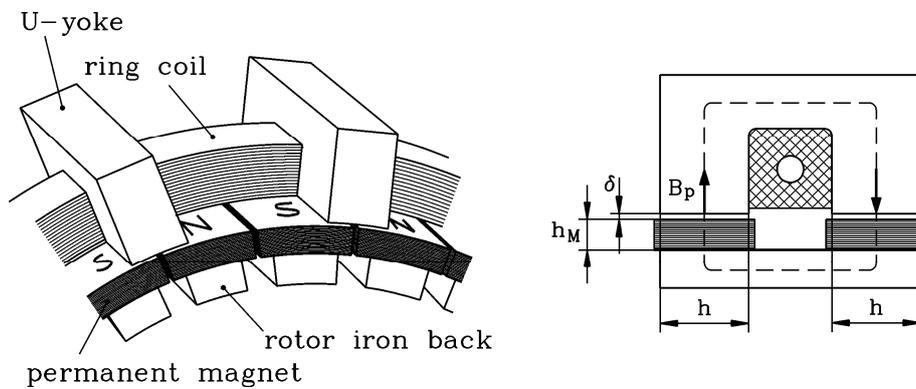

Fig. 4.1.5.-1: Transversal flux machine: Depiction of one phase, consisting of a ring coil, p U-yokes and $2p$ magnets of alternating polarity in two parallel rows with opposite polarity (left), excitation of rotor-PM-no-load field for current less ring coil, which closes over the U-yokes (right)
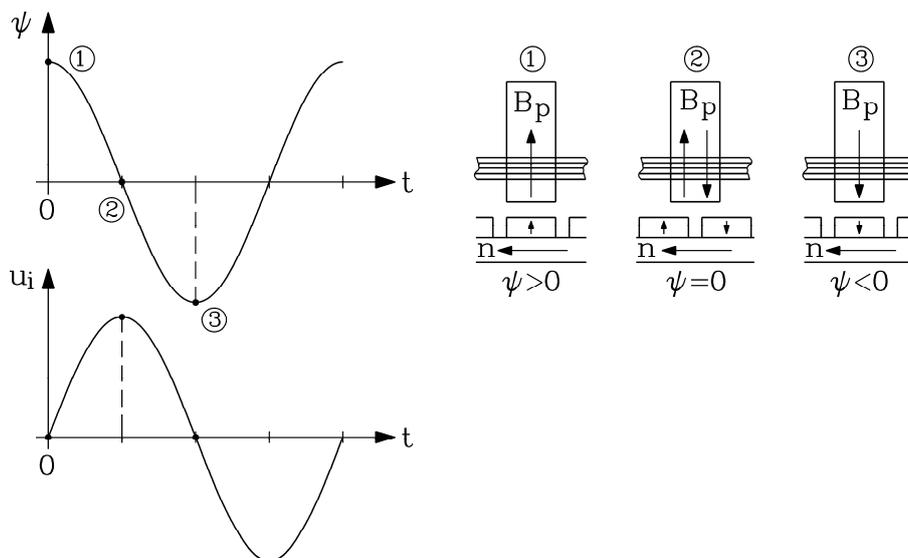

Fig. 4.1.5-2: Voltage induction into stator ring coil of a transversal flux machine: The alternating flux linkage ψ induces the back-EMF $u_i = u_p$
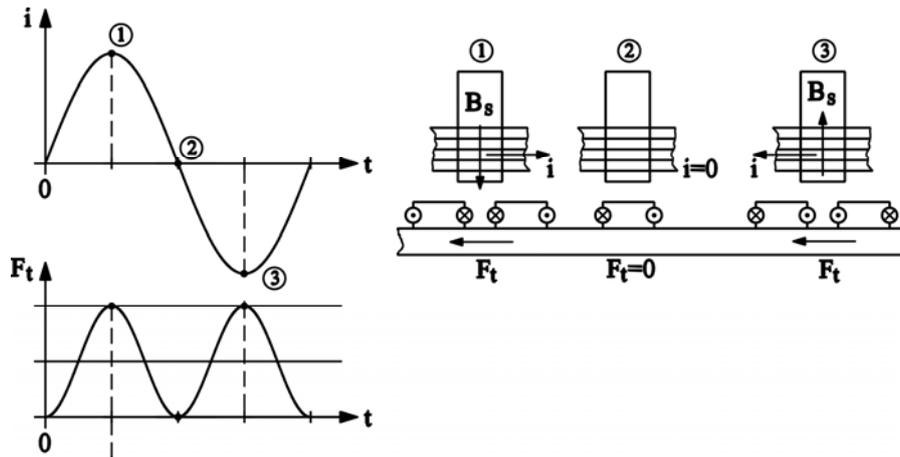
Fig. 4.1.5-3: The AC-current supply *i* of a stator ring coil generates a stator field B_s, which together with the equivalent ampere turns assembly of the magnets generates a tangential force according to *Lorentz*-force-law pulsating with double stator frequency 2*f*.

Two by a quarter of pole pitch displaced ring coils and U-yoke assemblies deliver two displaced pulsating tangential forces, so that the sum of tangential forces is theoretically constant for sinusoidal pulsation. In this way a two phase TFM concludes (Fig. 4.1.5-4). In the same way three- and poly-phase machines can be constructed, by assembly of e. g. three ring coils, which are displaced by 1/3 of double pole pitch. As the force pulsations are generally not sinusoidal a force ripple remains in the resulting tangential force similar to the switched reluctance machines. In the same way formidable noise excitation may occur.
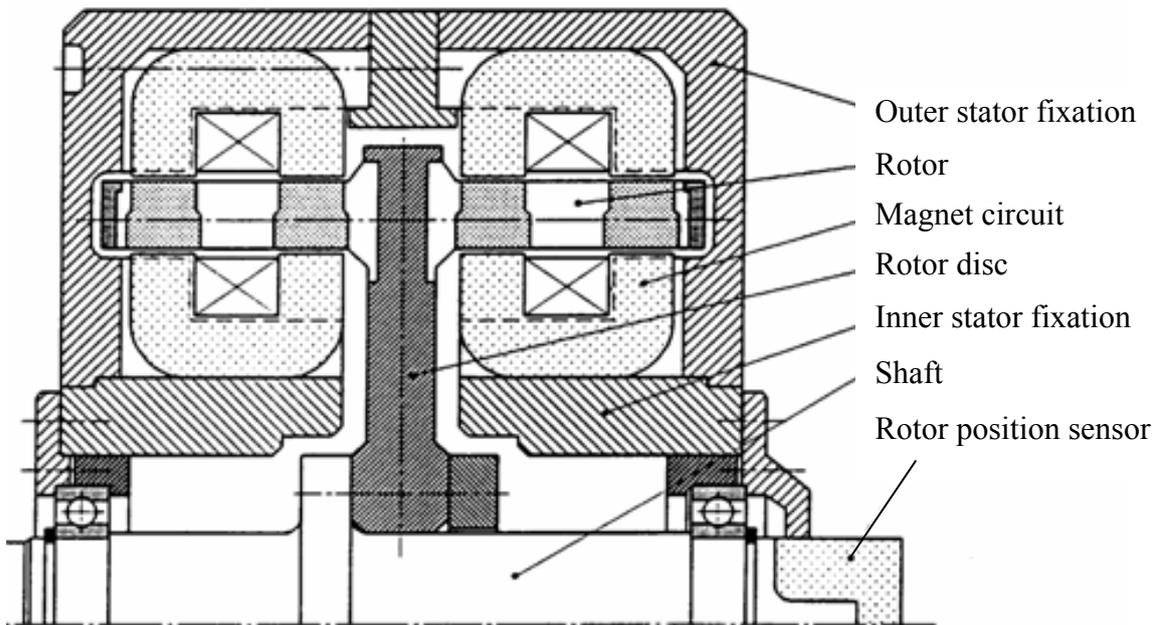

Fig. 4.1.5-4: Axial cut of two-phase transversal flux machine according to Prof. *Weh,* TU *Braunschweig*, rotor magnets is flux concentrating assembly, double acting TFM with each one ring coil above and beneath the magnet rows per phase

As a force contribution is delivered per U-yoke, torque can be increased by the increase of the number of U-yokes together with a decrease of magnet width in circumferential direction, which yields to high torque densities, but also to high pole counts. Thus the supply frequency for high speed is very high (in the range of kHz), what leads to high additional losses and reduces the efficiency significantly. By assembling a ring coil above and beneath the magnet rows the thrust can (almost) be doubled, if the magnets are placed perpendicularly in flux concentration assembly (Fig. 4.1.5-5). The TFM then has the

highest specific torque and can be applied as a direct motor without a gear close to the wheel. While ring coils are relatively simple the magnetic paths in the rotor are quite complex. For the application in line-manufactured vehicles the TFM is up to now sill not suitable, as it is mainly suited as direct drive. Bus drives as prototypes by the company *Voith* on the basis of patents by Prof. Weh are applied. The first generation is depicted in Fig. 4.1.5-6, while the second generation has an again increased power density are more and more deployed.
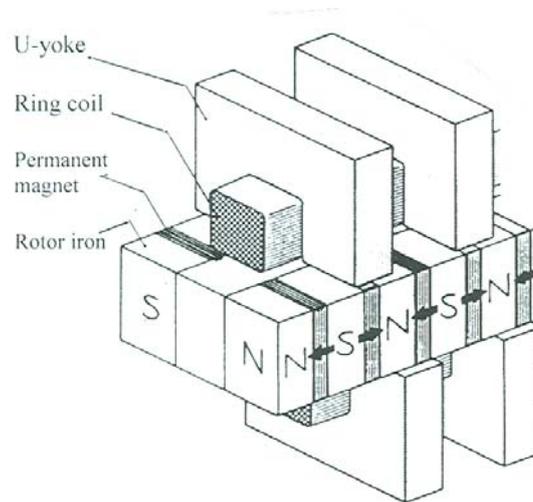

Fig. 4.1.5-5: Magnetic flux concentration in the rotor by upright placed rotor magnets with above and beneath assembled ring coils
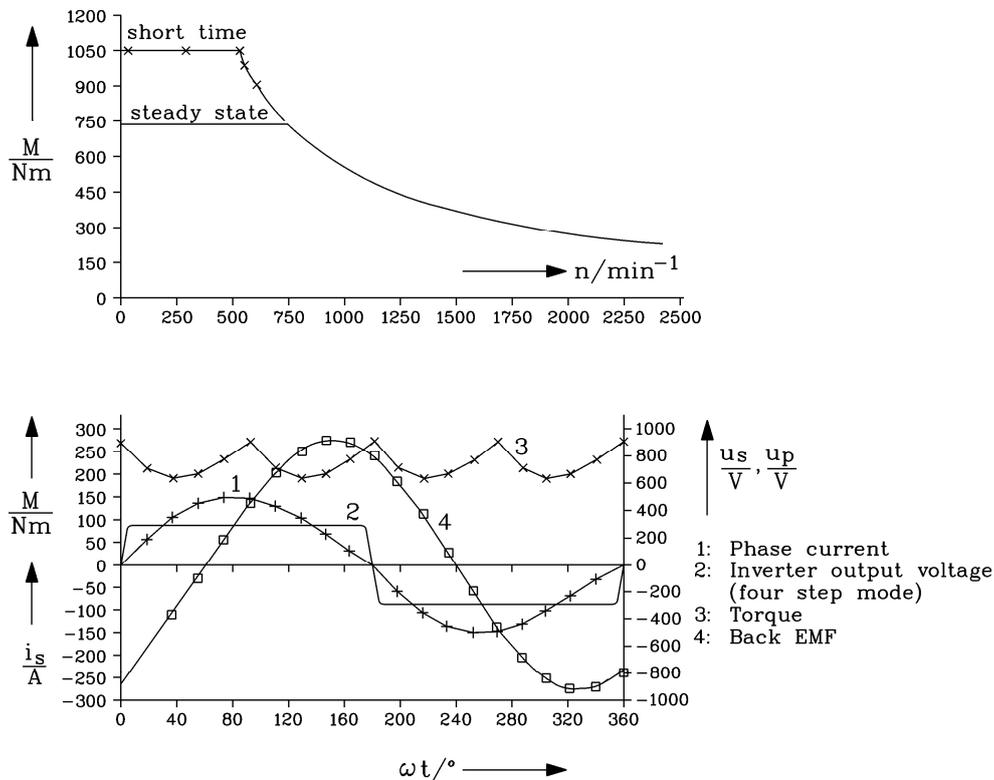
Fig. 4.1.5-6: 57 kW TFM: Calculated electric operation parameters for a city bus drive (*Voith, Germany*). Top: Torque-speed boundary line, Bottom: Calculated current i_s, back-EMF u_p, inverter output voltage u_s for block commutation at maximum speed 2500/min, torque. Torque ripple 17% with 4-times stator frequency 5.4 kHz.

The first generation of prototypes of a TFM-series for city busses (*Voith, Heidenheim, Germany*) had the following specification: n_{max} = 2500/min, M_{max} = 1050 Nm, f_{max} = 1375Hz, continuous power 57 kW,

outer diameter 420 mm, weight 115 kg, 300 V DC-link voltage, pole count $2p = 66$, number of phases $m = 2$.

Table 4.1.5-1: Operation range of TFM first generation prototype by Voith Company

Base speed range: Constant torque	0...750/min	725 Nm continuous torque 1050 Nm overload torque
Constant power range	750...2500/min	725...218 Nm continuous

4.2   Comparison of machine types

Whereas in older battery powered vehicles a formidable amount of DC-machines were used, they have almost disappeared in newer electric or hybrid vehicles. The trend is moving towards the usage of PSM in newer vehicles, which is due to the use of new high energy magnets made of rare earth metals and the high efficiency in lower speed range and at part-load. At high speed the efficiency is generally reduced by the field weakening d-current component, while the induction machine and the SRM do field weakening "automatically" by lower current consumption. Thus they provide a higher efficiency at high speed. Under use of two machines and the occurrence of a fail e. g. in the stator winding the induction machine and the SRM can be turned off and in fail-safe mode entrained without any problems. Due to the rotor magnets the PSM is in the state of fail-active. A voltage is induced into the damaged stator winding, which yields to fail-short-circuit-current in the short circuited windings even at turned-off machine, as long as it rotates. Even with open circuited windings entraining losses occur for rotating machine due to the iron losses in the iron stack, which generate a braking torque by eddy currents in the stator iron.
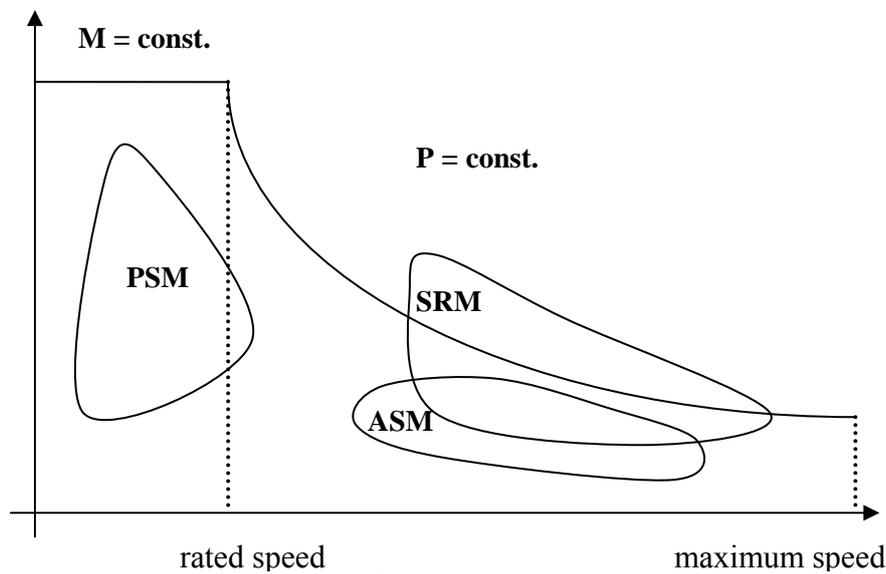
Fig. 4.2-1: Areas of maximum efficiencies of the three different drive concepts PSM (permanent magnet excited synchronous machine), induction machine (squirrel cage rotor), SRM (switched reluctance machine)
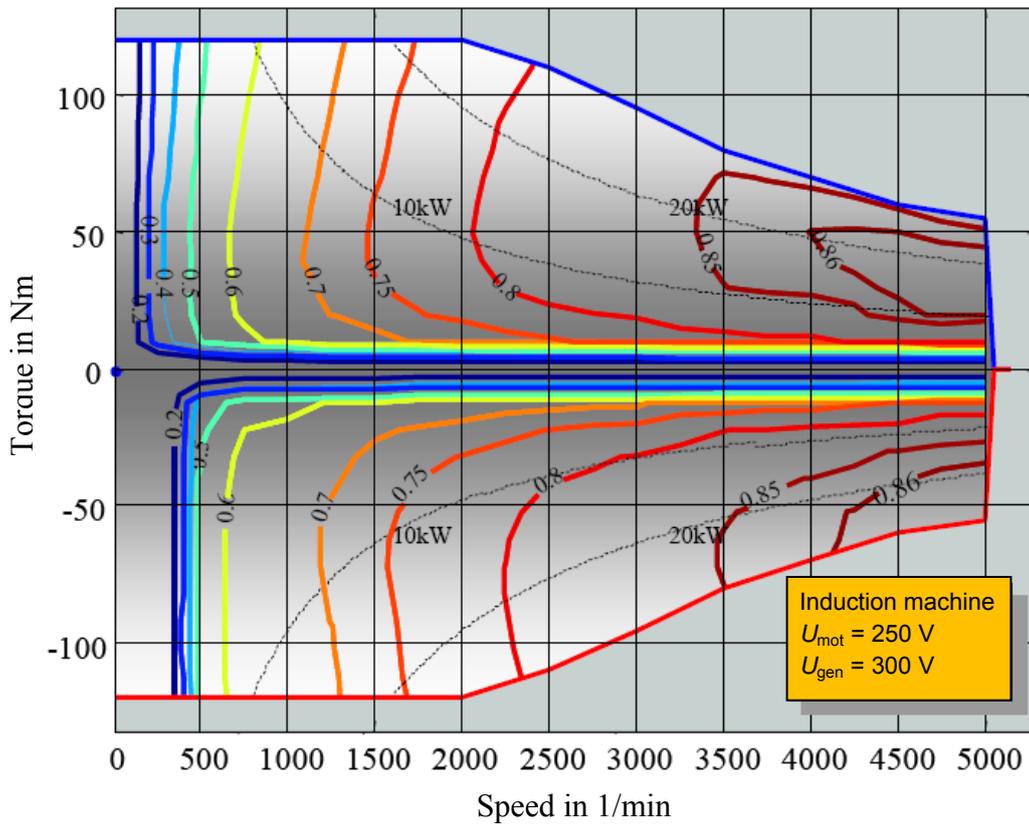
Fig. 4.2-2: Efficiency field of an induction machine designed for a hybrid vehicle (Source: Köhle, S.: Der Volkswagen Bora Hybrid, Entwicklungsziele, Fahrzeugbeschreibung und erste Messergebnisse of the *VW Bora* mit Hybridantrieb, 2003)

Fig. 4.2-3: Efficiency field of PSM machine designed for a hybrid vehicle (from: Köhle, S.: Der *Volkswagen Bora Hybrid*, Entwicklungsziele, Fahrzeugbeschreibung und erste Messergebnisse of the *VW Bora* mit Hybridantrieb, 2003)

<u>Table 4.2-1</u>: Advantages and drawbacks of the electric machines as traction drives
PSM (permanent magnet synchronous machine), induction machine (squirrel cage rotor), SRM (switched reluctance machine), TFM (transversal flux machine), DC-machine
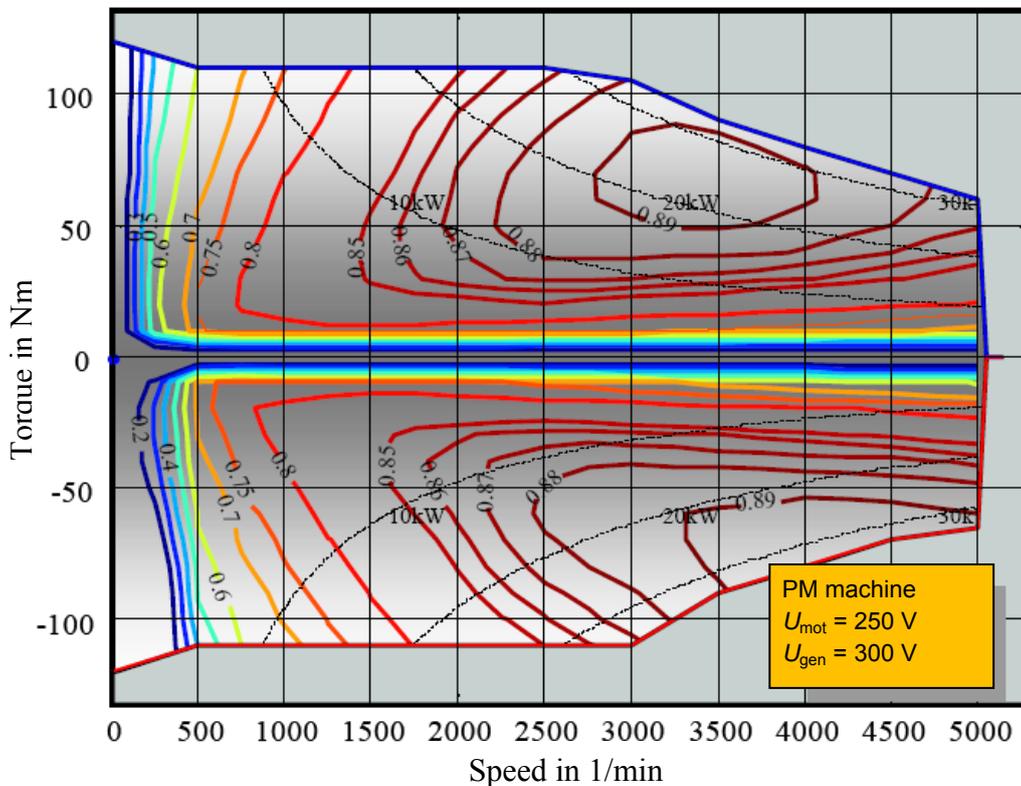
	Induction machine	**PSM**	**SRM**	**TFM**	**DC-machine**
Torque density	**o**	++	+	++	-
Efficiency	**o**	++	**o**	+	-
Weight	+	++	+	++	-
State of art	++	+	**o**	--	++
Inverter	+	**o**	--	--	++
Costs	**o**	-	++	-	-
Manufacturing	+	-	++	--	-
Noise	+	++	-	--	+

<u>Table 4.2-2</u>: Comparison of electric drive for electric vehicles

	Series wound motor	**Separately excited motor**	**Induction machine**	**Separately excited synchronous machine**	**PSM**	**SRM**
Costs	low	fair	fair	fair	fair	low
Efficiency	low	fair	high	very high	high	very high
State of art	high	fair	high	fair	fair	low
Maintenance	yes	yes	no	no	no	no
Characteristic	bad	good	very good	very good	very good	very good
Control effort	very low	low	high	high	high	fair
Recuperation	costly	no additional effort	no additional effort	no additional effort	no additional effort	no additional effort

Cost comparison between induction machine, PSM and DC-machine at 25 kW
Important criteria for the choice of the machine are the costs. In the Table 4.2-3 induction machine, PSM and SRM are compared with regard on manufacturing costs for the dimensioning on the same rated power.

The permanent magnet make the PSM more expensive compared to the induction machine and the SRM. While the induction machine only need a speed sensor the PSM, the SRM and also the transversal flux machine need a rotor position sensor, in order to determine the exact position of the rotor and obtain maximum torque. In some cases sensorless procedures can be used, e. g.
    a) By injected test signals into the stator winding with reluctance effects or
    b) By monitoring of the back-EMF
The rotor position is indirectly determined without the need of an extra sensor.
Optical incremental encoders or absolute encoders on the one hand (Fig. 4.2-4a) and (cheaper, but less accurate) electromagnetic resolvers on the other (Fig. 4.2-4b) are used as position sensors.

Table 4.2-3: Exemplary comparison between water-jacket-cooled E-motors for E-vehicles: Induction machine, PSM and SRM for 25 kW rated power

|		Induction machine	PSM	SRM
Rated power	kW	25	25	25
Max. torque	Nm	130	150	130
Max. speed	min^{-1}	13 500	11 500	13 500
Weight	kg	59	55	65
Stator diameter	mm	235	235	235
Stator length	mm	125	125	125
Air gap length	mm	0,5	1	0,4
ECE-Cycle range as hybrid drive		100 %	105 %	102,5 %
Max. inverter current	A	400	600	400
Torque ripple		2,5 %	3 %	10 to 15 %
Electromagnetic noise		generally low, depends on numbers of slots	generally low, depends on magnet pole edges	big noise, especially at high speed
Required specific iron losses in stator iron stack	W/kg 50 Hz 1.5 T	3,2 … 5,3*) *) standard material	3,2*) … 5,3 high quality material	2.0 (high quality material)
Power density	W/kg	5.3	3.2	2.0
System costs for 10.000 drives per annum		100 %	120 %	108 %

a)   b)
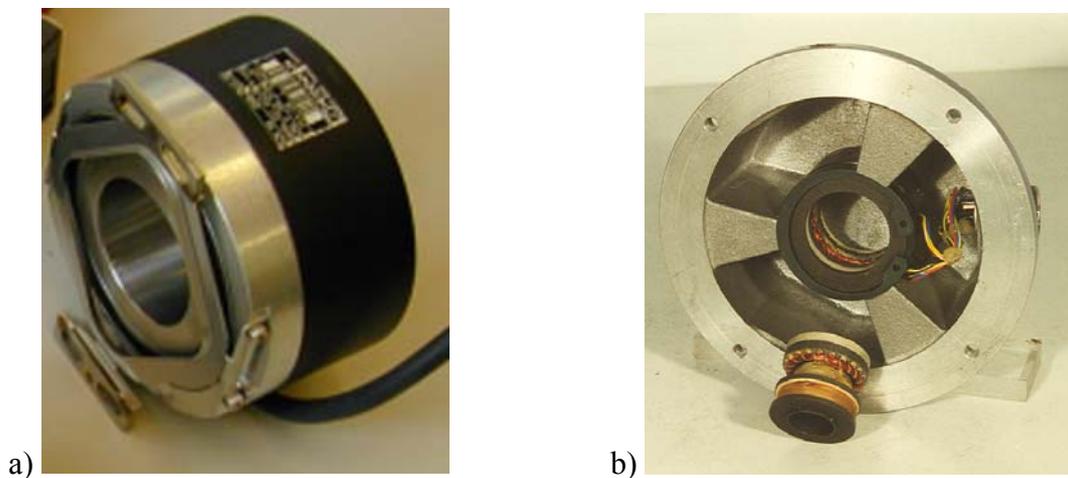
Fig. 4.2-4: Rotor encoder: a) Optical incremental encoder with A- and B-trail for direction recognition and zero trail for recognition of initial position, resolution 1024 lines on circumference, b) resolver rotor with transformer coil for 10 kHz operation frequency and sinus- and cosine-rotor coil, and stator mounted into the end shield. The evaluation electronics for a) and b) for calculation of rotor angle is included in the inverter.

For the development of E-motors with regard on higher power densities and efficiencies the following points are to be considered: Modern insulation materials have for the same voltage protection less thickness, so that a bigger conductor cross section, better thermal conductivity, lower current densities and hence lower losses and temperatures are possible. Insulating materials based on glass fiber allow continuous temperature of 180 °C (thermal class H). With the specific thermal class 200, which was developed for rail way applications continuous heating of 200 K are possible, so continuous temperatures of 240 °C. But all insulating materials have in common that with increasing temperature their lifespan

decreases. For E-motors in vehicles insulating materials are to be optimized for approximately 5000 h of operation. The *Montsinger*-law states that the lifespan of raisin-based insulating materials halves with the increase of continuous temperature by 10 K due to chemical reaction processes.
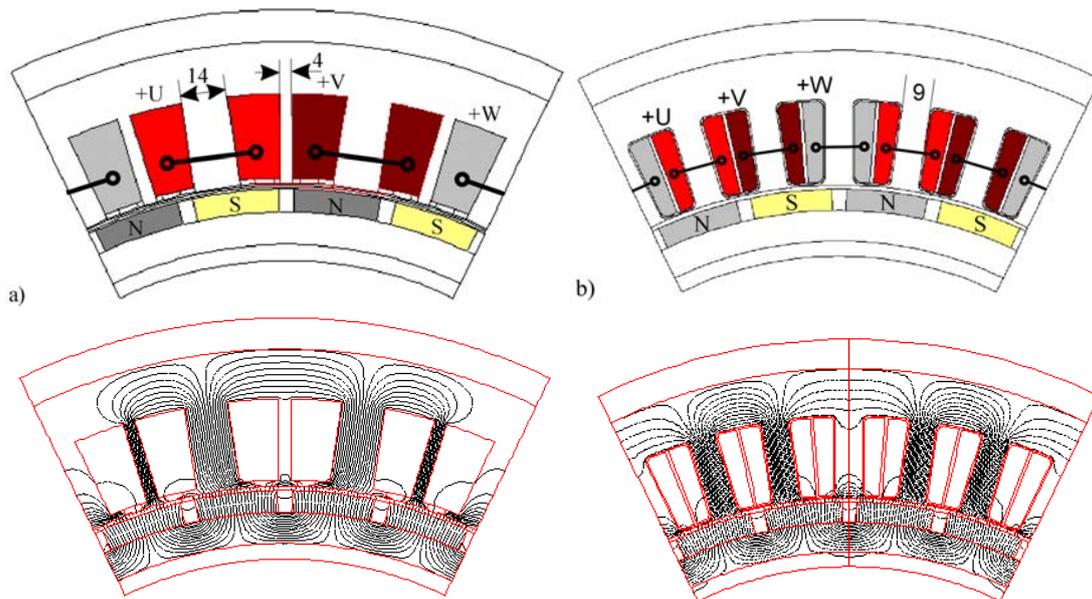

Fig. 4.2-5: Modular PM-synchronous machines have tooth coils instead of a distributed rotating field winding similar to switched reluctance machines: Numerically calculated field lines of magnetic flux density at no-load (stator current: zero) for 2 pole pairs of each a three phase PM-machine: a) Each one tooth coil U, V, W on four rotor poles: (with 4 mm big inter teeth between the coils for improvement of heat dissipation), b) Each one tooth coil of U, V, W on two rotor poles
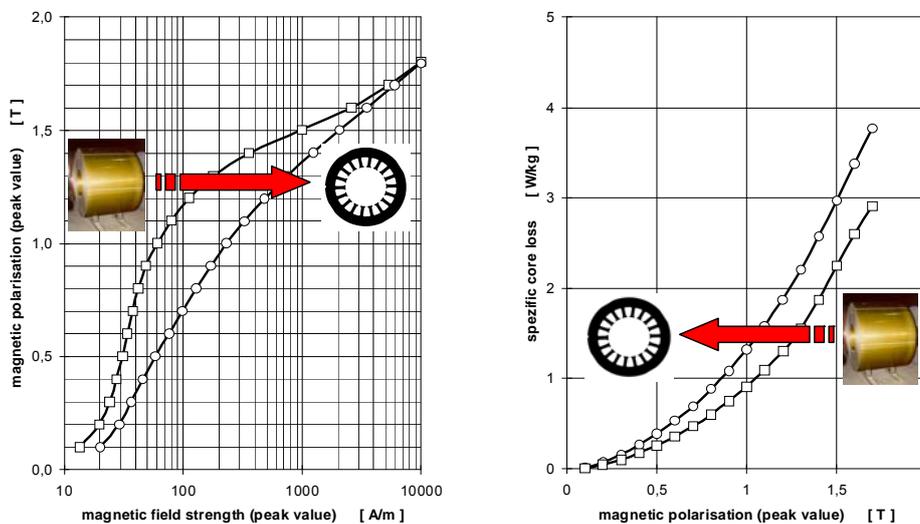

Fig. 4.2-6: Sheet punching: left: Decrease of magn. polarization, right: Increase of specific losses, (Dissertation Schoppa, A. P.: *Einfluss der Be- und Verarbeitung auf die magnetischen Eigenschaften von schlussgeglühtem, nichtkornorientiertem Elektroband,* Dissertation, RWTH Aachen, 2001)

Modern **high-energy permanent magnet materials** (PM) with high remanence flux densities and coercive field strengths (approx. 1.4 T at approx. 1000 kA/m) allow already now the construction of big permanent magnet excited synchronous machines in MW-range with high efficiencies of more than 93 % in spite of low speed, but the potential of development of PM is limited. But with PM-technology combination of low loss winding technologies of tooth coils (like in SRM) are possible (Fig. 4.2-5). This allows significantly more compact machines thanks to shorter winding overhangs and reduced ohmic losses. But the distribution of stator field in the air gap deviates formidably from the desired sinusoidal

shape. Especially at high speed eddy current losses in the magnet strongly increase, so that a careful design of the rotor with segmentation of the magnets becomes necessary. For high speed there is still development work to be done. The in the conductive magnets occurring eddy currents at variable speed (inverter fed) machines is a problem domain, which requires suitable precalculations and geometric configurations (buried or segmented resp. special layered magnets).

The **softmagnetic material** for the application in electric vehicles at high speed must have as low specific losses (eddy currents and hysteresis losses) as possible at high permeability and saturation induction for a wide frequency range. Due to cost reasons materials based on iron like iron-silicon-sheets (e. g. Fe6.5) for reduction of eddy currents, iron-nickel-materials (FeNi) and also iron-cobalt-materials (FeCo) are used. Sinter-materials based on iron (Soft Magnetic Composites, SMC) for the application at high frequency in kHz-range due to low eddy current losses have a permeability of only 1/10 of pure iron. Amorphs (MetGlass) and nano-crystalline materials have not gained acceptance yet. For middle-frequency-machines (high-speed-drives or TFM for higher spade) low loss thin electro sheets (e. g. HF20-sheet) are necessary for limitation of losses. Very difficult to implement in calculations are loss increasing influences due to mechanic machining of the sheets with the accompanying reduction of saturation polarization. Gentle processes (laser cutting instead of punching, recrystallization glowing) are partially applied from case to case (Fig. 4.2-5). The machining of SMC needs new approaches.

5. Inverter

For the use and control of the DC-voltage obtained by the energy storage the voltage has to be converted by an inverter into an AC-voltage. Industrial inverters at first rectify the 3-phase voltage of the public grid into a DC-voltage, which is afterwards smoothed by DC-link capacitors. In battery powered vehicles this DC-voltage source is the battery itself. The capacitor has to take in AC-current parts of the motor current, which occur due to pulse width modulation. In this way the AC-current part is kept away from the battery.

The bigger the capacity the smaller is the - with the DC-current superimposed - AC-current in the battery. If the energy flow from battery to motor is inversed for recuperation during braking, the inverter acts as a rectifier from the point of view of the battery, which generates a DC-voltage out of the induced AC-voltage by the motor, which is higher than the battery voltage, so that current flows into the battery. Due to the relatively high voltages of the battery of several hundred volts the fast switching MOS-FET-power switches are voltage-seen too small, in spite of being able to switch in the range up to 50 kHz with low losses. The combination of MOS-FET on the basis of common bipolar switching transistors – the so called IGBT (insulated gate bipolar transistor) – allows fast low loss switching up to 10 kHz at formidably higher voltages and currents than MOS-FETs. The silicon-based technology has temperature limits of approx. 125 … 150 °C junction temperature. The SiC-(silicon carbid)-technology provides already in low-power range Schottky-diodes and power transistors up to e. g. 5 A, which are for the application in electric vehicles far insufficient. The electric devices for inverter technology determine their energy efficiency.

In hard-switching voltage-source-inverters the losses of the power semiconductors are decisive, in resonant-switching and current-source-inverters the passive devices (e. g. inductive) affect the energy efficiency considerably. A halving of losses is predicted by close interaction between new devices and thus realizable inverter topologies. Power semiconductors made of SiC (silicon carbide) theoretically make steady operation up to 600 °C junction temperature possible due to the big band gap between valence and conductor band (currently Si-semiconductor: 125 … 150°C). The high critical field strength in SiC allows thinner devices with lower losses. The available connection-, mounting- and insulating technologies were developed only for silicon and are hence only suitable up to 200 °C. In order to use the potential of SiC concerning high temperatures, new materials have to be explored and connection-, mounting technologies have to be developed. For common silicon-based switching-transistors (Insulated Gate Bipolar Transistor, IGBT) the conduction and switching losses were more and more decreased; but the limit is reached here. In hard-switching inverters the reverse-current of Si-power-diodes creates a big contribution of turn-on losses of the IGBTs. A fundamental improvement is expected with the transition to SiC-power-semiconductors. Researches in this domain are well positioned in Germany, (worldwide first SiC-*Schottky*-power-diode 2002 by *Infineon* on the market). SiC-devices allow fast switching with low switching losses and low static losses (first realization of a hard switching inverter with JFETs: *Siemens*, *Rebbereh*, 2003). By intensive use of significantly higher switching frequencies the achieved system advantages can compensate the higher costs of SiC- devices.

The type of the used inverter depends especially on the type of the electric machine.

5.1 DC-converter

DC-machines need a DC-converter, which switches the voltage pulse-shaped to the motor. In the converter circuit a fixed DC-voltage U (battery voltage) is being pulsed by transistor switches. The pulse frequency

$$f_P = 1/T \qquad\qquad\qquad (5.1\text{-}1)$$

is due to the good switching properties of power transistors relatively high (e. g. 1 to 5 kHz). This pulsed voltage is applied to the DC-machine as armature voltage. The average value U_d of this pulsed armature voltage u_a can be **changed** by different ratios of pulse widths to breaks (Fig. 5.1-1b). During pulse width T_{on}, while the transistor is switched-on, current flows from the voltage source U to the machine. The freewheeling diode is currentless.

$$U_d = U \frac{T_{on}}{T} \qquad\qquad\qquad (5.1\text{-}2)$$

During the break, when the transistor is switched-off, the current has to continue flowing due to the self-induction voltage. This is over the **freewheeling diode** possible. Because of the relatively high pulse frequency and also due to the relatively big armature inductance, the current is well smoothed and almost harmonic-free. A small „saw tooth-ripple" with pulse frequency remains (Fig. 5.1-1b). The one-quadrant-converter from Fig. 5.1-1a can be expanded to a four-quadrant-converter by adding three more transistors and freewheeling diodes.
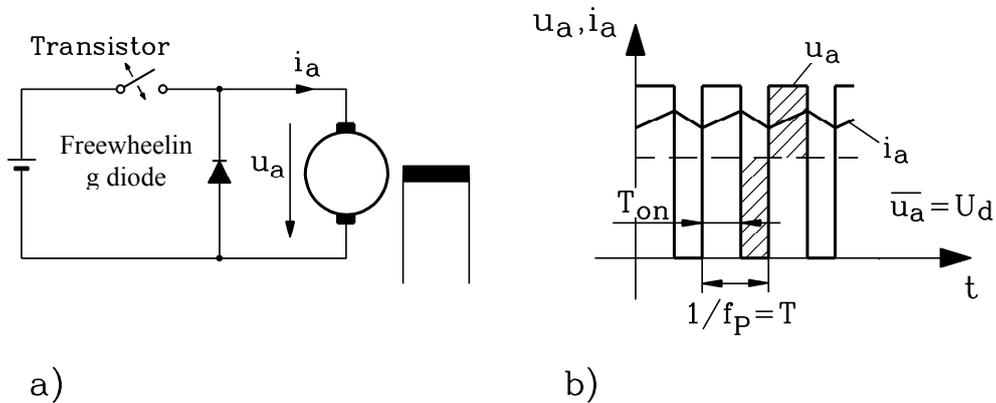

Fig. 5.1-1: DC-current-converter: a) Principle of a one-quadrant-converter, b) Pulsed armature voltage, the average value and the armature current as a function of time
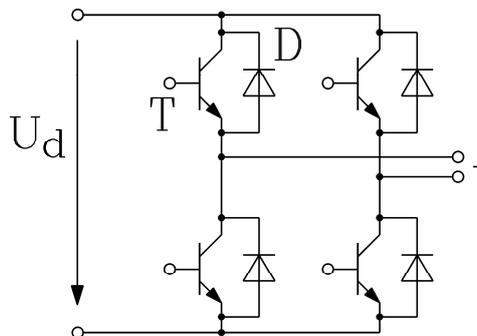

Fig. 5.1-2: Four-quadrant-converter (T: Switching-transistor, D: Freewheeling diode)

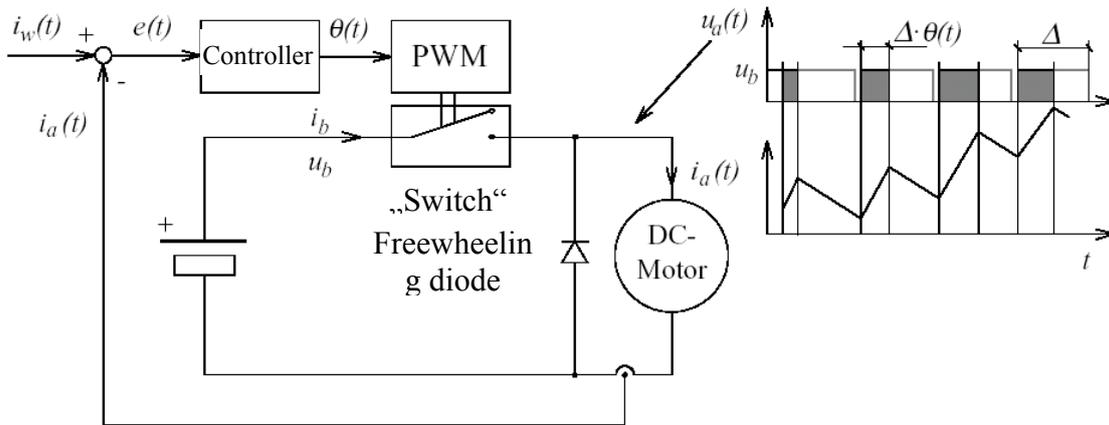For control of torque a control device is necessary.

Fig. 5.1-3: Principle of current-control of a one-quadrant-DC-converter by PWM

5.2 Inverter for rotating field machines

If rotating field machines are used (PSM, induction machine, 3-phase TFM), voltage supplying inverters in bridge-connection according to Fig. 5.2-1 are used. The self-guided pulse width inverter works in that way, that the three motor terminals are either supplied with positive or negative battery voltage. By this the applied voltage between the motor terminals (line-to-line voltage) is the pulse width modulated DC-voltage. If the duration of the pulse widths is changed sinusoidal at fixed switching frequency, a sinusoidal current with a superimposed switching ripple result due to the smoothing effect of the motor inductance (Fig. 5.2-2). This makes an operation of the machine at variable frequency and variable voltage amplitude possible.
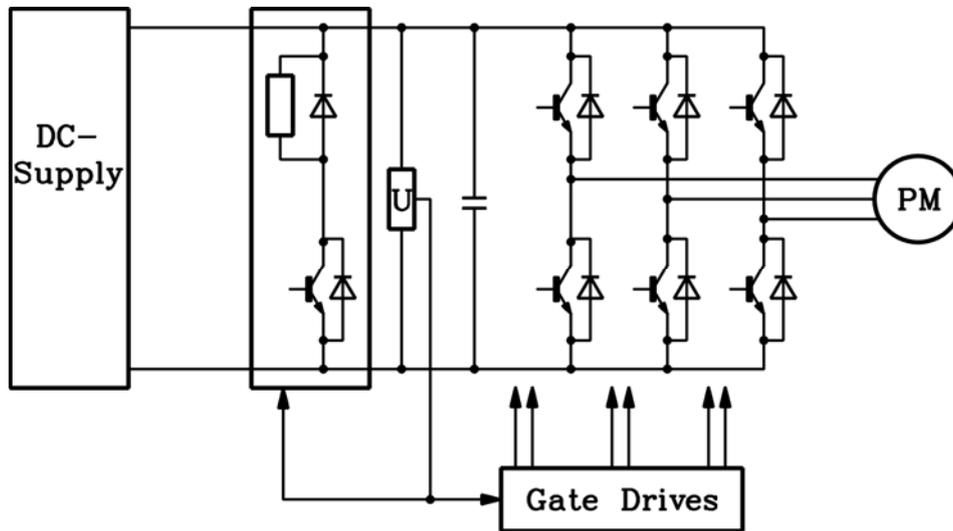

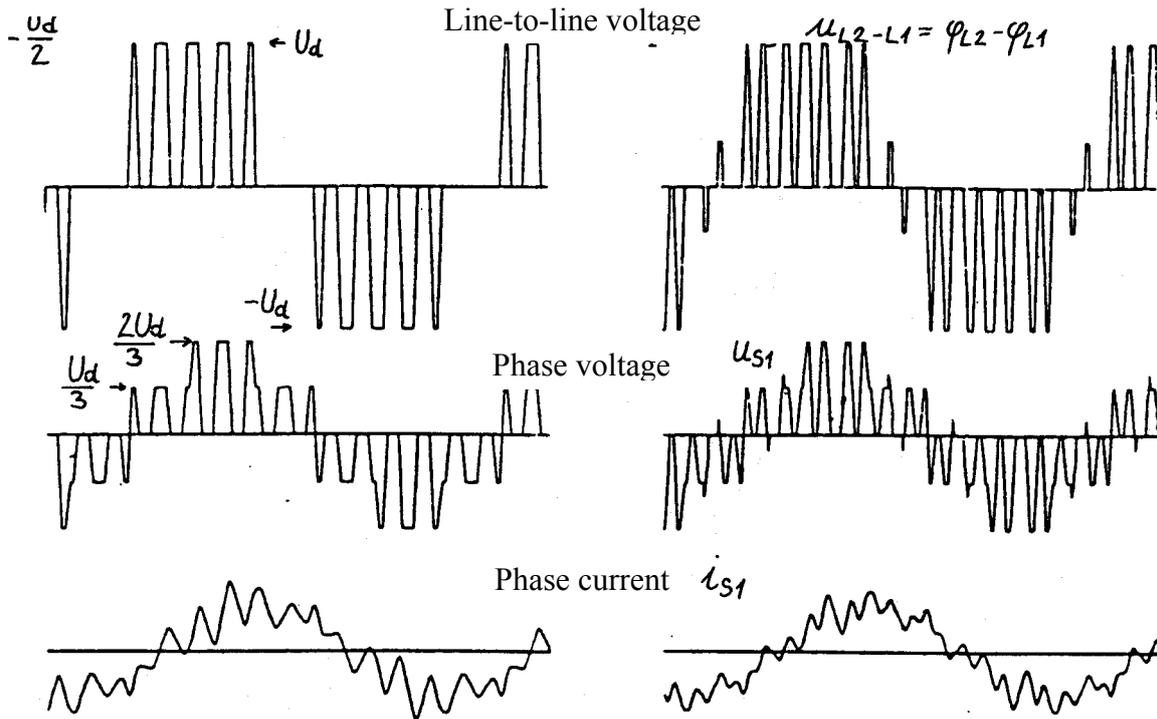Fig. 5.2-1: Voltage applying inverter for 3-phase-synchronous machines

Fig. 5.2-2: Voltage-pulse pattern and current shape for pulse width operation of an induction machine: ratio of switching frequency to fundamental frequency: left (square wave modulation): $f_{sw}/f_s = 6$, right (trapezoidal modulation): $f_{sw}/f_s = 9$

Depending on the modulation degree (ratio of voltage fundamental amplitude to battery voltage) the single and double switching frequent harmonic dominate in the voltage spectrum, which lead to the current ripple depicted in Fig. 5.2-2 (for relatively low switching frequencies), which causes additional losses in the motor. For the control of the motor the voltage fundamental is considered. For both induction machines and PSMs at constant motor flux and hence constant current according to (4-1) constant torque the PWM is done in that way, that the fundamental U_s of the pulse width modulated voltage (line-to-line and per phase) is changed proportional to the frequency of the fundamental (Fig. 5.2-2). Only at low frequencies, when the inducing effect of the magnetic field is small compared to the voltage drop over the armature resistance R_s, the voltage is increased, in order to compensate the voltage drop $R_s I_s$ (Fig. 5.2-3).
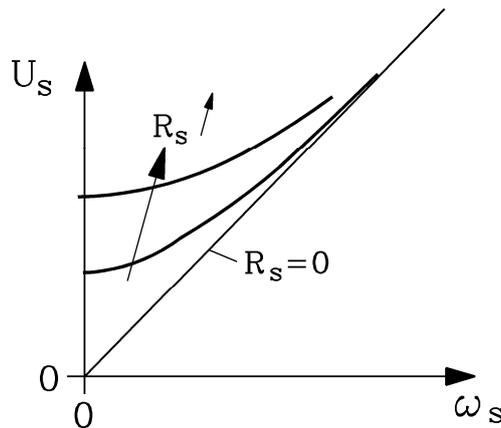

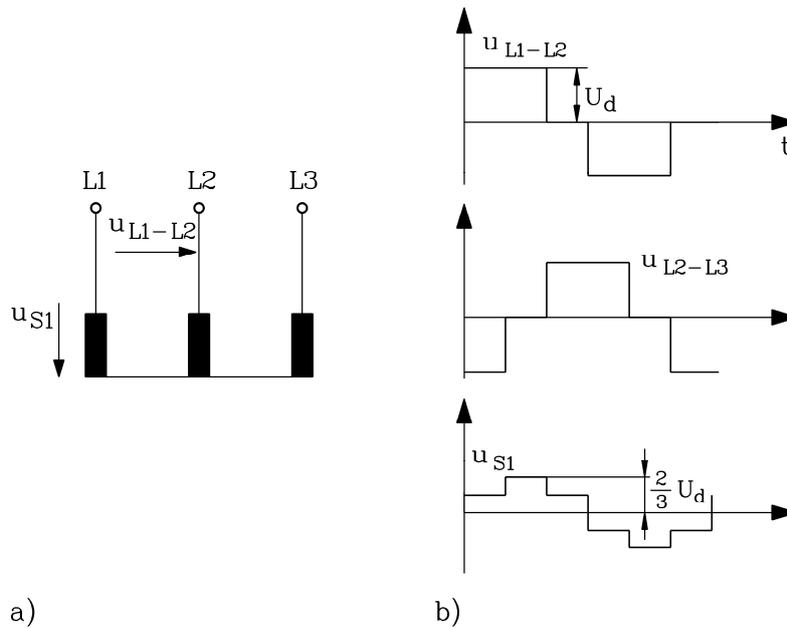Fig. 5.2-3: Control law $U_s(\omega_s)$ for small and middle frequencies

Fig. 5.2-4: Block commutation operation at star connection of the stator winding:
a) phase voltage u_S and line-to-line voltage u_L,
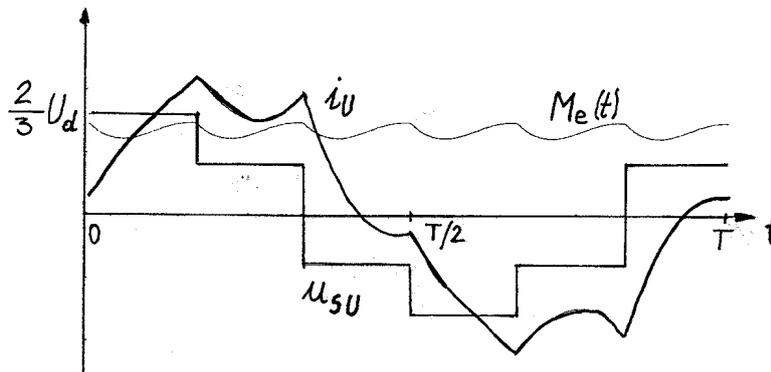b) line-to-line voltage u_L and phase voltage u_S as a function of time

Fig. 5.2-5: Calculated phase current i_U at block commutation operation (phase voltage depicted), and resultinig continuous and pulsating torque

By reducing the breaks between the voltage pulses the amplitude of the fundamental is increased. The maximum voltage is reached, when no breaks occur anymore (block commutation, Fig. 5.2-4). The associated motor current e. g. in an induction machine deviates considerably from the sinusoidal shape, which results into torque pulsations with 6-times the fundamental frequency $6f_s$.

The control of the drive requires e. g. for the PSM a calculative adjustment of d- and q-current, which is to be impressed as a resulting current to the three phases of the machine (with the correct phase angle and amplitude) by the inverter output voltage. A current transducer is normally not used due to cost reasons. At star connection the third current V determined from the measured currents U and W according to $i_V = -i_U - i_W$. The electric control processes are very fast, as the electric time constants of the windings T_e = L/R are in the range of well below 1 s. With field oriented control d- and q-current can be controlled separately according to Fig. 5.2-6. This is for induction machines the seperately adjustable magnetizing current and the torque generating component of the current, which is shifted to the magnetizing current by a quarter of period. Due to the fast microprocessors (e. g. 32 bit-computer architecture) in the inverter the digital control with its calculation operations is also for more complex motor models possible with a high speed. The sampling frequency of the analogue current signal limits the dynamic of the control (typical

current sampling time below 0.1 ms), which is sufficiently fast for the requirement in the E-vehicle with its inert weights.
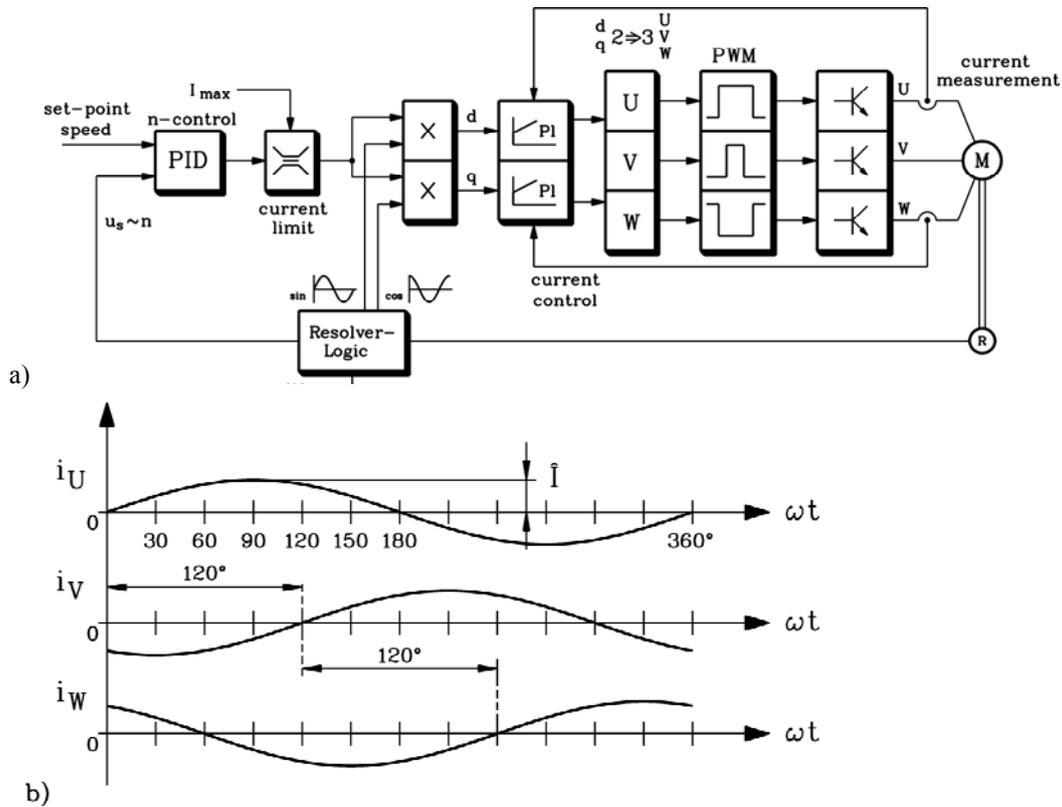

a)

b)

Fig. 5.2-6: PSM-Drive: a) Drive components: M: motor, R: Rotor position sensor (resolver). The motor current is measured in two phases and transmitted to the motor current controller, which compares the set value (calculated from d- and q-current via the torque, given by the speed controller) with the actual value of the current and adjusts the required motor voltages with PWM. The speed control is only active in cruise control. Otherwise the driver sets torque and hence current set value by the "gas pedal".
b) Ideal three-phase current system without any current ripple due to switching

For the two-phase TFM each of the two phases is triggered by a four-quadrant converter according to Fig. 5.1-2, so that instead of 6 transistor and 6 freewheeling diodes 8 of each type becomes necessary. For the three-phase TFM the inverter depicted in Fig. 5.2-1 can be used.

5.3 Inverter for switched reluctance machines

Also in three- and poly-phase SRM each of the winding phases is triggered with a separate converter, so that three or several phases can be triggered simultaneously. Thus the torque ripple can be reduced a little bit. As the current is fed unidirectional (Fig. 4.1.4-1) only 2 transistors and 2 freewheeling diodes instead of 4 each (like in Fig. 5.1-2) are needed, as it is no current inversion necessary. Whereas the voltage can be inversed in order to shut down current quickly. Depending on current feeding of the winding with respect to the position of the rotor teeth, the driving or braking torque is the generated and thus makes motor or generator operation possible.
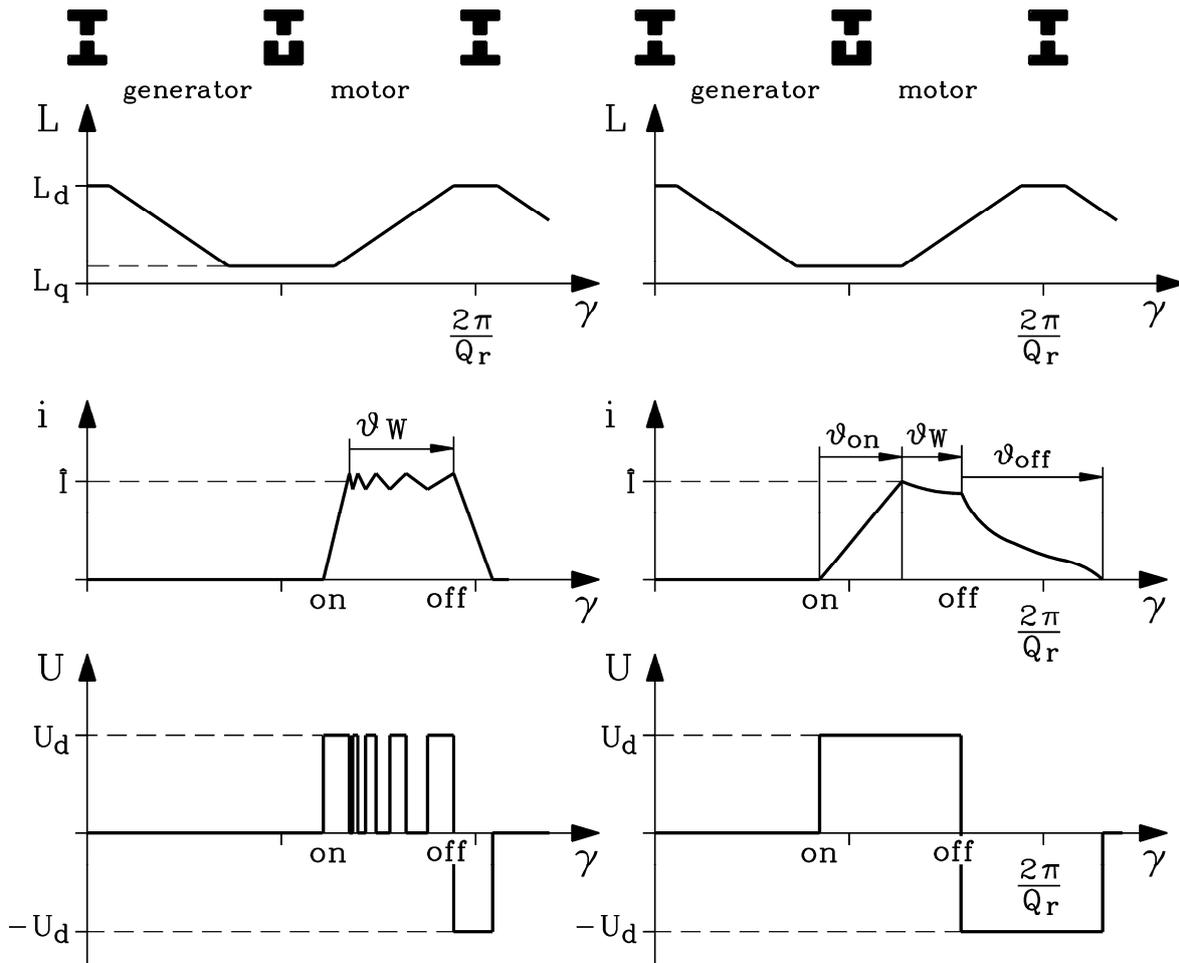
Fig. 5.3-1: Generation of current in the SRM: (γ: rotor position angle, L: stator winding inductance, Q_r: number of rotor slots)
Left: At low speed hysteresis control of current allows generating rather block shaped unidirectional current, which can be shut down quickly by an inversion of the voltage. Right: At high speed time is too short to chop DC link voltage, so only "voltage on" and "off" is possible, leading to distorted current pulse, which generates increased torque ripple

6. Battery systems for electric vehicles

An assembly consisting of two different electrode materials in an electrolyte is called **galvanic cell**. The occurring difference of electric potentials between its electrodes results from the amount of electrode ions, which go into solution into the electrolyte due to diffusion (reason for diffusion: different partial pressures of ions in the electrode and electrolyte). This amount of ions going into solution is different for each electrode material. Against the described pressure drop a reversing attracting force builds up on the ions, so that a force balance between partial pressure difference and electrostatic attraction accommodates. That is why the ions advance only up to the thickness d (*Debye-Hückel*-length)

$$d = \sqrt{\frac{\varepsilon_r \cdot \varepsilon_0 \cdot kT}{e^2 n_\infty}}$$

(6-1)

inside the electrolyte (ε_r: relative constant of dielectricity of electrolyte, constant of dielectricity of vacuum $\varepsilon_0 = 8.854 \cdot 10^{-12} \, \text{As}/(\text{Vm})$, *Boltzmann*-constant $k = 1.38 \cdot 10^{-23} \, \text{J}/\text{K}$, T: absolute temperature of the system (in K), electric elementary charge: $e = 1.602 \cdot 10^{-19} \, \text{C}$, n_∞: electron concentration in the undisturbed electrolyte (particle count/m^3)). Due to the higher concentration c_1 of electrode-ions inside the electrode compared to the ion concentration c_2 in the electrolyte a difference of electric potential ΔU

appears between those two within the *Debye-Hückel*-length („electronegativity"), which lies between approx. 3 V and + 1.5 V depending on electrode- and electrolyte material.

$$\Delta U = -(\mathrm{k}T / e) \cdot \ln(c_1 / c_2) \qquad\qquad (6\text{-}2)$$

The accommodating no-load voltage U_0 of the galvanic cell is the difference of the single voltages of the electrodes 1 and 2 against the electrolyte ΔU_1 and ΔU_2 according to

$$U_0 = \Delta U_1 - \Delta U_2 \quad . \qquad\qquad (6\text{-}3)$$

According to the specifications from above these no-load voltages per cell lie in the range of few volts. In order to reach higher voltages a lot of cells have to be connected in series. When galvanic cells are connected to a loading resistance, the remaining electrons in the electrodes flow through the resistance due to metallic conductance, while the ions in the electrolyte maintain the current flow and deposit on the other electrode (the more "noble" one with the lower electronegativity ΔU). Due to the drain of electrons new amounts of ions go into solution, hence the less "noble" electrode corrodes.

In order to achieve **rechargeable galvanic cells (accumulators)**, the electrodes must be able to regenerate when a voltage is applied externally (charge voltage), hence current direction in the electrolyte is inversed. In these systems the molecules of the electrolyte are dissociated into ions by the accommodating electric field which builds up between the electrodes (e. g. Pb-accumulator) when an external voltage is applied. The different positive and negative ions attach to the electrodes and join with the atoms of the outer electrode layers to new materials. In this way the externally supplied energy is stored in chemical binding energy. By the increase of the electrode surface (e. g. grid structure) the bound charge amount can be increased. Both electrodes have even for same source material a different material surface. Both build up electric potential differences - ΔU_1 and ΔU_2 according to (6-2) - together with the electrolyte due to the different accommodating partial pressures (concentrations) of the ions in each electrode to the electrolyte, which difference counteracts to the applied voltage and increases with charging time, until it is as high as the charging voltage. The charging current stops then – the accumulator is charged. The (different) chemical change of the surfaces of both electrodes and hence the generated potential difference ΔU_1 resp. ΔU_2 of the electrodes to the electrolyte is called the **electrolytic polarization of the electrodes**. It allows the usage of the accumulator as a galvanic cell (**discharge of the accumulators**). The chemical reactions happen automatically in inversed direction, whereby the surfaces of the electrodes change to their original state. The emerging ions from the degrading chemical compounds are equal to the current flow inside the electrolyte, where the positive and negative ions recombine to neutral molecules. The chemical binding energy is directly dissipated into heat in the load resistance. The process of charging and discharging is a reversible cycle. The stored electric charge in the accumulator in both electrodes (positive $+Q$ resp. negative $-Q$) is directly proportional to the amount of converted chemical substance at the surface of the electrodes A (1. *Faraday*-law), this is why large electrode surfaces are necessary, as the chemical reactions only happen at the surface which is in contact with the electrolyte. If the whole surface of the electrodes was chemically changed by charging, further charging would only lead to further dissociation of the electrolyte (electrolysis) , whereby the ions leave the electrolyte in gaseous form (**„gassing" of accumulator at overcharge**). The **capacity C of an accumulator** is the stored charge Q in the accumulator in „ampere-hours", the product of discharge current i and discharge time t.

$$Q = \int_0^t i(t) \cdot \mathrm{d}t \qquad\qquad (6\text{-}4)$$

The stored electric energy due to the charge voltage $u(t)$ is

$$W = \int_0^t u(t) \cdot i(t) \cdot \mathrm{d}t \quad . \tag{6-5}$$

Due to the internal resistance R of the electrolyte and the electrodes losses occur during charging and discharging, so that the efficiency can be defined as the ratio of the withdrawn electric energy during discharge and the supplied electric energy during charge.

$$\eta = W_{e,out} / W_{e,in} \tag{6-6}$$

The **charging process** is characterized by an amount of charge which is being charged by a current which is determined by the charging device. The charging device is supplied by the grid. So the charging current is limited by the maximum permitted current in the grid (e. g. 10 A or 16 A) and thus the charge time is determined. If e. g. a *VW CitySTROMer* with a consumption of about 20 kWh/100 km drives a distance of 50 km and is charged with a power of 2.2 kW (= 220 V · 10 A) afterwards, charge time is about 4 hours until full charge. Due to the different technologies of the different batteries the charging processes have to be adjusted for each case.

For hybrid vehicles the for high charge- and discharge powers dimensioned DC-link batteries are charged with much higher currents, which correspond to the ones during e. g. recuperation with braking energy, than "normal" charging currents (about $C/10$, so for C = 100 Ah with 10 A). Thus results from the relatively high braking power, which is available generally only for a short time.

Due to the losses during **discharge phase** the withdrawn battery charge Q_{in} (in Ah) is not the same as the withdrawable charge Q_{out} (in Ah). The charge describes the ratio of input and output power during one full cycle.

Charging factor $= Q_{in} / Q_{out}$ $\qquad\qquad\qquad\qquad$ (6-7)

For closed lead batteries the charging factor has a value smaller than 1.05.
The efficiency of a battery (6-6) can be formulated with the charging factor.

$$\eta = \frac{W_{out}}{W_{in}} = \frac{U_{out} \cdot I_{out} \cdot t_{out}}{U_{in} \cdot I_{in} \cdot t_{in}} = \frac{U_{out} \cdot Q_{out}}{U_{in} \cdot Q_{in}} = \frac{U_{out}}{U_{in}} \cdot \frac{1}{\text{Charging factor}} \tag{6-8}$$

Hereby $U_{in} > U_{out}$ is valid, as due to the internal resistance the voltage is higher when charging $U_{in} = U_0 + I_{in} R_i$ than when discharging $U_{out} = U_0 - I_{out} R_i$. The efficiency lies between 70 and 90%.

The maximum current for charging and discharging (building up resp. dissociating ions) is limited by the reaction velocity of the simultaneously happening reactions at different locations of the electrode surfaces and by the size of the surfaces themselves. Thus maximum current and **maximum electric power** conclude for discharge.

$$I_{max} \Rightarrow P_{max} = U_0 I_{max} \tag{6-9}$$

6.1 Technical requirements for vehicle batteries

Energy content:

For pure electric vehicles the requirement for high energy content for wide range dominates. Hence for a pure electric vehicle with mass of 1000 kg more than 20 kWh are estimated if a range of 150 km is considered.

Power:

Power of an electric vehicle should be approx. 30 kW per 1000 kg, in order to come close to the driving dynamic of a vehicle with an internal combustion engine.

For common electric vehicles batteries with a power of 20 to 50 kW and energy of 20 to 50 kWh are needed, so that the power-energy ratio (LEV) of such a battery should be about 1 h^{-1}. This is fulfilled by some batteries.

$$\text{LEV} = P/W \quad \text{(Unit: kW/kWh = 1/h)} \tag{6.1-1}$$

Table 6.1-1: Comparison of power-energy ratios of different battery systems

LEV (Pb conventional)	≈	2 h^{-1}
LEV (Zn-Br)	≈	1 h^{-1}
LEV (Zn-O_2)	≈	0,75 h^{-1}
LEV (ZEBRA)	≈	1,5 h^{-1}
LEV (Ni-MH, Ni-Cd)	≈	3 h^{-1}
LEV (Li-Ion)	≈	3 h^{-1}

Depending on the design of the vehicle the LEV value has a value of 5 to 20 h^{-1}. When this is not the case like in the zinc-air system, generally the energy is increased in order to achieve the required power. For some batteries it might be critical for real driving profiles where very high starting and acceleration powers are needed.

Chargeability:

The common house-hold grids allow a maximum charging power of 3 kW. With this an electric vehicle with a battery of 20 kWh needs 7 h for a charging process. Nevertheless shorter charging times of less than one hour are being preferred, which is possible with special junctions.

Lifespan:

Energy storages of electric vehicles should have a lifespan, which approximately corresponds to the lifespan of the vehicle, so a "mileage" of approx. 200.000 km resp. a lifespan of 10 years, in order to avoid a costly battery replace.

Efficiency:

Due to the frequent charging and discharging processes an efficiency of 90 % should not be deceeded.

Table 6.1-2: Comparison of requirements for electric and hybrid vehicles

		Electric vehicles	Hybrid vehicles
Energy density	(kWh/1000 kg)	20	1,5
Power density	(kW/1000 kg)	30	30 – 60
Chargeability	(kW/1000 kg)	> 3	10 – 30
Lifespan		200.000 km or 10 years	
Efficiency		90%	

6.2   Overview - Electrochemical energy storage systems

Following five battery systems were of are applied in electric vehicles:
- ♦ Lead-batteries (Pb/PbO$_2$)
- ♦ Nickel-cadmium-batteries (NiCd)
- ♦ Nickel-metal-hydride-batteries (NiMH)
- ♦ Sodium-nickel-chlorineid-high-temperature-batteries (NaNiCl$_2$)
- ♦ Lithium-ion-batteries (Li-Ion)

Apart from further developments of the conventional lead battery researches also focus on the further development of **Nickel-metal-hydride-** and **Lithium-ion**–batteries.

Up to now the following battery systems could not compete yet:
- o Nickel-sulfur
- o Nickel-iron (NiFe):   instable iron electrode → hydrogen gassing → high-maintenance
- o Nickel-zinc (NiZn):   fine short circuit problems → Zn-dendrite-generation
- o Zinc-bromine / -chlorine: unmanageable security deficits

Energy storage of the same type can vary in their energy and power containment depending on construction, geometry and chemical composition. Generally higher energy content leads to a reduced power.

Lead-batteries (Pb/PbO$_2$)
The technical types are distinguished in
- - Pb-liquid-acid-batteries
- - Pb-Gel-batteries
- - Pb-AGM-batteries (**a**bsorbant-**g**lass-**m**aterial)

The construction of the lead battery differs in the construction of electrodes, cell geometry and electrolyte. Generally the electric power can be increased with the use of thinner electrodes; this mostly yields to a reduction of energy density and lifespan. Special types of the Pb-battery system are **wound cells**. This type allows higher loading (especially at low temperature) and a bigger lifespan compared to battery in plate shape. Pb-batteries have limited cycle strength.

Nickel-cadmium-batteries (Ni/Cd):
Nickel-cadmium-batteries are - like lead batteries – interesting especially for full electric vehicles. However they have the advantage of a bigger lifespan compared to lead-batteries. This advantage faces the higher manufacturing costs. The quick chargeability of Ni/Cd-batteries cannot be used everywhere due to the infrastructure.

Nickel-metal-hydrid-batteries (NiMH):
The NiMH-battery is considered to be the successor of the NiCd-battery. Similar to the other battery systems the energy and power depend on the brought in active material as well as on the technical design of electrode and cell geometry. The construction of the collector structure on the one hand and the choice of type of active material on the other have big influence on the power of the battery.

Sodium-nickel-chlorineid-batteries (Na/NiCl$_2$)
The Na/NiCl$_2$-Battery belongs to the high temperature batteries (resp. high energy batteries) and is also called ZEBRA-Battery (Zero-emission-battery). The enrgy density of the Na/NiCl$_2$-Battery exceeds the ones of the lead-, nickel-cadmium- resp. nickel-metal-hydrid-batteries considerably. Further more it has a bigger lifespan. One set of batteries allows up to 150.000 km mileage as "life-span". Decisive for the power and lifespan of the system are the properties of the ceramic separators and the seal. Another

advantage of the Na/NiCl$_2$-battery, compared to the other battery systems, is that in case of a break or a failure of the ceramic separator that cell remains conductive and has no influence on the functionality of the remaining cell compound. A drawback is the high operating temperature of approx. 300 °C, which influences the efficiency negatively at a daily mileage of 40 km by thermal losses of about 5 W per kW.
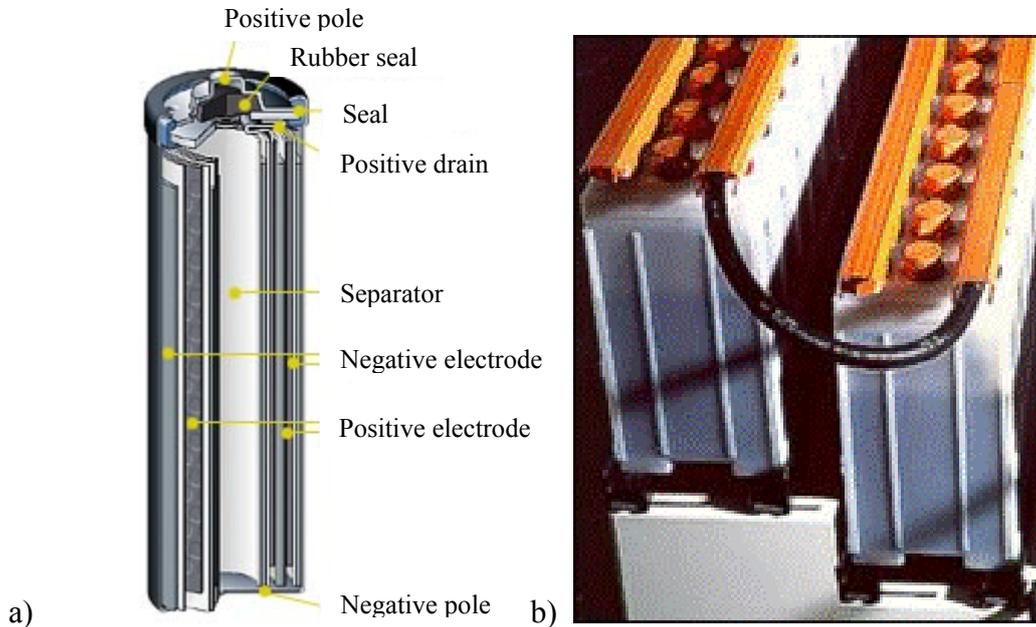
Fig. 6.2-1: NiCd-battery: a) schematic construction, b) technical design (http://www.elektroauto-tipp.de)

Fig. 6.2-2: NiMH-Battery by *Toyota* (*Toyota Hybrid System THS II*, press information, www.toyota.co.jp, 2003)

Fig. 6.2-3: ZEBRA-battery by *VARTA* (http://de.varta.com/index.html)

Lithium-ion-battery (Li-Ion):
The Lithium-ion-batteries represent the technical most recent development in the domain of battery technologies and is characterized by relatively high manufacturing efforts. A battery compound

consisting of Li-ion-batteries can be realized with a relatively low number of cells, which is thanks to the high voltage of every single cell controlled by an active battery management. This results in a small space demand and weight reduction. Nevertheless according to current development standard the calendric lifespan is still not sufficient for the application in an electric vehicle. Furthermore there is still need for clarification concerning security and costs.
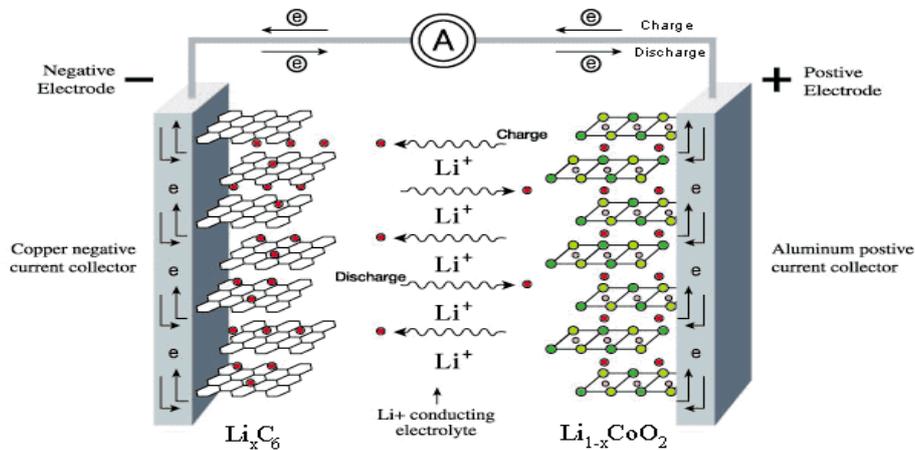

Fig. 6.2-4: Schematic construction of a Lithium-ion-battery (http://www.ict.fhg.de/deutsch/scope/ae/Libattery.gif)

Table 6.2-1: Energy density, power density, lifespan and costs of different battery types (* = prognosis);
(Gerl, B.: Innovative Automobilantriebe: Konzepte auf der Basis von Brennstoffzellen, Traktionsbatterien und alternativen Kraftstoffen, Landsberg/Lech: Verlag Moderne Industrie, 2002)

Battery type	Energy density		Power density		Lifespan		Costs
	Wh/kg	Wh/dm^3	W/kg	W/dm^3	Cycles	Years	Euro/kWh
Lead	30-50	70-120	150-400	350-1000	50-1000	3-5	100-150
Nickel-cadmium	40-60	80-130	80-175	180-350	> 2000	3-10*	225*-350
Nickel-metal-hydride	60-80	150-200	200-300	400-500	500-1000	5-10*	225*-300
Sodium-nickel-chlorine	85-100	150-175	155	255	800-1000	5-10*	225*-300
Lithium-ion	90-120	160-200	ca.300	300	1000	5-10*	275*
Lithium-polymer	150	220	ca.300	450	< 1000	-	< 225*
Zinc-air	100-220	120-250	ca.100	120	-	-	60

In the following the battery systems are discussed in datail.

6.3 Lead-acid-accumulator

The Lead-accumulator is distinguished between
- Open system,
- Closed system,
- sealed system

Due to the danger of leaking out an open accumulator for the application in electric vehicle is not possible. Advantages like no maintenance lead to the fact that only sealed gas-tight batteries can be used in electric vehicles. In the gas-tight system VRLA (valve-regulated lead-acid-battery) each cell has a valve, over which hydrogen can escape at over pressure. Furthermore the penetration of air is prevented.

Electrodes:

Negative electrode:	Lead sponge (on lead-calcium-antimony-alloyed grid)
Positive electrode:	Porous lead oxide (on lead-calcium-antimony-alloyed grid)
Electrolyte:	Water-sulfuric-acid mixture
Separator:	Either glass fiber for absorption of liquid electrolyte or plastics resp. vinyl plates with gelled electrolyte.

Cell reactions:

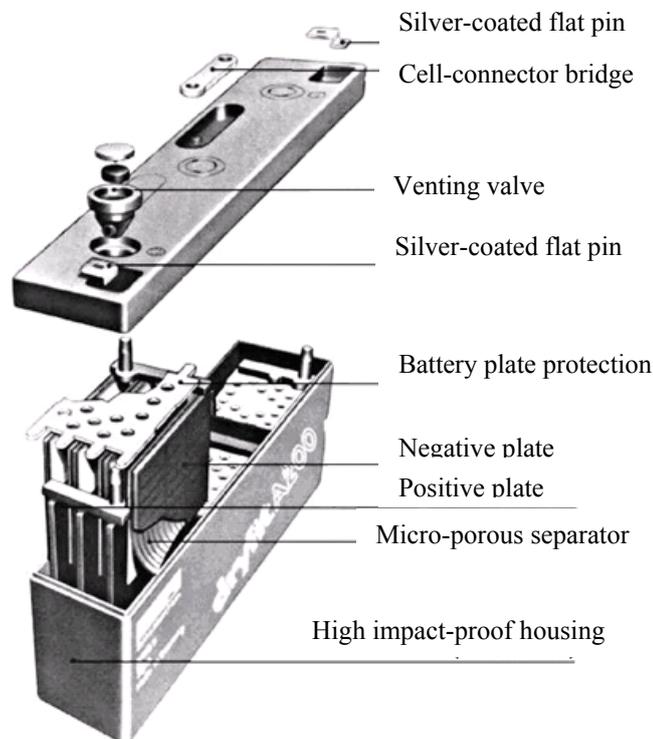|	
- Anode:	$Pb + (2 H+ + SO42-) \leftrightarrow PbSO4 + 2 H+ +2e-$
- Cathode:	$PbO2 + (2 H+ +SO42-) + 2 H+ + 2e- \leftrightarrow PbSO4 + 2 H2O$
Total cell reaction:	$Pb + PbO2 + 2 H2SO4 \leftrightarrow 2 PbSO4 + 2 H2O$

Fig. 6.3-1: Construction of a sealed lead accumulator with grid plates (Akkumulatorenfabrik *Sonnenschein GmbH*)

In the charged state the positive tubular plates („armor plates") consist of lead dioxide (PbO_2) and the negative grid plates consist of lead sponge. At discharge the lead dioxide and the lead is turned into lead sulfate ($PbSO_4$). This lead sulfate and the generated water are compounds, which have a lower energetic level than the lead dioxide, lead, and the sulfuric acid (electrolyte). The energy difference is released in form of electric energy. The electrolyte made of sulfuric acid (H_2SO_4) is either gel or a glass fiber separator called AGM (= absorbed glass material). Thus it is possible in a sealed system that at full recharge the water corrosion and water loss is prevented. The oxygen diffuses through channels to the negative plate where it recombines with the hydrogen to water. The electrolyte is involved in the reaction, so that the acid concentration decreases during discharge. For charged accumulators the acid density is between 1.26 and 1.29 g/cm³ and for discharged ones between 1.12 and 1.10 g/cm³. The

lead-calcium-antimony-alloy guaranties the mechanic stability of the plates and increases the gassing voltages.

In the 90s a lead-accumulator was placed into the hybrid vehicle *Audi-Duo* due to the low development standard of other battery systems at that time. The no-load voltage of the 22 in series connected modules was 264 V and the energy content was 10 kWh at five hour discharge. The weight of the system was about 320 kg.

Charging and discharging:

For traction batteries two charging methods are possible:

1. Charging with constant charging voltage
2. Charging with constant charging voltage and constant charging current

For the first method a constant charging voltage of about 2.3 V is applied to the electrodes of each cell at temperature between 20 and 25 °C. The battery is fully charged, when the charging current stabilizes
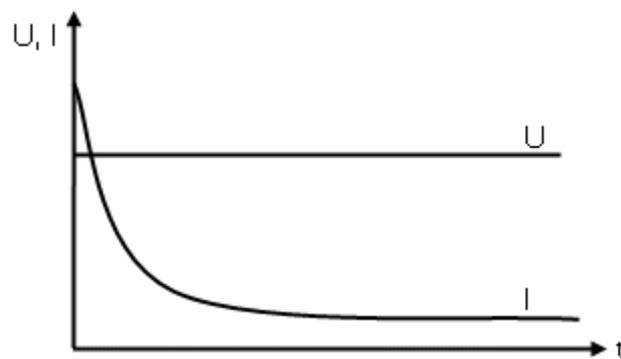

Fig. 6.3-2: Current and voltage as a function of time during charging with constant voltage

For the second method at first a constant current is applied until the charging voltage reaches a certain value. From this point on the battery is charged with a constant voltage.
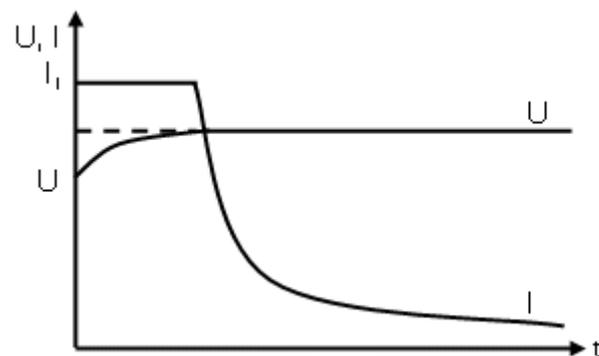
Fig. 6.3-3: Current- and voltage as a function of time during charging with constant current as long as the voltage is lower than a certain value (*I-U*-charging method)

During charging the water as a part of the electrolyte is being dissociated into hydrogen and oxygen and the negative electrode absorbs the oxygen. The battery is being overcharged, if the battery generates more oxygen than the cathode can absorb. The abundant gas escapes through the valve, what means a reduction of the amount of the electrolyte. Thus the chemical reactions become inefficient. The consequence is a considerable reduction of battery power. An overcharging with 1 Ah leads to a water loss of 0.33 g. The gas mixture (detonating gas), which is generated during charging, can explode, if the volume share of hydrogen is the same or higher than 4 %. This leads to some security measures, which have to be obeyed in any case:

- Batteries should be only charged in well ventilated rooms
- No smoking close to the batteries, also open flames or sparkle building are to be avoided
- The charging device is not to be placed above the battery; gases out of the battery can erode and damage the device.

The charging voltage, above which a battery starts to gas considerable is called **gassing voltage**. For lead-accumulators this voltage is about 2.40 V/cell. With the help of the discharge curves one can recognize, that with increasing discharging current the lead-accumulator can be deeper discharged. I_{20} is the value of the constant current, which discharges the accumulator to 80 % in 20 minutes.
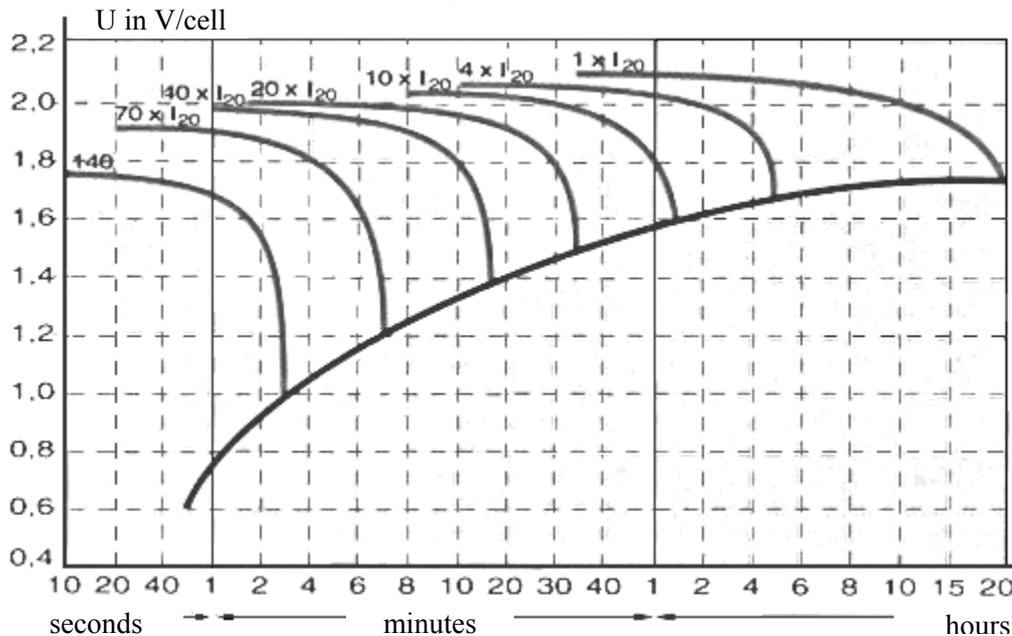
Fig. 6.3-4: Discharge curves of the lead-accumulators model A500 by the company *Sonnenschein*
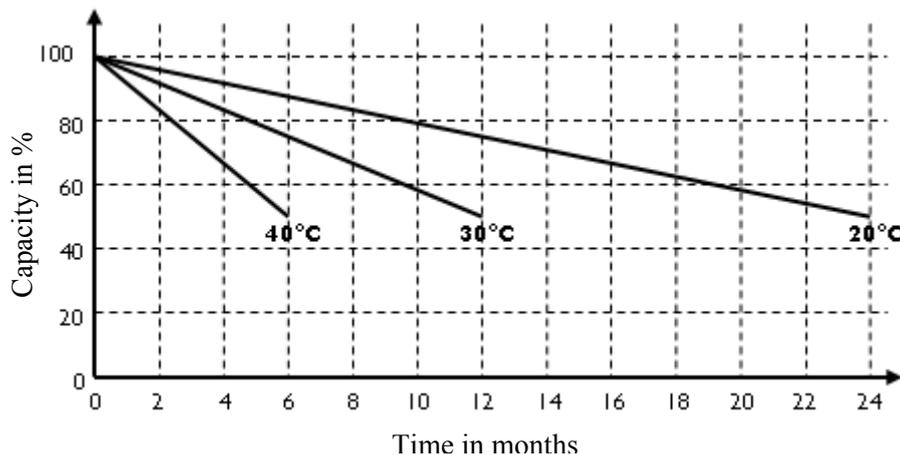
Fig. 6.3-5: Self discharge of the lead-accumulators depending on the temperature (company *Sonnenschein*)

The **deep discharge** considerably reduces the conductivity of the electrolyte. Another problem is the lead sulfate generation, which results in a volume excess and represents a mechanical stress for the system. Battery manufacturers have developed methods, in order to counteract these damages due to deep discharges resp. to reduce them. By the use of very pure lead as grid material for the electrodes the self discharge could be considerably reduced. At room temperature the capacity loss is about 6 to 8% per month. Higher temperatures lead to an increase of the self-discharge rate.

6.4 Nickel-cadmium-accumulator

Electrodes:

Negative electrode:	Cadmium hydroxide (discharged); A plastic enforced electrode is used. This is produced, by mixing the active mass with polymer foam, which is applied on a nickel covered steel grid for several times. This way of manufacturing is much cheaper than the common sinter electrodes
Positive electrode:	Nickel(II) hydroxide (discharged); foam-electrode
Electrolyte:	Potash lye (KOH); does not take part in the reaction, its concentration remains almost unchanged
Separator:	High-porous polymer fleece (polyamide- or polypropylene foil)

Cell reactions:

- Anode: $Cd + 2\,OH^- \leftrightarrow Cd\,(OH)_2 + 2e^-$

- Cathode: $2\,NiOOH + 2\,H_2O + 2e^- \leftrightarrow 2\,Ni(OH)_2 + 2\,OH^-$

Total cell reaction: $Cd + 2\,NiOOH + 2\,H_2O \leftrightarrow 2\,Ni(OH)_2 + Cd(OH)_2$

The Nickel-cadmium-accumulator was already developed in 1899 by the Swedish *Waldemar Jungner (1869 - 1924)*. Because of the properties like quick and easy charge, robustness, low-maintenance, etc. the Nickel-cadmium-accumulator is suitable as tractions battery. Nevertheless drawbacks like the later explained memory-effect or the poisonous ingredients have to be accepted. The development of the nickel-cadmium-battery is based on the different designs of the electrode. In the first designs masselectrodes, namely pocket- resp. tubular plates, were used. Hereby the active masses (cadmium, nickel hydroxide) are sealed in pockets or tubes made of perforated steel sheets. The sinterelectrode was already developed in the 30s. This type of electrode has the advantage, that it can be loaded with very high current. The basis of the sinter-electrode is a sinter body made of nickel with about 80% pore volume. The active material is brought in by precipitation of a solution of nickel- or cadmium-salts. A thin layer of active material, which lies close to the current drain, is characteristic for this electrode. In the 80s the foam-electrode (also called fiber-structure-electrode) appeared on the market. A nickel frame with about 95 % free volume is generated by chemical (currentless) nickeling of porous polymer (foamed polyurethane) and afterwards by pyrolysis of the polymer body. As the pore volume of the foam-electrode is bigger than the one of the sinter-electrode, the foam-electrode has a bigger capacity for the same volume. The active material is brought in as a paste; the final thickness of the electrode is set by milling afterwards.
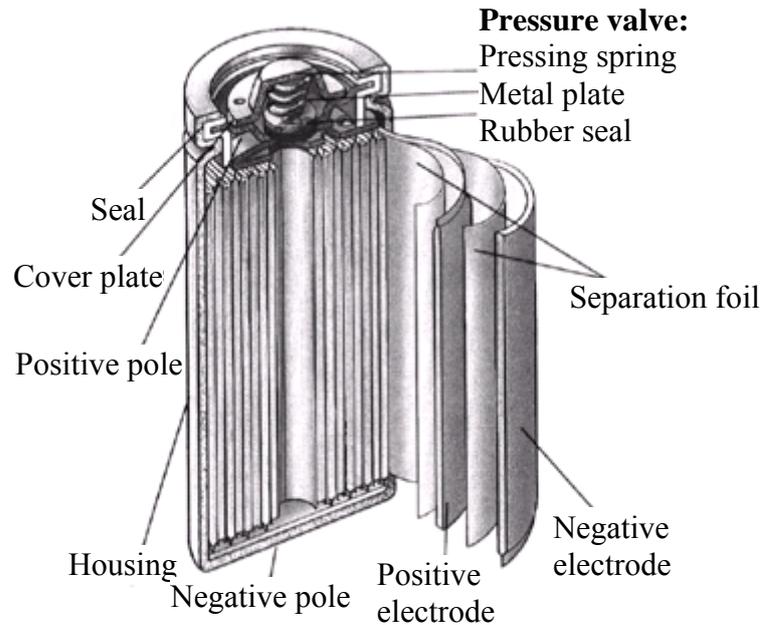
Fig. 6.4-1: Schematic structure of a cylindrical nickel-cadmium-cell (*Sanyo Rechargeable CADNICA Batteries*)

Charging and discharging:
There are different methods to charge a nickel-cadmium-accumulator. Depending on the type of application it is being distinguished between a) work- and b) support battery. In vehicles the energy storage is used as work battery. The charging methods suggested by *Panasonic* are listed in Fig. 6.4-2.
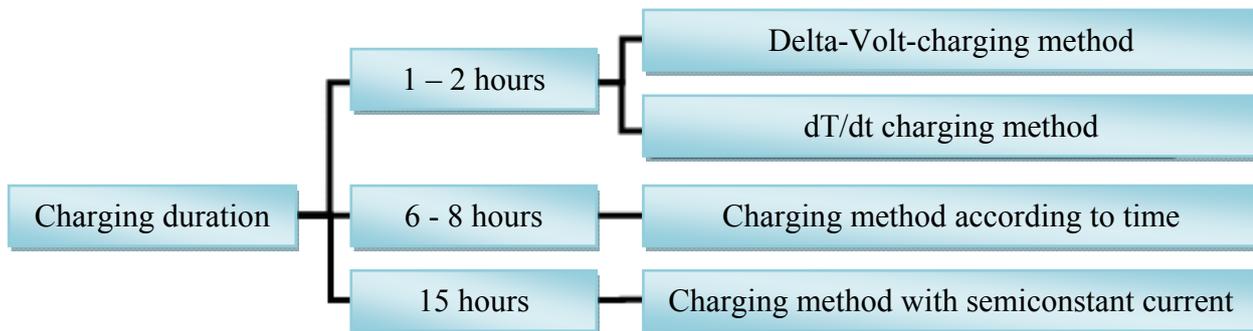
Fig. 6.4-2: Charging methods for nickel-cadmium-cells (*Panasonic*)

a) **The delta-volt-charging method** – also called delta-peak-charging method – is a quick-charge-method, in which charging current is kept constant. The charging current is 50% to 100% of nominal current. The "voltage knee" at the end of the charging curve is used for recognition of full charge and for turn-off.

b) Also the charging method with observation of change of temperature dT/dt as a criterion for turn-off is a quick-charge-method. The charging current is 50% to 100% of nominal current. The absolute temperature of the batteries only serves as a security criterion. The temperature change ΔT since the beginning of charging or the actual change („slope") of temperature are possible criteria. Depending on the initial value the admissible „slope dT/dt" is 1 to 6 K per minute.

c) The charging method according to **time criterion** is cheap and easy to realize. However there is one drawback: without consideration of any further turn-off criterions, depending on the initial state it may come to undercharge, overcharge or to correct turn-off.
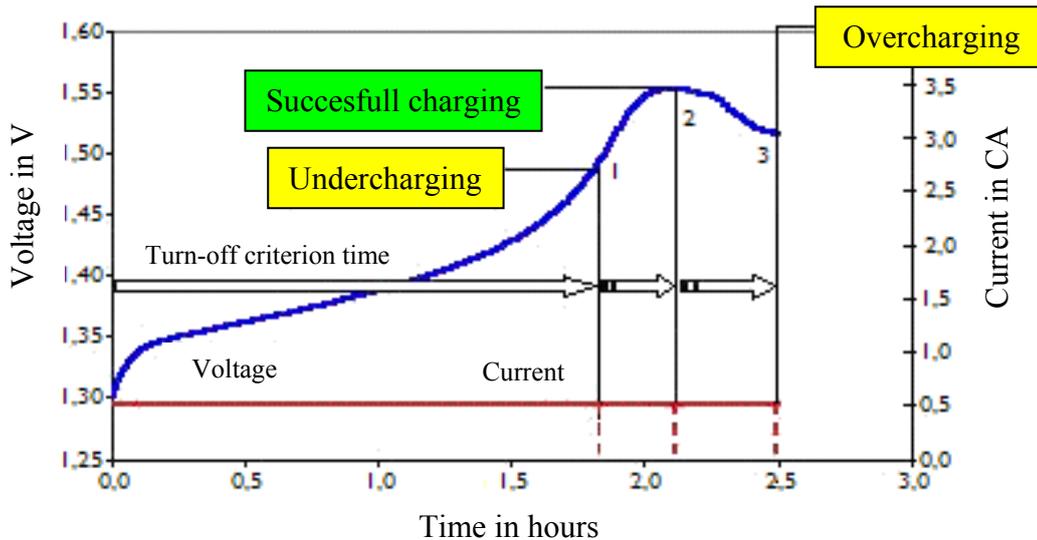
Fig. 6.4-3: Charging method according to time criterion of a Nickel-cadmium-cell (*Panasonic*)

d) In the charging method of semi constant current a resistance R is connected between battery and voltage source, in order to have stable discharging current. By keeping the charging current low, no heat is generated and the process does not need any further surveillance. The charging current is calculated according to:

$$I_{Charge} = \frac{U_0 - U_B}{R} = \frac{U_C \cdot N \cdot (K) - U_C \cdot N}{R} \tag{6.4-1}$$

with: I_{charge} - Charging current

$\quad\quad U_0$ - Output voltage of energy source

$\quad\quad U_C$ - Cell voltage (average 1.45 V/cell a charging current of 0.1 I_N and 20 °C)

$\quad\quad N$ - Number of used cells

$\quad\quad U_B$ - Battery voltage ($U_C \cdot N$)

$\quad\quad R$ - Resistance for stabilization of charging current

$\quad\quad (K)$ - Stability constant (is chosen according to application)

The discharge characteristic of nickel-cadmium-accumulators depends among other things on the temperature and the discharging current. Compared to dry batteries the discharging is more stable and also at high discharging current there is no big loss of the capacity.

The specification of **charging- and discharging current** refers to nominal capacity. Denotations like $C/10$ (resp. $0.1\ C$) are common. „C" refers to nominal capacity and „10" on the duration of charging resp. discharging (e. g. 10 hours). Thus the specification C/10 of a 1-Ah-cell means, that the charging current is 0.1 A (= 1 Ah/10 h).
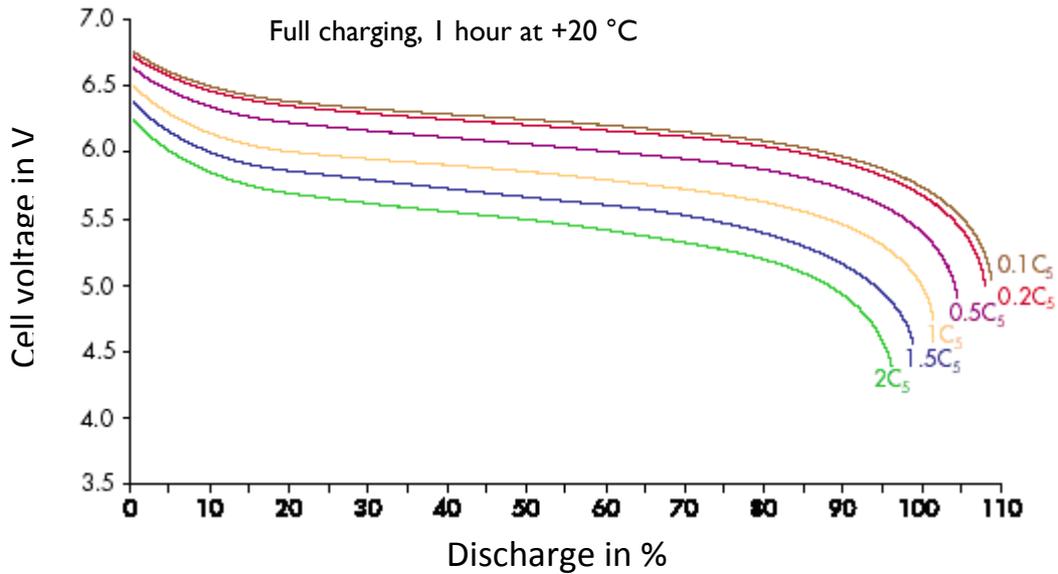
Fig. 6.4-4: Dependence of module voltage U_C in volts depending on discharge in % of battery capacity, C_5 (in Ah) at discharge with different currents (NiCd-accumulator) (http://www.saftbatteries.com/130-Catalogue/PDF/data_STM_en.pdf)
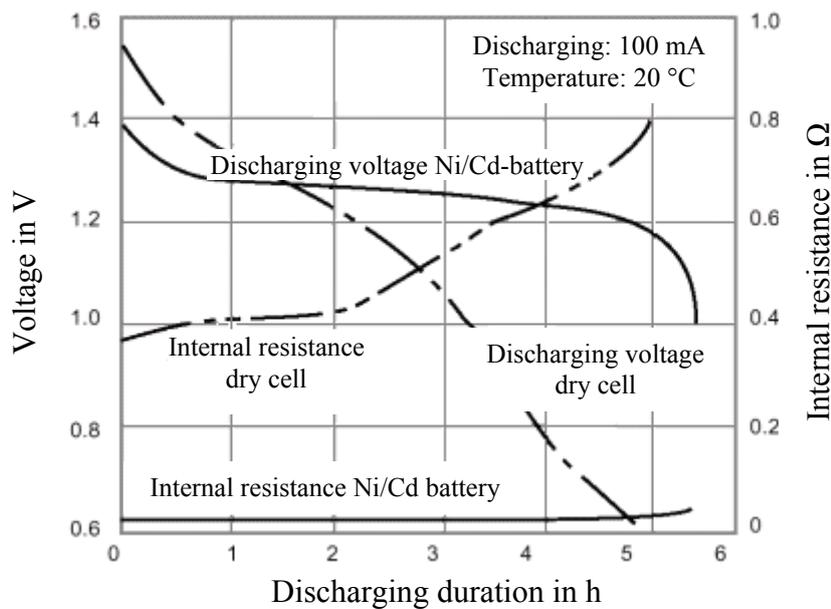
Fig. 6.4-5: Comparison of discharge curve of a nickel-cadmium-battery and a dry battery (http://www.ni-cd.net/accusphp/theorie/decharge/nicd.php)

If the accumulator is only partially discharged and then immediately charged, the (remaining) part of the unturned cadmium can build up big crystals. If the Ni-Cd-accumulator is afterwards loaded beyond this previous discharge depth, the internal resistance increases at this point. This results in a break in the progress of the discharge voltage, which is the more significant the higher the discharging current is. This memory-effect occurs mainly at high discharging current. It appears as if the cell has „memorized" exactly that point to which it was previously discharged. When the memory-effect has occurred, only the defined discharging with small current (< 0.3 C) until 1 V/cell can provide remedy. Something like that happens, when a nickel-cadmium-accumulator is permanently charged by small continuous currents. Small charging currents support the growth of big crystals. Those provide less reaction surface for the electrolyte. So the internal resistance of the cells increases. Contrary to the real memory effect this

influences the whole discharge characteristic. Charging pulses with current breaks or short discharge impulses in between (reflex charging) are better than small continuous charging currents.

Also starting out from the negative electrode is the so-called dendrite growth. The crystal size reaches dimensions that the crystal peaks penetrate the separator and approach to the positive electrode. Thus local short circuits are generated. Such "sick" cells are fully conductive, but they do not have any terminal voltage anymore. This uncontrolled crystal growth is supported by too low, long lasting continuous charging currents and high temperatures. There are „special methods" known, which remove those dendrites by melting with the aid of short time current pulses ($I > 100$ A). Nevertheless harmful consequences of the previous short circuits - like leakage due to heat affection - remain.

6.5 Nickel-metal-hydride-accumulator

The nickel-metal-hydride-accumulator is considered as the direct successor of the nickel-cadmium-battery. The main advantages of the nickel-metal-hydride-system are the higher energy densities on the one hand and the environmental friendliness due to the dispensation of the poisonous cadmium. The drawback is the low power density.

Electrodes:

Negative Electrode:	Hydrogen storing alloys like a metal-hydride (MeH_2) (charged state)
Positive electrode:	Nickel hydroxide (charged state)

Electrolyte: Watery potash lye with a small part of lithium hydroxide

Separator: Fine fibers

Housing: Premium steel

Cell reactions:

- Anode: $MH + OH^- \leftrightarrow M + H_2O + e^-$
- Cathode: $NiOOH + H_2O + e^- \leftrightarrow Ni(OH)_2 + OH^-$

Total cell reaction: $MH + NiOOH \leftrightarrow M + Ni(OH)_2$

The structure can either be prismatic (Fig. 6.5-1) or cylindrical (Fig. 6.5-2). The latter has the advantage, that no empty rooms are formed so that the volumetric energy density is higher. Like in the nickel-cadmium-battery in system the anode consists of nickel hydroxide. The Cathode is made of hydrogen absorbing alloys. The unique property of these alloys is the capability of storing one hundred times its own hydrogen content at a pressure, which lower than the ambient pressure. Used alloy are:

     a) AB_5-alloys, like $LaNi_5$,
     b) AB_2-alloys, like $TiMn_2$ or $ZrMn_2$.

The nickel-metal-hydride-accumulator is used in the *Toyota Prius* (Fig. 6.2-2) and in the *Honda Civic Hybrid.*
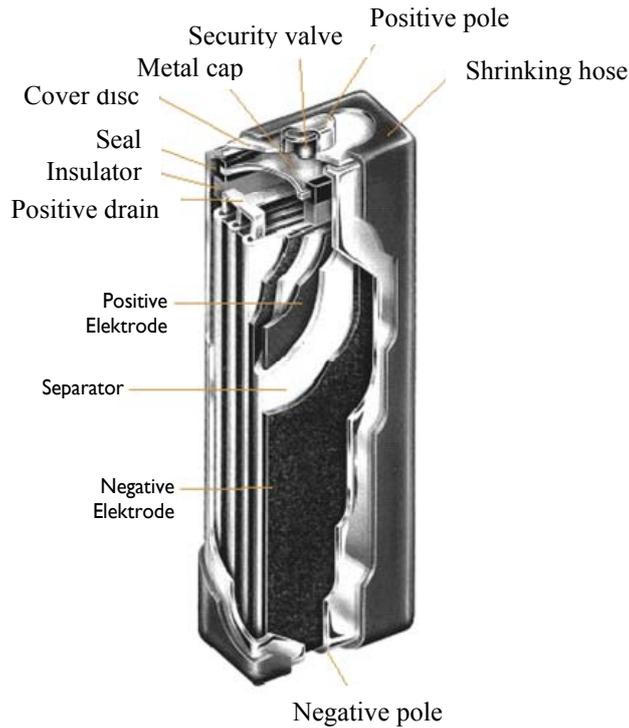
Fig. 6.5-1: Ni-MH-accumulator with prismatic structure (*Duracell*, http://www.duracell.com/oem/Pdf/others/TECHBULL.pdf)
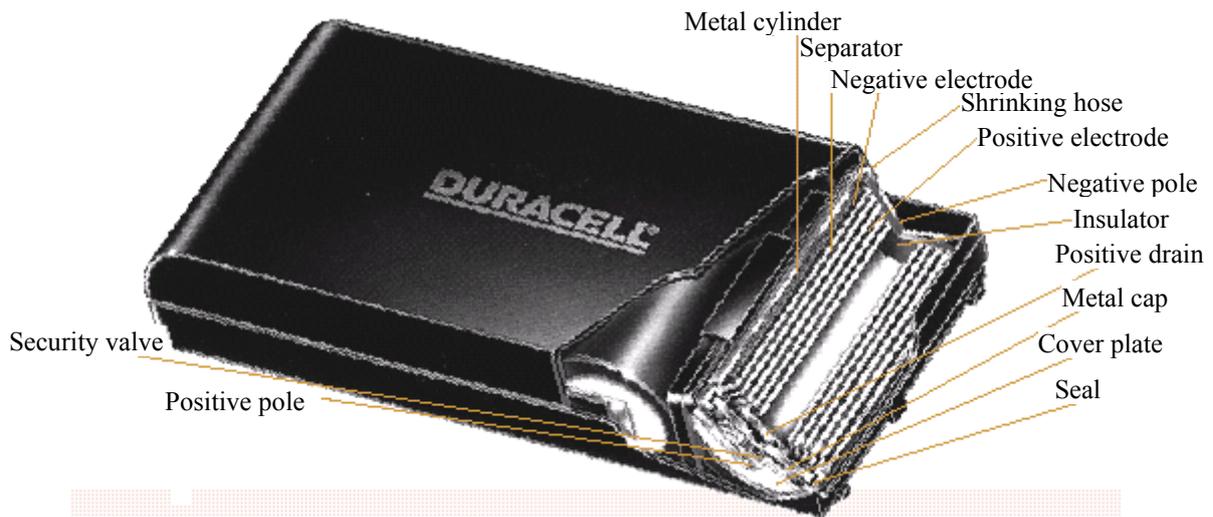
Fig. 6.5-2: Ni-MH-accumulator with cylindrical structure
(*Duracell*,http://www.duracell.com/oem/Pdf/others/TECHBULL.pdf)

Table 6.5-1:   Battery data of the *Toyota Prius* and the *Honda Civic Hybrid*

		Toyota Prius	*Honda Civic Hybrid*
Nominal voltage	V	201,6	144
Number of modules		28	20
Capacity	Ah	6,5	6,5
Energy	Wh	1310	936
Weight	kg	39	unknown

Charging and discharging:
For charging of the nickel-metal-hydride-accumulators three main criteria are decisive:
1. Choice of the suitable charging speed
2. Limitation of temperature
3. Choice of a suitable charging technique

The charging properties of the nickel-metal-hydride-system are similar to the one of the nickel-cadmium-Systems, whereby nickel-metal-hydride-system is more sensitive against overcharging. The most common method is the **charging with constant current**. By the current limitation an excessive temperature increase and an excessive oxygen recombination, which leads to undesired gassing, is avoided.
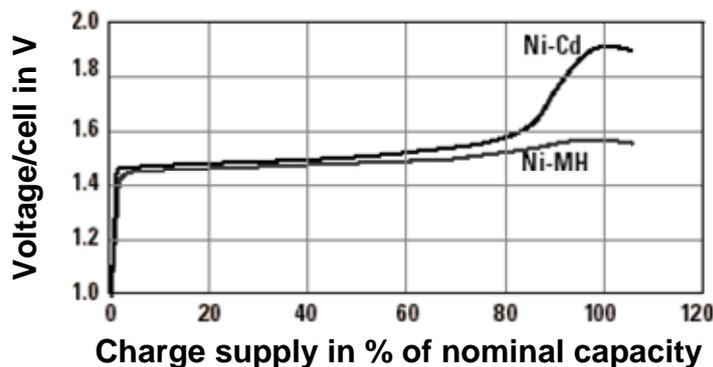
Fig. 6.5-3: Typical charging curves of Ni-MH- and Ni-Cd-Batteries
Conditions: Charging with 1·C at 21 °C until voltage change of -10 mV per cell
(*Duracell*, http://www.duracell.com/oem/Pdf/others/TECHBULL.pdf)

When comparing the charging voltage curves of the Ni-MH- and Ni-Cd-systems one recognizes that after reaching about 80% of the capacity the voltage of the Ni-MH-accumulator increases. The reason for this is the oxygen generation at the positive electrode. As soon as the battery is being overcharged the voltage decreases again. This effect is stronger for the nickel-cadmium-system than for the nickel-metal-hydride-system.

Fig. 6.5-4: Typical temperature curves during charging of Ni-MH- and Ni-Cd-Batteries
Condition: Charging with 1·C at 21 °C up to a voltage change -10 mV per cell
(*Duracell*, http://www.duracell.com/oem/Pdf/others/TECHBULL.pdf)

The stronger increase of the temperature during charging up to 80% of nominal capacity of the Ni-MH-accumulator is due to the exothermal property of the charging reaction. In contrast the reaction of

the nickel-cadmium-systems is of endothermic nature, which explains the smaller increase of the temperature curve. From a state of charge of about 80 % … 85 % on a bigger temperature 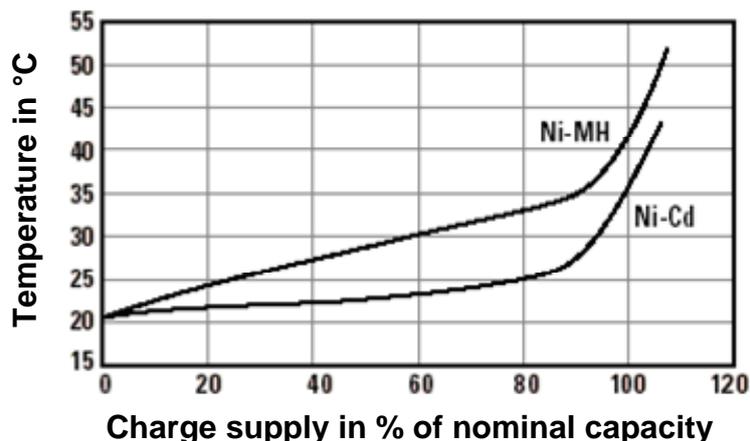increase result for both systems. This is due to the exothermic oxygen reaction. Like for the nickel-cadmium-system also for the Ni-MH-system the beginning voltage decrease ($-\Delta U$) after reaching the maximum voltage (Fig. 6.5-4) and the temperature increase (Fig. 6.5-5) during charging are used as indicators for the reaching of full charging. The voltage trajectory during charging depends on several factors especially on the temperature and the current. The voltage during charging proceeds on a higher level at lower temperatures. Also the charging efficiency is influenced by the temperature, because the higher the temperature the oxygen is generated at the positive electrode. Hence charging at high temperature influences the capacity negatively. Also the voltage during charging is higher the higher the charging currents are chosen.

The **discharging behavior** of a nickel-metal-hydride-accumulator is comparable to the one of the nickel-cadmium-accumulators. For both systems the voltage depending on the withdrawn amount charge proceeds during the whole charging process relatively flat Fig. 6.5-5). Hereby the capacity of the nickel-metal-hydride-cell is generally by 40% higher than the ones of the nickel-cadmium-cell for the same cell sizes.
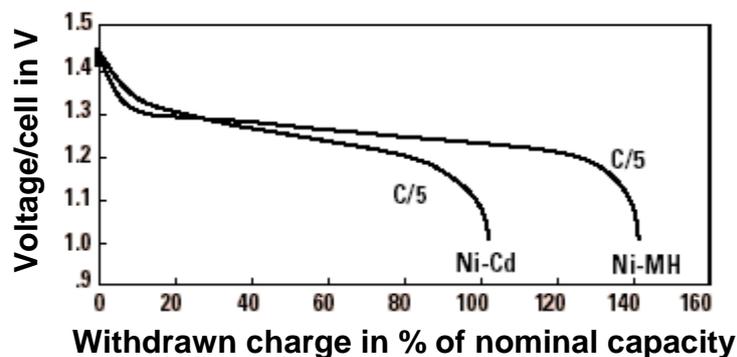
Fig. 6.5-5: Voltage in V depending on the withdrawn charge in % of nominal capacity: Comparison of discharge curves of a Ni-MH- and a Ni-Cd-cell of same size; condition: Charging previously with $C/3$ over 5 hours; temperature: 21°C (*Duracell*, http://www.duracell.com/oem/Pdf/others/TECHBULL.pdf)

For higher discharge currents the discharging curve of the battery voltage proceeds on a lower voltage level. Also the usable capacity of the Ni-MH-Battery is lower then. The same is observed, if the Ni-MH-battery is discharged with the same current but at a lower temperature. When nickel-metal-hydride-accumulators are stored, the state of charge resp. the capacity decreases depending on the temperature and storage duration (Fig. 6.5-6). The **self-discharge** is reasoned in the reaction of the hydrogen which remains in the battery with the positive electrode. Also the slow and reversible dialysis of the positive electrode gives a contribution to this. The higher the storage temperature the higher is the self-discharge rate. The loss of capacity due to self-discharge can be recovered by suitable charging.

A drawback of nickel-metal-hydride-batteries, which can occur in case of incautious discharge, is the **reversible lazy-battery-effect**. In principle this is comparable to the memory-effect. It occurs due to an incomplete discharge of the accumulator during operation resp. due to a continuous charge with a too low, non-specification-conform current. Similar to the memory-effect crystals build up on the positive nickel-hydroxide-electrode. In the lazy-battery-effect the voltage does not break down at the point of partial discharge, but it slightly drops over the whole discharge period. Due to inappropriate maintenance the capacity of nickel-metal-hydride-accumulators can decrease over the whole discharging time.
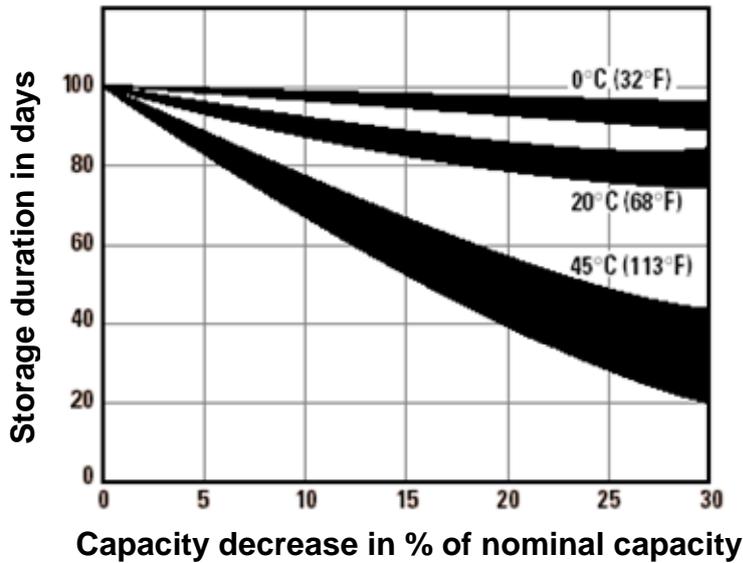
Fig. 6.5-6: Capacity decrease of the Ni-MH-battery in % of nominal capacity depending on storage in days: Self-discharge at different temperatures; condition: Charging with $C/3$ over 5 hours; afterwards discharging with $C/5$ to 1.0 V at 21 °C (*Duracell*, http://www.duracell.com/oem/Pdf/others/TECHBULL.pdf)
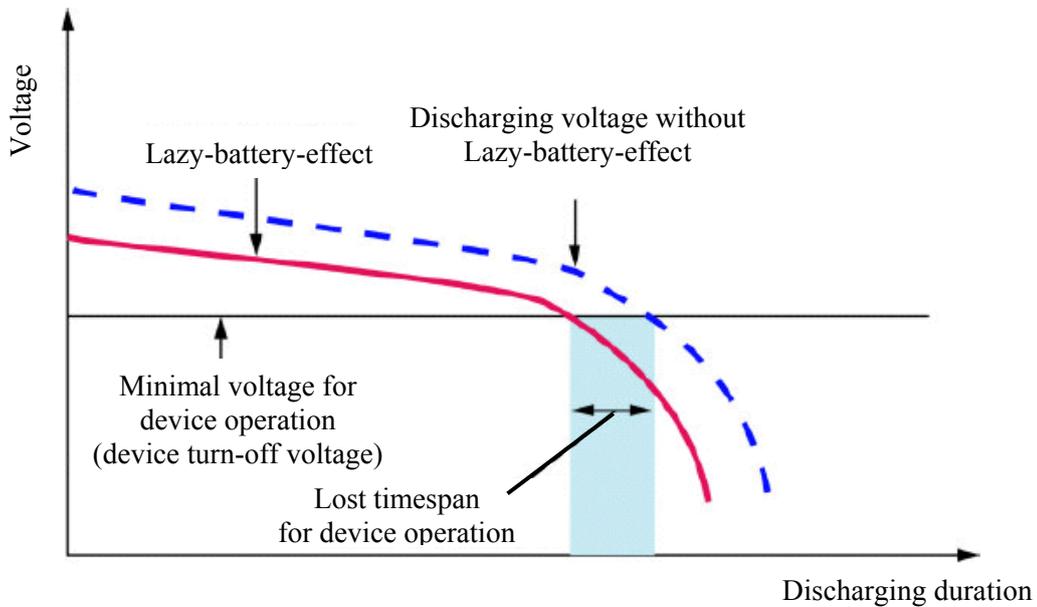
Fig. 6.5-7: Ni-MH-battery: Effects of the lazy-battery-effect on the battery voltage
(http://www.tecchannel.de/hardware/1191/8.html)

The lazy-battery-effect is less dramatic than the memory-effect. The accumulator voltage is below nominal voltage during charging, but the lifespan is only slightly decreased. In order to prevent these negative properties, the accumulator has to be 2 or 3 times successively fully discharged. Like for the memory-effect a modern charging device with the appropriate charging- and discharging functions can help to recover the original performance of the accumulator.

6.6 Sodium-nickel-chloride-accumulator (ZEBRA)

The ZEBRA-battery is a version of the sodium-sulfur-accumulator, which is not further described here. It differs in the material of the positive electrode. Instead of sulfur nickel-chloride is used. Another difference is the assembly of the electrodes. In this system the sodium surrounds the ceramic from the

outside. The cells, which have a capacity of 40 Ah each, are connected in series and parallel to a battery. Due to the high operating temperature of about 300 °C the cells are in a housing, which has a vacuum insulation. Thus the surface of the battery housing remains cold and the heat flow from the battery is small. At start-up or after cool-down the battery first has to be heated up to operating temperature. This is done by an integrated electric heating. As soon as the battery reaches a temperature of about 200 °C, the charging process can start.

Electrodes:

Negative electrode:	Molten liquid sodium
Positive electrode:	Nickel-chloride, in discharged state NaCl (common salt) and nickel
Solid electrolyte and separator:	Tube made of β"-aluminum oxide
Second electrolyte:	Molten liquid sodium-aluminum-chloride inside the solid electrolyte tube
Remark:	Both electrolytes do not take part in the reaction, but serve only for the sodium ion conduction
Housing:	Premium steel, hermetically welded, with a thermal insulation

Cell reactions:

- Anode: $2\,Na \leftrightarrow 2\,Na^+ + 2e^-$
- Cathode: $NiCl_2 + 2\,Na^+ + 2e^- \leftrightarrow Ni + 2\,NaCl$

Total cell reaction: $2\,Na + NiCl_2 \leftrightarrow Ni + 2\,NaCl$

Charging and discharging:
The ZEBRA-battery is made up of tube shaped cells. The positive solid electrode is inside of the ceramic electrolyte tube and has a circular cross section with a current drain in the middle. During charging the reaction zone radially drifts from the electrolyte ceramic radial towards the current drain. With proceeding charging reaction the reaction zone moves into the solid electrode. Thereby the reaction surface becomes smaller. The charging method has to take this fact into account. In order not to have an increased current density with proceeding charging, the charging current has to decrease, in order to keep a constant current density. Hence the *I-U*-charging method is especially suitable for this cell type (Fig. 6.3-3). It is being charged with constant current, as long as the voltage stays below a certain value. After reaching the maximum voltage current is permanently decreased until the end of charging is reached. If very small currents are chosen for the constant-current-phase, the constant-current almost lasts until the end, so that for charging with small currents the method of charging with constant current can also be applied. But then the charging duration is longer than the one of the *I-U*-charging.
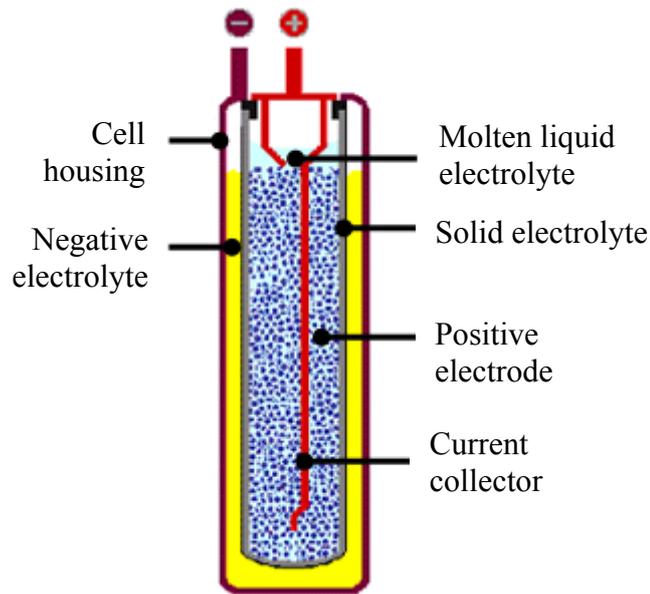
Fig. 6.6-1: Structure of a sodium-nickel-chloride-accumulator (http://www.basytec.de/batallg/batallg.htm)

Beneficial for the practical operation is the insensibility against overcharging and deep discharging. The running reactions are reversible and do not damage the cell. This advantage is possible by a sodium excess. Fig. 6.6-2 demonstrates the voltage and the corresponding chemical reactions depending on the state of charge.
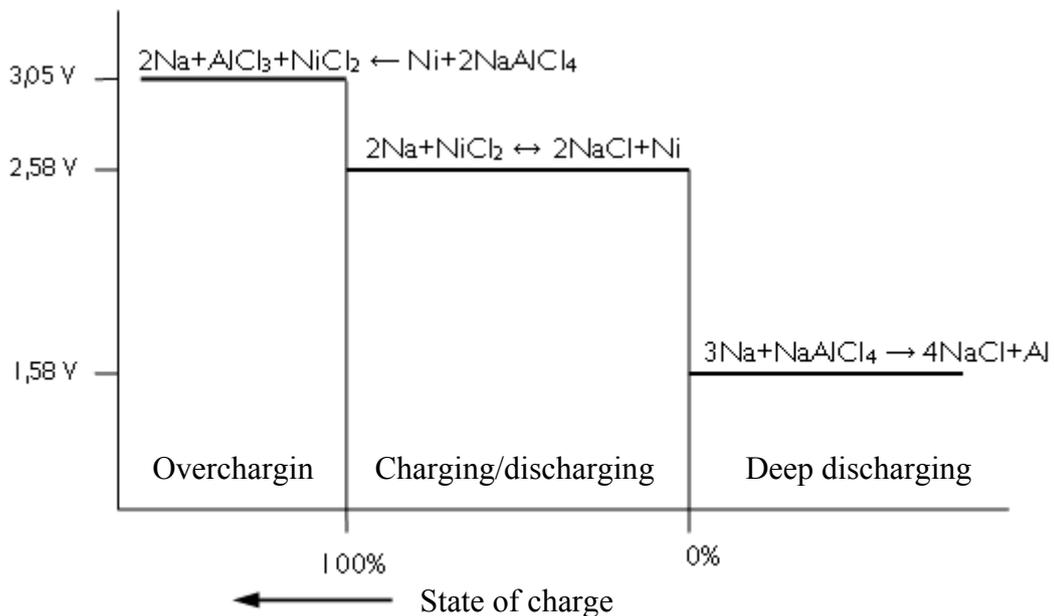
Fig. 6.6-2: Charging and discharging reaction inside a *ZEBRA*-cell (from: Naunin, D. [Hrsg.]: Elektrofahrzeuge: Entwicklungserfolge und Perspektiven. DGES-Tagung 29./30. April 1999. Karlsruhe)

If a very high power is withdrawn from the battery over a long time during discharging, the battery heats up because of the internal resistance. In order to limit the heating, the battery has to be cooled by air ventilation when exceeding a given temperature. The ZEBRA-system shows no electrochemical self-discharging, as the ceramic electrolyte prevents the self-discharge (Ah-efficiency 100%). But a thermal self-discharging of approx. 5.5 W per stored kWh is unavoidable.

6.7 Lithium-ion-accumulator

The first works on Lithium batteries began in 1912 under *G. N. Lewis*, but the first rechargeable lithium batteries were commercially not available until 1970. Different approaches to develop a rechargeable lithium battery mainly failed because of security problems. Due to the natural instability of metallic lithium – especially during charging – the development moved towards to a non-metallic lithium battery, in which only lithium ions would be used. This accumulator delivers a slightly lower energy density than an accumulator made of metallic lithium, but this design is more secure, assuming that certain security measures are done for charging and discharging. In 1991 *Sony Corporation* commercially introduced the first lithium-ion battery into the market. Other manufacturers followed. A lithium compound is used for the cathode in the litium-ion system, which can consist of cobalt-, mangan- or nickel-oxide. The anodes are made of a graphite compound.

Electrode:

Negative electrode: Graphite

Positive electrode: Lithium-storing-capable metal oxide, e. g. cobalt dioxide, ($LiCoO_2$), nickel oxide ($LiNiO_2$) or mangan oxide ($LiMn_2O_4$)

Electrolyte: E. g. lithium-phosphor-hexafluoride

Separator: Polyethylen film

Cell reactions: Under use of cobalt dioxide

- Anode: $LiCoO_2 \rightarrow Li_{1-x} CoO_2 + xLi^+ + xe^-$

- Cathode: $C + xLi^+ + xe^- \rightarrow CLi_x$

Total cell reaction: $LiCoO_2 + C \rightarrow Li_{1-x} CoO_2 + CLi_x$

Lithium is a highly reactive light metal. This easy ignitable material can explode at strong heating. In order to provide the necessary security, the lithium-ion-battery must have a security circuit and a valve for pressure release. Additionally the cells are set into a pressure-proof housing. The function of this security circuit is the limiting of peak voltage of each cell during charging and the prevention of a too low cell voltage during discharging. The cell temperature is watched, in order to avoid extreme temperatures. The maximum charging current is limited to $1 \cdot C$ and the maximum discharging current to $2 \cdot C$. Due to these precautions a lithium-metalizing, which might occur at overcharging, is practically avoided. These security measures result in relatively high costs for the Li-ion-system. Hence a rechargeable lithium-ion-battery is by 30 % more expensive compared to a nickel-metal-hydride-accumulator.
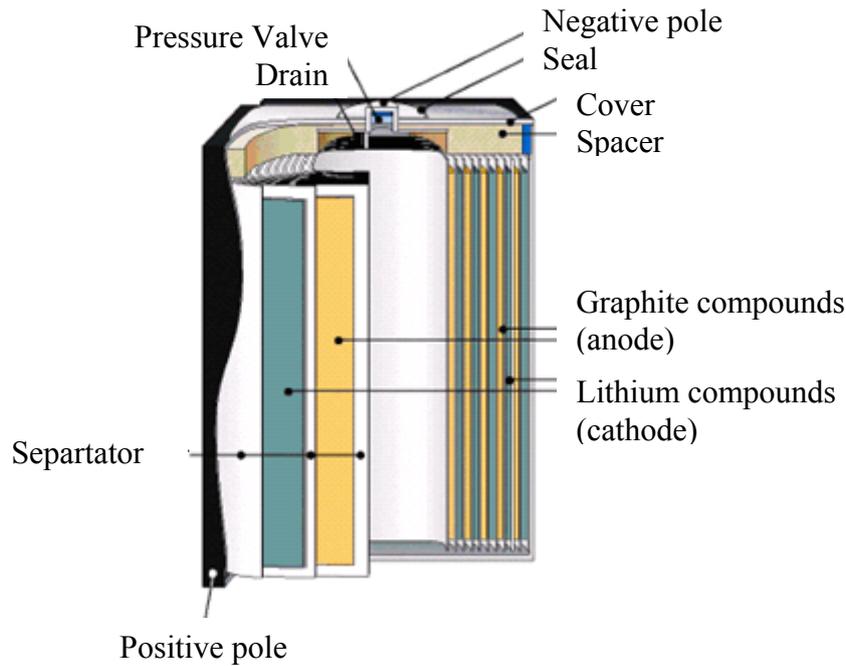
Fig. 6.7-1: Structure of a lithium-ion-accumulator (http://www.tecchannel.de/hardware/1191/8.html)´

The **aging** of lithium-ion-batteries is currently still a problem of this system. A reduction of battery capacity can already be noticed after one year, whether the battery was used or not. The battery often malfunctions after two or three years. Also other battery systems in principle underlie a decrease of storage capacity due to aging, especially nickel-metal-hydride-batteries, if they have experienced too high temperatures.
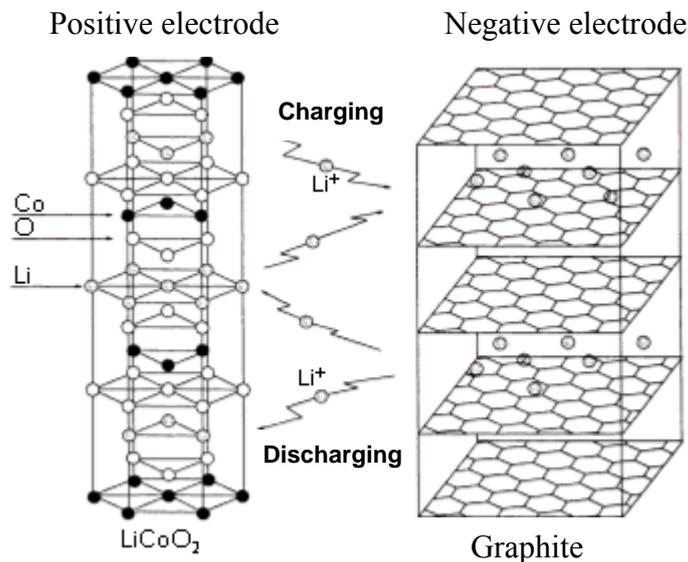
Fig. 6.7-2: Scheme of the chemical reaction of a lithium-ion-accumulator
(*Panasonic* http://www.panasonic.com/industrial/battery/oem/images/pdf/Panasonic_LiIon_Overview.pdf)

Charging and discharging:
In the lithium-ion-system following chemical reaction runs during charging: During charging the lithium in the positive electrode is being ionized. The Li-ion move to the single grid layers of the hexagonal crystal plane structure of the negative graphite electrode, where they embed. During discharging the ions move from the negative electrode back to the positive one.

The lithium-accumulator is generally charged according to the *U*-characteristic (Fig. 6.7-3), whereby during the initial phase a current limitation may be necessary. The manufacturer's specification of maximum charging current is between $0.5 \cdot C$ and $1 \cdot C$. A fixed charging end voltage has to be satisfied.

a)   b)
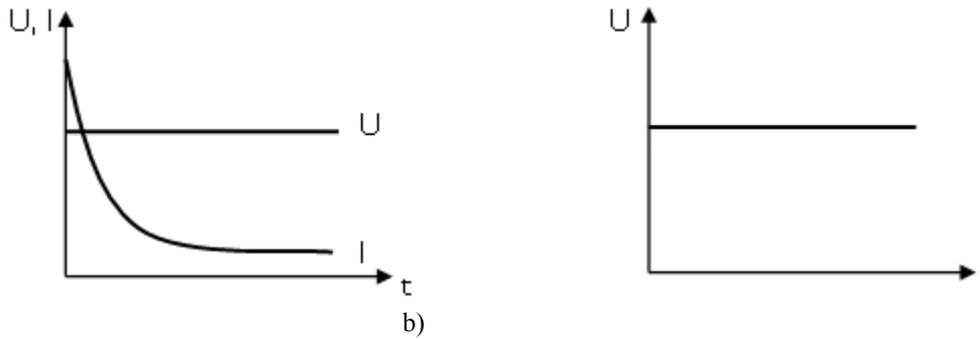
Fig. 6.7-3: Charging with constant voltage: a) Current and voltage over time, b) Voltage and current characteristics
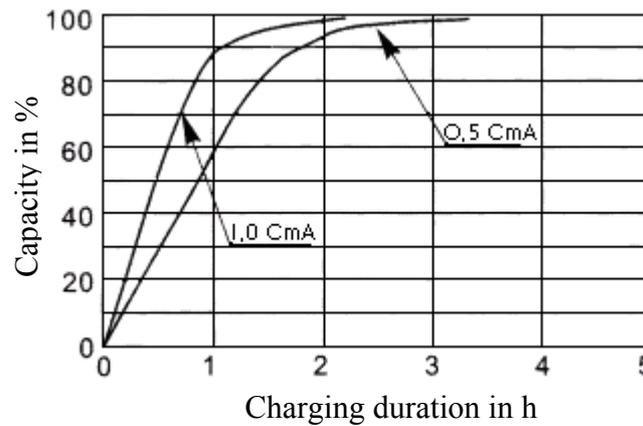
Fig. 6.7-4: Capacity depending on time during charging of a Li-ion-accumulator (http://www.huanyubattery.com/en/product-1-1.asp?sort=Characteristics&sort2=Li-ion%20Battery)
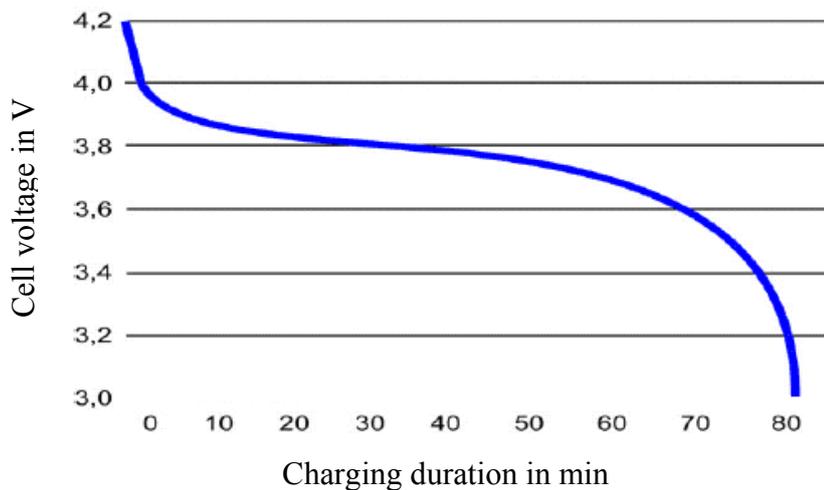
Fig. 6.7-5: Battery voltage in V depending on discharging duration in minutes: discharging curve of a lithium-ion-accumulator (http://www.tecchannel.de/hardware/1191/9.html)

With the given charging current of $0.5 \cdot C$ to $1 \cdot C$ lithium-ion-batteries reach within 70 to 120 minutes 90% of their nominal capacity (Fig. 6.7-4). *Panasonic* describes the charging of a one-cell battery pack with a flowchart in Fig. 6.7-6, where it is at first being charged with constant current and afterwards with

constant voltage *(I-U-approach)*. The occurring abbreviations and denotations are explained in the following.

CV   - Charging with constant voltage
i_L - Charging current
i_{set1} - fixed current-set-value 1
i_{set2} - fixed current-set-value 2
OCV   - No-load voltage of battery
t_{bat} - Temperature of battery
t_{min} - Minimum threshold temperature, fixed value
t_{max} - Maximum threshold temperature, fixed value
T_1 - Time counter for total time
T_2 - Time counter for full charging
T_3 - Time counter for recharging

From Fig. 6.7-5 it can be seen, that during discharging the voltage is above nominal voltage of 3.6 V nearly over the entire timespan.
Negative phenomena like the memory- or lazy-battery-effect do not occur in Li-ion-systems.

START

Checking wether battery pack is inserted

No ← Battery pack inserted?

Yes → (A)

T_1 counts total time

Counter cancel decision

Yes ← $T_1 > 720$ Min

Checking battery temperature

$t_{min} \leq t_{bat} \leq t_{max}$ → No Waiting → (A)

JA

Voltage check 1; voltage higher than discharging voltage? (4.2 V)

No ← OCV < 4,2V

JA

Voltage check 2

OCV > 2,9V → No

Yes

0.7 CmA charging　　　0.1 CmA charging

After transition to CV-mode
Charging current check　Overcharging check

(A) ← No　auf CV $i_L < i_{set1}$　　OCV > 3V → JA → (A)

Yes　　　No

Charging complete Timer on T_2　　Recharging Timer on T_3

Charging complete counter
Cancelling decision　　Recharging counter Cancelling decision

$T_2 < 120$ Min →　　$T_3 < 120$ Min → Yes → (A)

Yes　Charging stop　　No

current check

(A) ← No　$i_L < i_{s.2}$

Yes

Error: Time exceedance　　Error: Overcharged　　Charging complete

Fig. 6.7-6: Charging of a lithium-ion-accumulator
(http://www.panasonic.com/industrial/battery/oem/images/pdf/Panasonic_LiIon_C)

6.8 Zinc-bromine-accumulator

Electrodes:

Negative electrodes:	Zinc
Positive electrodes:	Bromine

Electrolyte: Watery solution of zinc-bromine and quaternary ammonium salts

Separator: Micro-porous polyethylene

Cell reactions:

- Anode: $Br_2 + 2e^- \leftrightarrow 2\ Br^-$
- Cathode: $Zn \leftrightarrow Zn^{2+} + 2e^-$

Total cell reaction: $Br_2 + Zn \leftrightarrow ZnBr_2$

The development of the Zn-Br-battery started in the 70s at first at *EXXON* in the *USA* and from 1983 on in *Europe* by intensive work by the *„Studiengesellschaft für Energiespeicher und Antriebssysteme" (SEA)* in *Austria*. From 1990 on vast laboratory tests and tests in E-vehicles were done. The Zinc-bromine-battery deviates in the structure from the „classic" cell, because the active material of the positive electrode is not embedded in the electrodes, but is in charged state as well as in uncharged state in dissolved form. It is stored in a separate tank. Thus more material can be provided, than the amount which normally stored in the electrode. For the negative electrode (Zn) it is important, that during charging a galvanic separation from the flowing electrolyte is done. In this way a homogenous separation can be achieved and the common problems with liquid electrodes is not observed. Another special property of this system is that two electrolytes are required, each a three-molar zinc-bromine solution and a bromine solution. To the latter a four-molar potassium chloride for increase of conductivity, and ammonium bromine as complexing agent is added. The electrolytes circulate in separated circuits; anode- and cathode chambers are separated by a micro-porous polymer-memrane from each other. With an impressed warts profile even at a deformation of the electrodes a minimal gap for the electrolyte solutions remain. In order to reach high current densities, to control the temperature and to provide a homogenous separation of zinc during charging, the electrolytes have to circulate between the electrodes. Two pumps are necessary in order to perform this. The active material of the negative electrode is dissolved in discharged state as zinc bromine ($ZnBr_2$) and is partially in the tank on the left side in Fig. 6.8-1. Polyethylene is used as electrode material, which reaches a conductivity of 1 S/cm by the insertion of carbon. The electrodes are designed bipolar, that means they act as anode on the one side and as cathode on the other. Due to the use of bromine the use of metals is impossible; even titanium would corrode. The reaction surface is increased, by covering a big area of the positive side of the electrode with carbon.
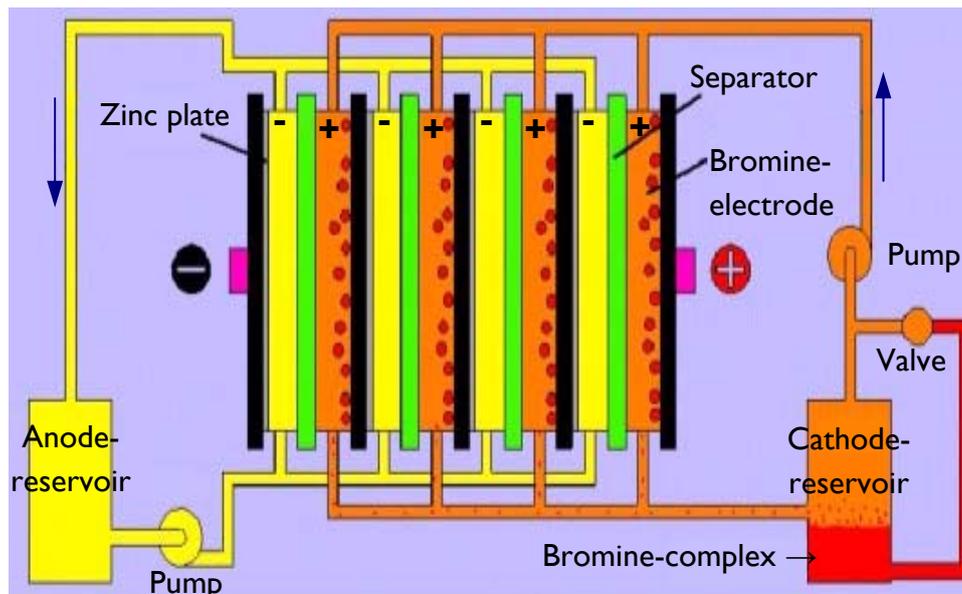
Fig. 6.8-1: Electrolyte flow system in the Zn-Br-battery (http://www.zbbenergy.com/technology.htm)

The zinc-bromine-accumulator make ranges of 150 to 200 km for an electric vehicle possible. The Zn-Br-system has problems concerning the complex structure and aggressiveness of the halogen. Also the power density and the cycle lifespan are not very high. During a car race in spring 1992 in *Phoenix* (*Arizona, USA*) an accident occured with an electrified *Opel Kadett*, in which a zinc-bromine-accumulator was built. Since that the acceptance of this system has decreased.

Charging and discharging:
During **charging** zinc is deposited on the negative electrode, while bromine is bound as liquid complex, bromine- and ammonium-ions and stored in a reservoir in form of a swamp. During **discharging** zinc- and bromine-ions come up at the corresponding electrodes. The bromine-complex is directed by an automatically acting valve back to the electrolyte and pumped through the cell pack. The bromine is being electrochemically discharged at the anode bromine. Instantaneously the zinc film on the cathode disperses. The micro-porous separator between the electrode surfaces prevents the bromine from going back to the zinc layer. Thus the direct chemical reaction is reduced and consequently also the self-discharging of the cell. The circulation of the electrolyte reduces the building of zinc dendrites and simplifies the thermal management of the battery. Charging and discharging of zinc-bromine-accumulators are done at current densities of 15 to 30 mA/cm². The amount of charge depends on the zinc content, at which the state of charge of 100% is defined. This amount is less than the whole amount of dissolved zinc-ions in the electrolyte.

6.9 Lithium-polymer-accumulator

The structure of lithium-polymer-accumulators is identical to the one of the lithium-ion-battery except for the electrolyte. The electrolyte of this system is not watery and thus safe from leaking out. The liquid reaction substance was replaced by a gelatinous polymere electrolyte. The advantage of the solid electrolyte is the design freedom for the housing.
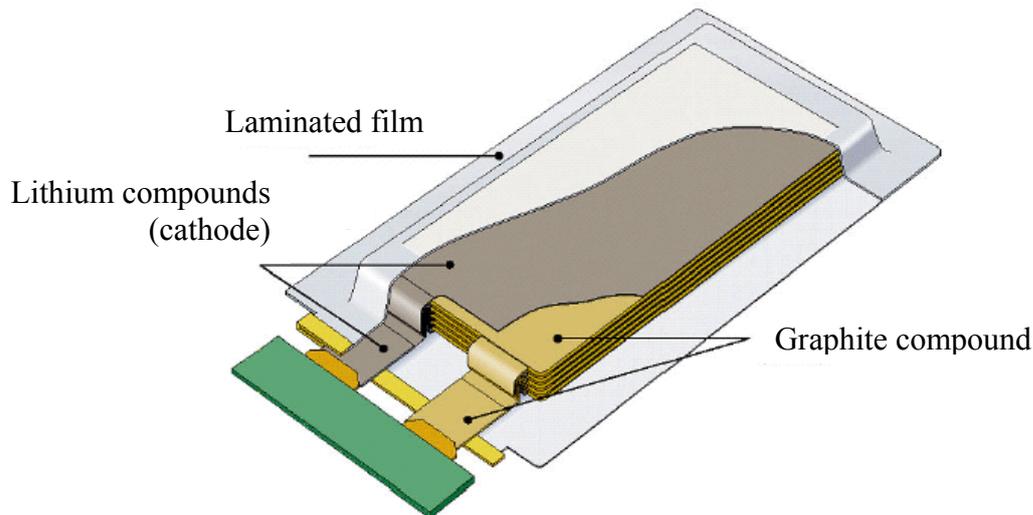
Fig. 6.9-1: Structure of a lithium-polymer-accumulator (http://www.tecchannel.de/hardware/1191/10.html)

6.10 Zinc-air-battery (ZOXY)

The development of the zinc-air-battery goes back to the American inventor *Thomas Alva Edison (1847-1931)*. The battery consists of a positive electrode made of porous carbon, a negative electrode made of zinc and an electrolyte made of potash lye (KOH). The operating temperature is 60 °C. The positive electrode is in contact with air, oxygen from air is being reduced. That means, that the active material is no longer contained in the electrode, but it can be withdrawn from the atmosphere if required. The battery is charged mechanically, by replacing the zinc which is stored in cassettes. The zinc is being recovered in facilities and processed to new electrodes. The specific energy of the zinc-air-battery is 120 to 160 Wh/kg and the power density 50 W/kg. A *VW* City E-car ("*VW City Stromer*") was provided with such a system. The battery consisted of 179 cells with a total energy content of 45 kWh. The weight was 358 kg.

6.11 Lithium-iron phosphate (LiFePO$_4$)

This is one of the most recent implementations of lithium-ion-batteries. Lithium iron phosphate, which was modified by nanoparticles, is used as material for the cathode. Thus a better cell stability against temperature influences as well as against chemical influences is achieved. Further advantages are the increased number of cycles, the increase of charging current and the elimination of explosion risks. Furthermore it is not necessary anymore to watch every single cell during charging. Nevertheless the lifespan can be increased by watching. A drawback of this implementation compared to other lithium batteries is the lower energy density, which is due to the partially smaller voltage of 3,0 - 3,3 V.

6.12 Comparison of accumulators

Traction batteries are judged according the following criteria:
- Energy content
- Power
- Volume
- Weight
- Quick chargeability
- Lifespan
- Low-maintenance
- Security

- Availability
- Maturity phase
- Costs
- Environmental friendliness and recyclability

For electric vehicles the energy density because of wide range, for hybrid vehicles especially the power density because of quick charging and discharging due to the cooperation of the electric drive system with the ICE is of major importance. The values of energy and power density of an energy storage is visualized in the *Ragone*-diagram (Fig. 6.12-1). With this diagram also the ranges for different speed can be graphically depicted (Fig. 6.12-2).
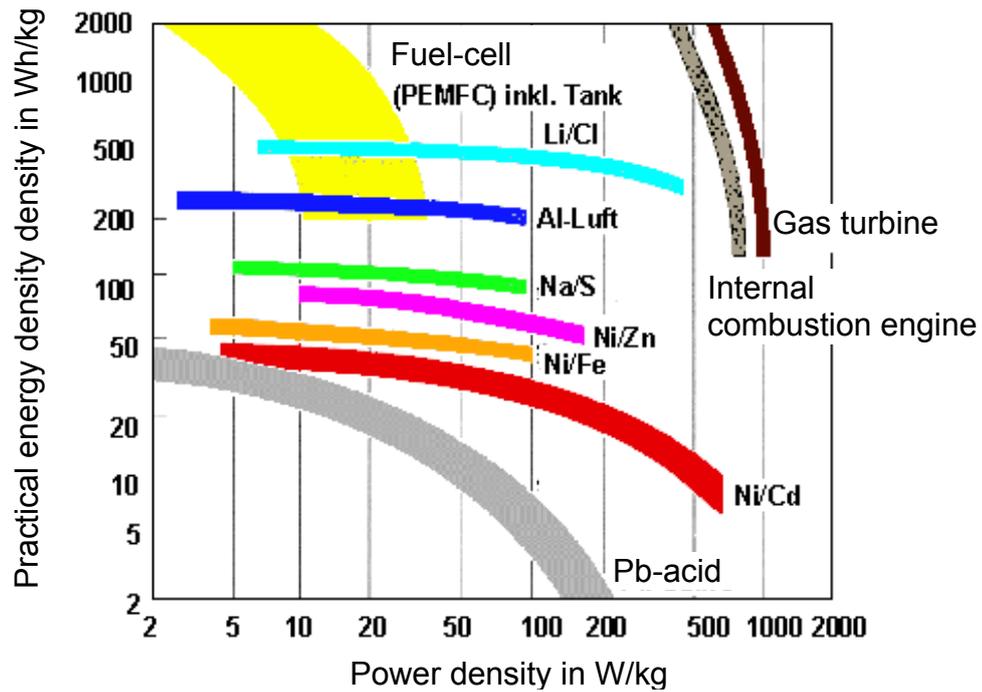
Fig. 6.12-1: *Ragone*-diagram of different energy storages compared to combustion drives and PEM-fuel cells
(http://www.iwe.uni-karlsruhe.de/plainhtml/lehre/bb/v8/sld014.htm)
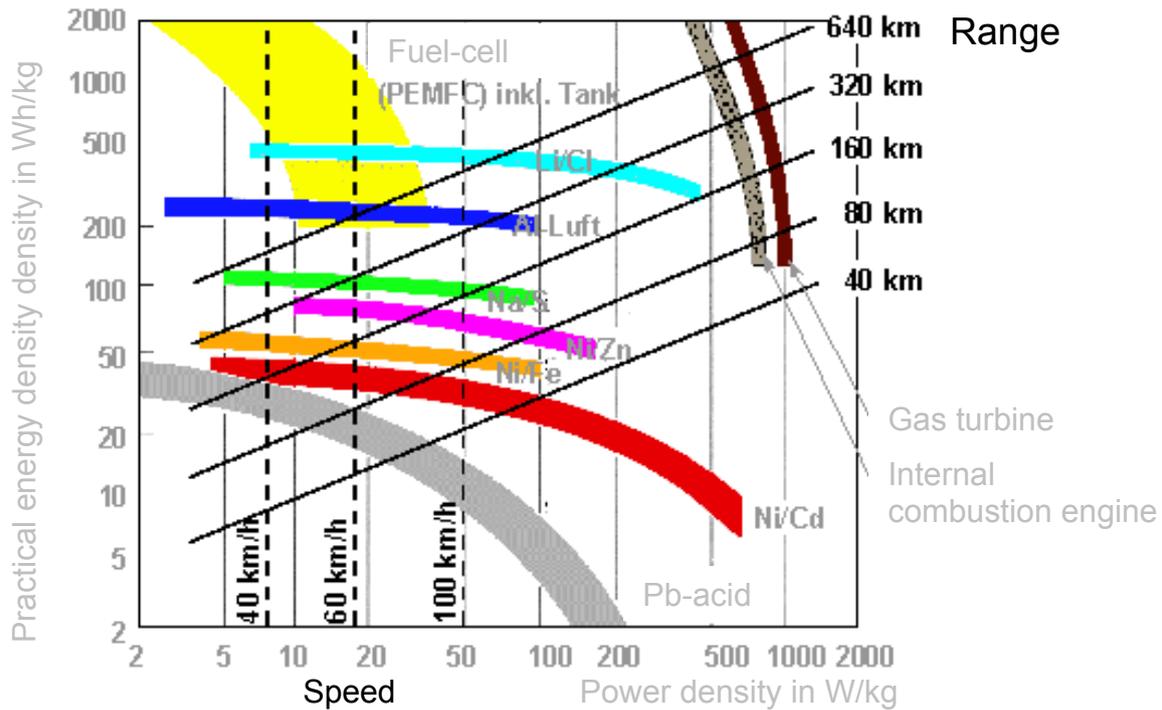
Fig. 6.12-2: Ranges and speeds of electric vehicles
(http://www.iwe.uni-karlsruhe.de/plainhtml/lehre/bb/v8/sld015.htm)

From the Tables 6.12-1 to 6.12.4 by different authors the lithium-ion-battery comes off as the most promising system concerning high energy and power density. Up to now the short lifespan is a drawback, as well as the complicated manufacturing and the resulting high costs. There is also still demand of development concerning operating security. Also the nickel-metal-hydride-accumulator has good values of energy and power density and is therefore mainly used in hybrid vehicles (Fig. 6.12-3).

Table 6.12-1: Energy density, power density, lifespan and costs of different battery systems
(Baumann, W./ Muth, A.: Batterien Daten und Fakten zum Umweltschutz. Berlin u.a. 1996. Springer-Verlag.)

System		Lead	Ni-Cd	Ni-MH	Na-NiCl	Li-Ion	Li-Poly	LiFePO$_4$	Zn-air	Target value
Energy density	Wh/kg	30 - 35	45 - 50	60 – 70	90 - 100	90 - 140	110 - 130	90 - 110	100 – 220	100 – 200
Power density	W/kg	200 - 300	80 - 175	200 - 300	160	300 - 600	ca. 300	> 3000	ca. 100	75 – 200
Lifespan	Years	2 - 3	3 - 10	10	5 - 10	< 5	n.a.[*)]	n.a.	n.a.	10
	Cycles	300 - 400	> 2000	> 1000	1000	500 - 750	< 600	n.a.	n.a.	1000
Costs	€/kWh	100 - 150	< 600	300 – 350	< 300	300 - 600	300	n.a.	60	100 – 150

[*)] no detailed values available

Table 6.12-2: Energy density, power density, lifespan and costs of selected battery systems ([Hartkopf, T. (2001): Skript zur Vorlesung: Rationelle Energieverwendung. Institut für El. Energiesysteme, Fachgebiet Regenerative Energien, TU Darmstadt)

System			Lead	Ni-Cd	Na-S	Na-NiCl	Zn-Br
Resting voltage/cell		V	1,93	1,24	2,08	2,59	1,79
Energy density gravimetric	theor.	Wh/kg	161	210	795	n.a	430
	pract.	Wh/kg	50	50	110	90	75
Energy density volumetric	theor.	Wh/dm³	690	700	1.200	n.a.	1.600
	pract.	Wh/dm³	100	110	130	110	85
Power density practical	grav.	W/kg	220	260	250	110	110
	vol.	W/dm³	240	360	140	130	130
Efficiency		%	< 80	65	90	90	75
Lifespan (80% discharge)	Calendric	Years	5 - 15	10 - 20	3 - 8	2 - 4	1 – 2
	Cycles		2000	3000	1500	1500	1500
Deep dischargeability			bad	very good	very good	very good	n.a.
Operating temperature		°C	20	20	300	300	20

Table 6.12-3: Comparison of different battery systems for the application in hybrid vehicles (Naunin, D. [Hrsg.]: Elektrofahrzeuge: Entwicklungserfolge und Perspektiven. DGES-Tagung 29./30. April 1999. Karlsruhe)

Accumulators with high power density (for hybrid vehicles)					
		Pb/PbO$_2$	Ni-Cd	Ni-MH	Li-ion
Energy density gravimetric	Wh/kg	32	35	40	70
Energy density volumetric	Wh/dm³	68	100	100	150
Power density gravimetric	W/kg	430	700	1.200	2.000
Power density volumetric	W/dm³	910	2000	3000	4200

Table 6.12-4: Comparison of different battery systems for the use in electric vehicles (Naunin, D. [Hrsg.]: Elektrofahrzeuge: Entwicklungserfolge und Perspektiven. DGES-Tagung 29./30. April 1999. Karlsruhe)

Accumulators with high energy density (for electric vehicles)						
		Pb/PbO$_2$	Ni-Cd	Ni-MH	Na/NiCl$_2$	Li-ion
Energy density gravimetric	Wh/kg	35	50	70	120	100
Energy density volumetric	Wh/dm³	90	150	200	190	250
Power density gravimetric	W/kg	200	200	140	180	200
Power density volumetric	W/dm³	510	600	400	270	500

However a cheap availability of the raw material nickel is a problem. The price of this raw material increased on the metal market. An older estimation of the availability of the used metals for assumed constant demand (1994) shows Table 6.12-5.

Table 6.12-5: Availablity of some raw materials used in accumulators (Naunin, D. [Hrsg.]: Elektrofahrzeuge: Entwicklungserfolge und Perspektiven. DGES-Tagung 29./30. April 1999. Karlsruhe)

Raw material	Lead	Nickel	Lithium	Zinc	Sodium
Availability in years	40	110	400	40	6.000

The in the table given availability is calculated according to:

$$\text{Availability} = \frac{\text{Resources}}{\text{yearly consumption 1994}} \qquad (6.12\text{-}1)$$

Here it can be seen, that the lead system reaches its limit, but this system is best known and most developed; other battery systems are still at the beginning of their development. With 43% (2004) the nickel-metal-hydride-accumulator dominates the percental part of the used accumulators in hybrid vehicles.
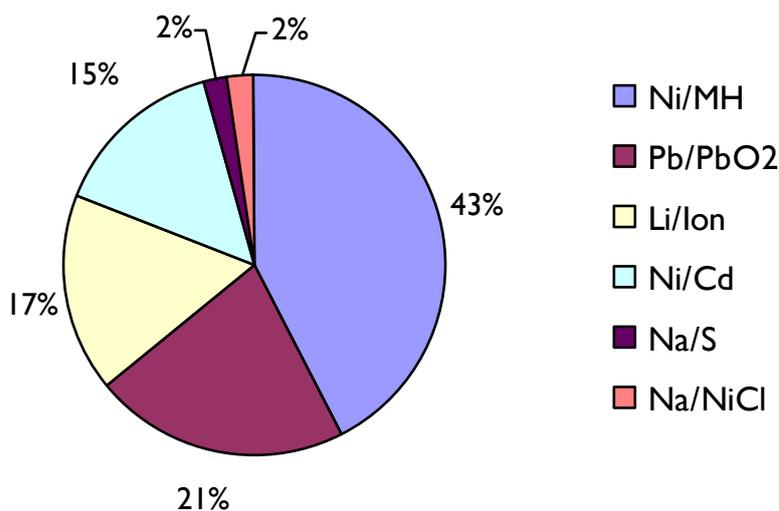
Fig. 6.12-3: In hybrid vehicles used battery-systems (2004)

7. Electrochemical capacitors

While batteries store electric charge by storing chemical energy on the electrodes, capacitors store electric energy between a positively charged and a negatively charged electrode with a dielectric in between. The voltage U which is applied to the capacitor electrodes is directly proportional over the **capacity C** to the positive and negative charge $+Q$ and $-Q$ which is cumulated on the electrodes.

$$Q = C \cdot U \qquad (7\text{-}1)$$

This capacity C (in Farad: 1 F = 1 As/V) is not to be mixed up with the capacity C of accumulators (in Ah). The **electric field E** resp. **electric flux density** $D = \varepsilon E$ ("dielectric displacement") in an idealized plate capacitor (Fig. 7-1) determines the potential difference U between the electrodes (distance of electrodes d) resp. the charge Q on the electrodes (electrode surface A):

$$U = E \cdot d \qquad Q = D \cdot A \qquad\qquad (7\text{-}2)$$

This yields to the capacity of the plate capacitor C:

$$C = \frac{Q}{U} = \frac{D \cdot A}{E \cdot d} = \varepsilon \cdot \frac{A}{d} \qquad\qquad (7\text{-}3)$$

High permittivity ε of the dielectric (material between the electrodes), big electrode surfaces and small electrode distances lead to high capacities. The dielectric consists of molecules, whose positive charge centroids (atomic nucleus) and negative charge centroids (electron shell) cannot fall together due to their molecule structure (polar molecules). Hence in an external E-field they experience a resulting electrostatic force, which tries to align them in the direction of the E-field. The permittivity describes the amplification of the electric field in the dielectric by the aligned polar molecules of the dielectric, which are aligned by the electric field. Their self-field P (dielectric polarization) is super-imposed with the E-field to the resulting field D, which determines the accumulation of the charge Q on the electrodes.

$$\vec{D} = \varepsilon_0 \vec{E} + \vec{P} = \varepsilon \cdot \vec{E} \qquad\qquad (7\text{-}4)$$

In the homogenous isotropic dielectric the dielectric constant ε is a scalar. The **energy density w** (= energy per volume unit) in the electric field pair D, E is

$$w = \int_0^E \vec{D} \cdot \mathrm{d}\vec{E} = \frac{D \cdot E}{2} = \frac{\varepsilon \cdot E^2}{2} = \frac{D^2}{2\varepsilon} \qquad\qquad (7\text{-}5)$$

The stored electric energy W in a **capacitor** (plate distance d between plus- and minus plate, plate area A) (Fig. 7-1) is the product "volume $\times$ energy density":

$$W = (A \cdot d) \cdot \frac{\varepsilon \cdot E^2}{2} \qquad\qquad (7\text{-}6)$$
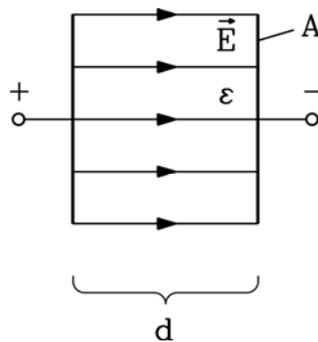

Fig. 7-1: Stored electric energy in an idealized plate capacitor (external field neglected, assumed homogenous internal field)

With (7-1), (7-2) the stored energy is expressed by the capacitor and the voltage.

$$W = \frac{C \cdot U^2}{2} \qquad\qquad (7\text{-}7)$$

If the capacitor is discharged over a resistance R, the current $\hat{i} = \dfrac{U}{R}$ flows in the first instance, and the instantaneous power $\hat{p} = \dfrac{U^2}{R}$ is generated in the resistance. The stored energy W is converted inside the resistance into thermal power $p(t)$, in which the charge from the plates flow off. Thus the voltage at the capacitor $u(t)$ and discharging current $i(t) = dQ/dt$ exponentially decrease with the time constant $T = R \cdot C$.

$$i(t) = \frac{U}{R} \cdot e^{-t/T} \qquad u(t) = U \cdot e^{-t/T} \tag{7-8}$$

Two types of capacitors are distinguished:
   a) physical capacitors
   b) electrochemical capacitors

a) **Physical capacitors** are based on the above described electric flux density D and the electric field E, between the amounts of electric charge Q, which are separated by a dielectric. At charging resp. discharging a displacement of conducting electrons in in the metal electrodes occurs, while in the dielectric only the alignment of the polar molecules happen, but no mass is moved (dielectric polarization is not to be mixed up with the electrochemical polarization of the accumulator electrodes (see chapter 6)). For the storability of energy the dielectric constant ε of the dielectric is decisive. For high permittivity D and Q is high, but E is small (7-4), so that the voltage U is sufficiently small and possible flashovers between the capacitor plates are not expected.

Table 7-1: Relative dielectric constants (permetivities) of different materials (dielectrics) (Clausert, H./ Wiesemann, G.: Grundgebiete der Elektrotechnik 1. Gleichstromnetze, Operationsverstärkerschaltungen, elektrische und magnetische Felder. 6. verb. Aufl., München 1993. Oldenbourg Verlag GmbH.)

Material	ε_r
Vacuum	1
Polyethylene	2,2 – 2,4
Aluminum oxide	9,3 – 11,5
Tantal oxide	27,6
Water	80

The specific capacity per cm^2 of electrode surface has for physical capacitors a magnitude of some 100 pF/cm², and is thus relatively low. But relatively high voltages U up to 400 V are possible.

b) **Electrochemical capacitors:**
The capacitor principle can also be build up by electrochemical electrodes. This charge separation system is based on the effect described by *Hermann Ludwig Ferdinand von Helmholtz (1821 - 1894)* already in 1856. It is about the building up of an electric double layer when applying a voltage to an electrode which is plunged in a conductive liquid, like it is described in chapter 6 for the galvanic cell. This double layer is characterized by series connection of an electronically (e. g. metal electrode) and an ionically conducting electrode (e. g. electrolyte) (chapter 6). In equilibrium it comes to a charge transition from one phase to the other because of the Fermi-energy-level at the border area (phase transition) between them („partial pressure compensation" – diffusion law and reversing electrostatic force). The consequence is a accumulation of charges at the phase border in the **electrochemical double layer**, which thus builds a capacitor, which has a very small „electrode distance" d. This results into very small voltages U, but very high capacities C. For this double layer capacitor the distance d of the charge separation lies in the range of ion radius (~ 10 Å resp. 1 nm). Depending on the physical principle of

operation, used materials or storable amount of energy different denotations are used (table 7-2, according to *B. Conway*).

Table 7-2: Nomenclature for electrochemical capacitors according to *B. Conway* (VDI-Gesellschaft Energietechnik: Energietechnik für elektrische Netze. Tagung Gelsenkirchen, 10./11. November 1998. VDI-Berichte 1404. Düsseldorf 1998. VDI-Verlag.)

Principle of operation	Material	Energy quantity
Double layer storing: *Double layer capacitor (DSC), electrical double layer capacitor (EDLC)*	Carbon: *Carbon capacitor*	*UltraCap*
Faraday storing: *Faraday capacitor, Redox capacitor*	Ruthenium: *Ruthenium capacitor*	*SuperCap*
	Conductive polymers: *Polymer capacitors*	

The different types of capacitors of Table 7-2 are explained in the following sections.

7.1 UltraCaps
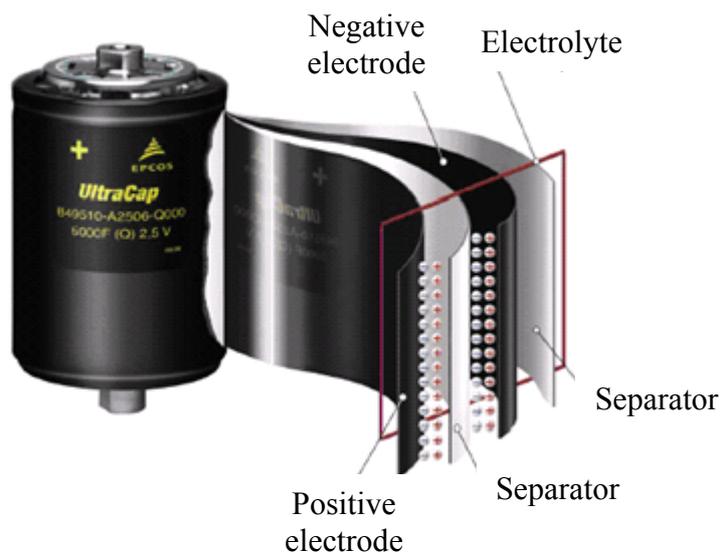
Fig. 7.1-1: Structure of an UltraCapacitor (http://www.epcos.com/inf/20/35/ds/ultracap_2005.pdf)

UltraCaps are storage systems, which close the gap between batteries and common capacitors concerning energy and power density.

Table 7.1-1: Comparison of typical values for power and energy densities of the three energy storage systems of „phsyical capacitors", Ultracaps, accumulators (batteries) (http://www.epcos.com/inf/20/35/ds/ultracap_2005.pdf)

		Physical capacitors („conventional" capacitors)	UltraCaps	Battery
Power density	W/kg	> 10000	5000	300
Energy density	Wh/kg	0.1	4	40
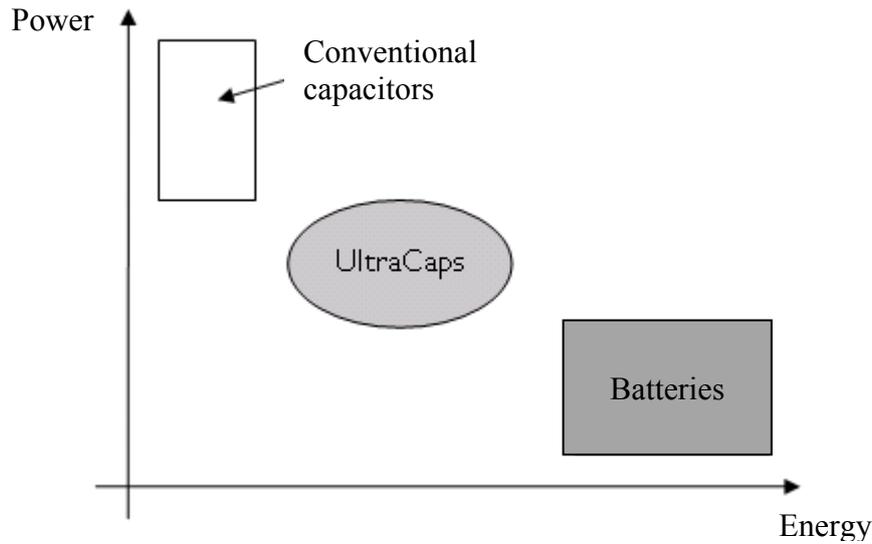
Fig. 7.1-2: *Ragone*-diagram the three energy storage systems „physical (= conventional) capacitors", UltraCaps, accumulators (batteries) (VDI-Gesellschaft Energietechnik: Energietechnik für elektrische Netze. Tagung Gelsenkirchen, 10./11. November 1998. VDI-Berichte 1404. Düsseldorf 1998. VDI-Verlag.)
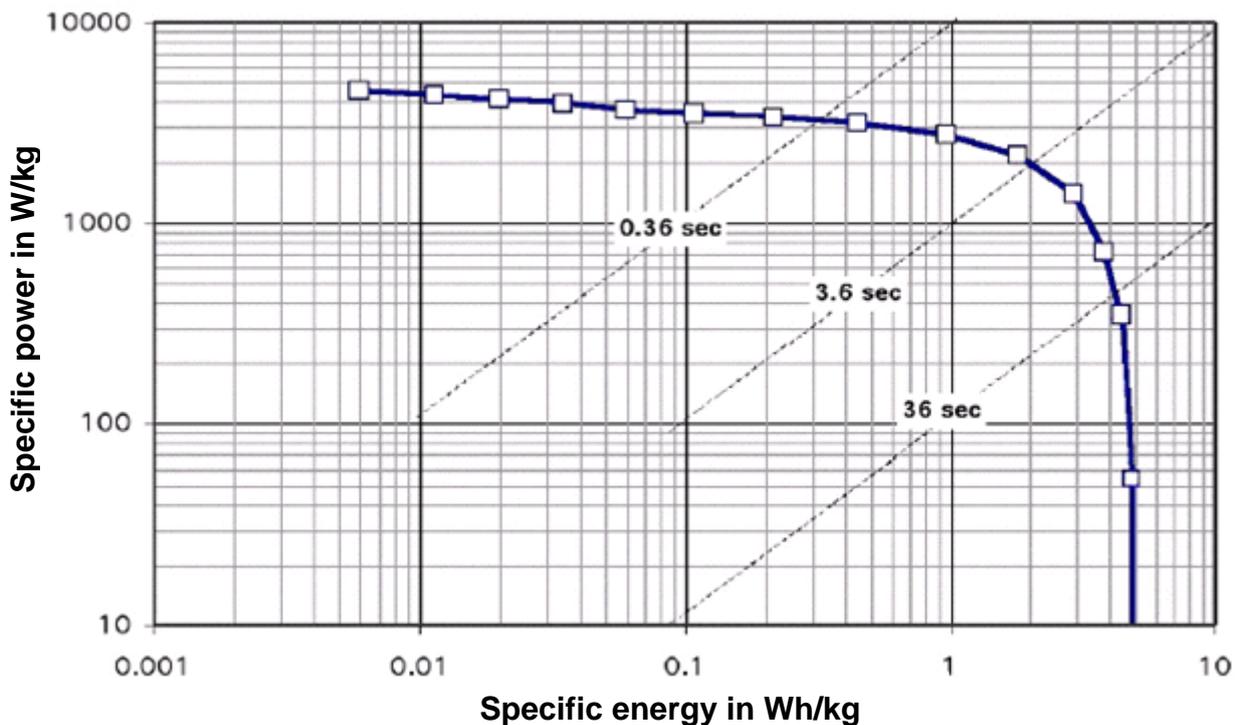
Fig. 7.1-3: *Ragone*-diagram of a typical double layer capacitor with organic electrolyte
(Kasseler Symposium Energie-Systemtechnik: Kötz, R.: Doppelschichtkondensatoren – Technik, Kosten, Perspektiven. http://ecl.web.psi.ch/Publications/cap_pub/ISET2002.pdf)

The significance of these maximum values is of small importance for the practical application. The reason is that the maximum energy is available only at low power and maximum power can only be withdrawn for short time (*Ragone*-diagram Fig. 7.1-3). For its creation a double layer capacitor with organic electrolyte and a capacity of 1800 Farad was used. Under assumption of a linear approximation the data were calculated with measuring of the impedance. The operating range of the capacitor has a time constant $T = RC$ of about 4 seconds; here almost half of nominal energy can be used at half of nominal power.

The double layer capacitors reach capacities of 5 up to 5000 Farad, the values of voltage are around 2.5 V. With 500.000 cycles the capacitors are robust against aging compared to batteries.
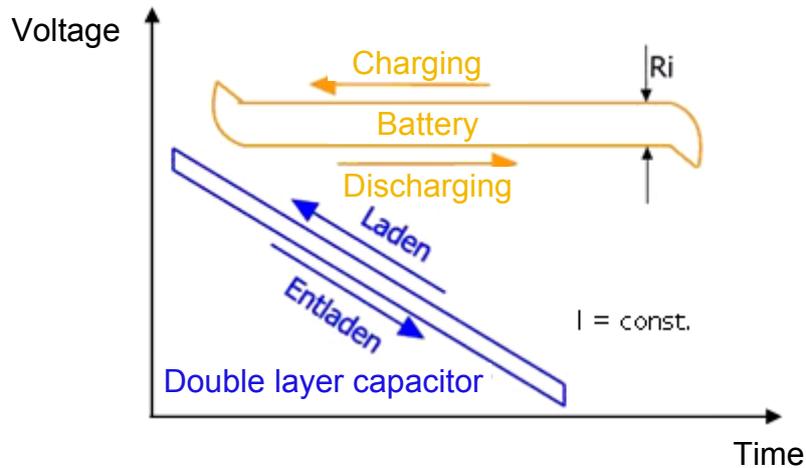
Fig. 7.1-4: Comparison of charging and discharging curves of double layer capacitor and battery
(http://www.udomi.de/Fuellcell/ultracap-basics.html)

In UltraCaps active carbon is used as electrode material. Mainly organic electrolytes on the basis of quaternary salts like tetra-acetyl-ammonium-borofluoride (TEABF) and acetonitrile or propylene-carbonate are used as solution. Organic electrolytes allow a cell voltage of about 2.5 V. Higher voltages can be applied for short time, but they reduce the lifespan of the capacitor. The relatively low specific conductivity of organic electrolytes of about 20 mS/cm is a drawback („high internal resistance R_i"), which reduce the power density of the UltraCap ($\sim \dfrac{U^2}{R_i + R}$). Watery electrolytes like potash lye (KOH) or sulfuric acid (H_2SO_4) are only used in few capacitors. Although cells with watery electrolytes only have a rated voltage of maximum 1.2 V, the higher conductivity of the electrolyte of about 1 S/cm leads to a significantly smaller internal resistance and thus allows higher power densities.

UltraCaps have due to the porosity of the carbon a surface of up to 2000 m²/g (per gram carbon). A little bit more than 20 to 40 µF/cm² can be stored. For these capacitors the charge separation does not depend on the plate distance but on the diameter of the ions. The following figure shows the interplay between porosity of the carbon electrode and the size of the ions.
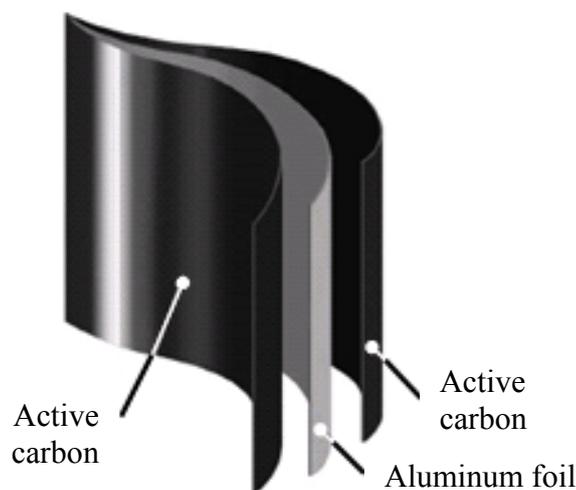
Fig. 7.1-5: Structure of an electrode of an UltraCap (http://www.epcos.com/inf/20/35/ds/ultracap_2005.pdf)
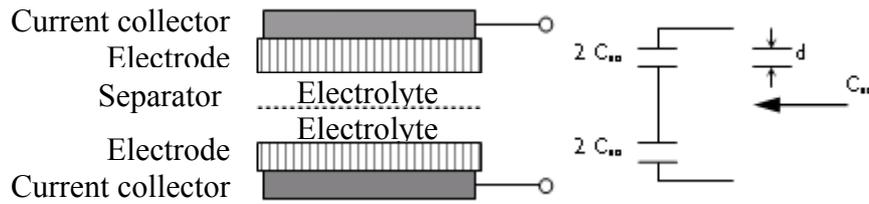
Fig. 7.1-6: Schematic structure of an UltraCaps end electric equivalent circuit (Miller, J. M.: Propulsion systems for hybrid vehicles. London 2004.)
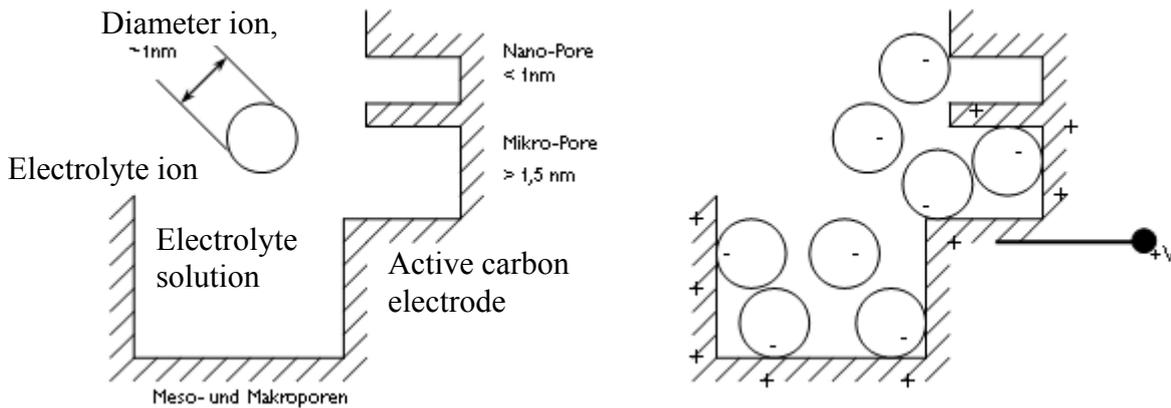
Fig. 7.1-7: Schematic sketch of a double layer capacitor (Miller, J. M.: Propulsion systems for hybrid vehicles. London 2004.)

Pores, which size is in the range of nanometer, cannot be occupied by ions. If the pores are only in this size, the for double layer capacitors typical effect does not occur neither for watery nor for organic electrolytes. The number of charge carriers cannot be arbitrarily increased, because with increasing charge the voltage increases. If the voltage and hence the energy of the electrons becomes too high that they can pass the phase border, the capacitor generally degenerates. This is identical with the „breakthrough" of the conventional capacitor. In electrochemistry these reactions, which are related with such high charge flow through the double layer, are called *Faraday*-reactions. The voltage and the number of charge carriers in the double layer should be kept as small as possible, so that no *Faraday*-reaction can occur. The charge storing in the double layer is done non-*faradaic* and only on an electrostatic basis. The breakthrough voltage is hence determined by the degeneration voltage of the electrolyte. This voltage depends on the material and the temperature and is for watery electrolytes about 1.5 to 2 V. Therefore the maximum limit of the operating voltage is maximal 1.5 V for double layer capacitors. For organic electrolytes electrolyte degeneration voltage is higher and has a value of about 3 to 4 V. As the conductivity of organic electrolytes is considerably lower than the ones of watery electrolytes, everywhere, where relatively high energies, but not extremely high powers are required, the organic electrolytes will be preferred. In electric and hybrid vehicles ultracapacitors are used to cover power peaks and additionally for the feedback of braking energy. Energy densities of 5 Wh/kg are required for this application. As according to Table 7.1-1 power density of batteries is limited, especially for short time accelerating and braking in hybrid vehicles, a combination of a battery together with an electrochemical capacitor is sensible (Fig. 7.1-8). Also for purely electric vehicles this combination can be used in order to protect the batteries. The specifications from Fig. 7.1-8 were recorded with an electric vehicle in city traffic, once with UltraCap and once without. The capacitor was connected in parallel to the battery. A significant difference in the battery power can be observed. While without UltraCap the battery has to face the power peaks, the power remains quite constant with UltraCap. The power peaks are hereby caught by the capacitor.
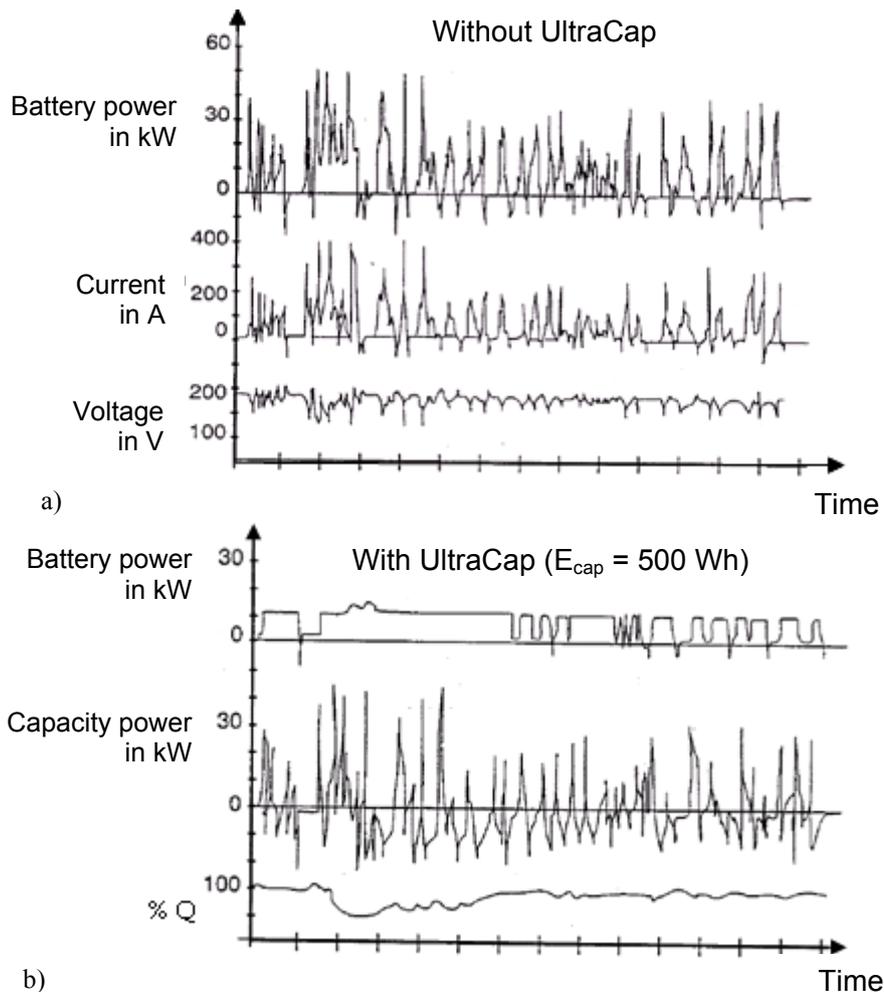
Fig. 7.1-8: Driving cycle of a battery powered E-vehicle in city traffic a) without, b) with UltraCap in parallel to the battery (http://www.nesscap.com/prod/Articles/Univ.%20of%20Alberta.pdf)

Catching the power peaks with an UltraCap helps to protect the battery. For example lead-batteries face a faster aging due to the high power peaks in city traffic. Also the withdrawable capacity decreases at a discharge with constant current. Furthermore the ultracapacitor can store the partially high braking powers of electric and hybrid vehicles. In order to store the maximum amount of energy in an UltraCap the applied voltage has to reach its maximum value. UltraCaps with organic electrolytes are – like mentioned – limited to 2.7 V. When 3 V are exceeded, the cell starts gassing. When the voltage increases above 4 V, the cell bursts after short use.

Due to the low cell voltage, many cells have to be connected in series, in order to reach a sufficient high operating voltage. Furthermore power electronic DC/DC-converter (= pulsed step-up converters) are used, in order to raise the low operating voltage of the UltraCaps to a higher DC-voltage level. Due to small differences from cell to cell (the real capacity value can be up to 10 % below or 30% above nominal capacity), the voltage would not be distributed evenly over the cells in series connection. This can lead to considerable over voltage and hence over loading and early failure, which leads in a domino effect to over voltages in the remaining cells, which again lead to failures of those cells and finally to total failure. Common techniques for cell voltage compensation (consistent cell voltage) are passive or active components resp. high loss or low loss equalizer. These initial problems, due to which the voltage of in series and parallel connected UltraCaps has to be watched and symmetrized, in order to avoid over loading, are overcome by continuous development of UltraCaps. Due to their high power density and the hope of increasing the number of cycles a big future is forecasted for this power electronic storage.

7.2 SuperCaps

Only for few electrochemical reactions the electric behavior of voltage decrease with discharging of a capacitor is observed, although the charge flow through the electric double layer happened. When charge penetrates the double layer it may come to grave structure changes due to redox reactions (*Faraday*-reaction). Redox reactions are chemical reactions, which consist of the part reactions oxidation and reduction. In the in Fig. 7.1 described electrochemical reactions this is not the case.

The for the *Faraday*-reaction typical electric behavior of a strong voltage change at the electrodes at charging discharging, which is due to the maintaining of the crystal structure with an simultaneous changing of oxidation state, is modeled in the electric equivalent circuit by a "pseudocapacity".
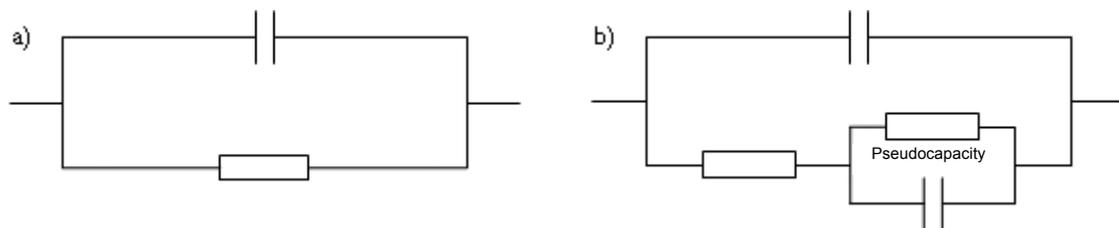
Fig. 7.2-1: Equivalent circuit of electrochemical capacitor electrodes
a) EDSC-electrode; b) electrode with *Faraday*-reaction
(Kasseler Symposium Energie-Systemtechnik: Kötz, R.: Doppelschichtkondensatoren – Technik, Kosten, Perspektiven. http://ecl.web.psi.ch/Publications/cap_pub/ISET2002.pdf)

Especially the so called intercalation reactions show a *Faraday*-behavior.
There are two material classes of bigger practical interest:
      a) Ruthenium oxides   → Proton intercalation
      b) Conductive polymers   → Li^+- and anion intercalation

a) For the use of **ruthenium-materials** capacity values of up to 720 F/g (je per gram electrode material) were measured. The high specific capacity compensates the low cell voltage of 1 V. The reason for this low value is that ruthenium oxide can only be used with watery electrodes. The material costs of ruthenium oxide are very high. For that reason capacitors made of this material are only suitable for special applications or smaller capacitors. Here the costs lose their importance

b) The developments of **conductive polymers** mainly concentrate on poly-acetylenes, polypyrroles, polyanilines, polyphenylenes and the polythiophenes. The achieved specific capacity values are similar to those of the ruthenium oxide. For instance a value of 400 F/g for polypyrroles was reported. The biggest development problem is the permanently decreasing capacity during operation over the lifespan. This effect comes from chemical instabilities like traces of water oxidation appearances.

8. Battery management system

In a battery system the weakest module determines the whole electric operating behavior. Hence it is necessary to guarantee a good operational behavior for the weakest module. In modern battery systems battery management systems (BMS) are included, which aim for the following goals:
-       Increase of lifespan
-       Increase of reliability
-       Increase of economy
-       Determination of state of charges for calculation of the remaining range in a battery powered vehicle resp. for information of the energy management system of drive components in a hybrid vehicle. For this purpose the BMS has to observe and control charging and discharging process.

Because of the decentralized structure of modern battery systems the communication between each single component is realized by a bus system. The battery has to fulfill the following requirements, so that an optimal operating behavior can be provided:

- Cell resp. module voltage within permitted limits
- Control of charging and discharging process in the given frame, where necessary with charge compensation
- Current limiting as deep discharging protection
- Battery tempering in operating range
- Temperature compensation between every module

The storing of operating data for diagnosis purposes and for regulations of von warranty claims is another point. To fulfill these requirements the following measurable quantities are available to BMS:

- Battery module resp. battery cell voltage
- Battery current
- Battery temperatures

By the evaluation of these physical quantities and by satisfaction of the requirements by the BMS it shall be ensured, that no deviations in the operating behavior of the battery modules occur and thus the aging behavior of each cell have a similar course. Thus e. g. a voltage and temperature sensor can be associated to each module (Fig. 8-1). Every partial voltage is measured and evaluated by the BMS and by a comparison of these data defect modules can be detected. The task of the battery management system can be an after treatment (e. g. by charge compensation) or a request to the user resp. to the service to replace the detected module.
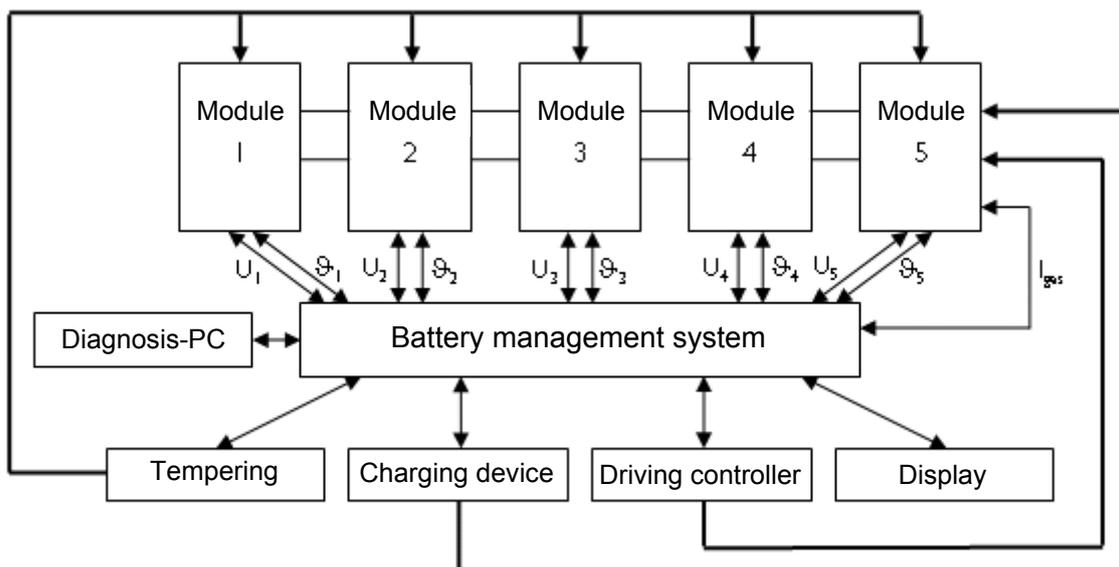
Fig. 8-1: Basic structure of a battery management

A current monitoring is necessary for controlling of charging current and for detecting short circuits. A controlled cooling resp. heating system with air or water realizes the tempering. The position of braking- and „gas pedal" is recognized; both pedals are included in the driving controller.

Overcharging and deep discharging can damage the battery resp. accelerate their aging. The BMS is supposed to avoid these operating states. Within the frame of the battery aging the parameters of each module vary. For instance the internal resistance can increase and the withdrawable capacity can become smaller. An indicator for a beginning **deep discharging** is a certain voltage level. For lead batteries this voltage is about 1.7 V. As protection against deep discharging the battery management system

automatically limits the current. Hence the vehicle can only be run with reduced power. Only in danger situations the current limit can be removed by a „kick-down" of the driving pedal.

For older battery systems an uneven module capacity may occur, which should be compensated for lifespan increase, because otherwise damages may occur. The problem is, that e. g. during charging some modules have already exceeded full charging - and are hence over charged and start gassing - , while other ones are still not fully charged. A method for charge compensation is the **shunting (by-passing).** In this procedure a part of the charging current is bypassed past the fully charged modules by a power electronic switching device. The weaker modules receive the stronger charging current. The charging efficiency decreases with the amount of modules with active by-pass.
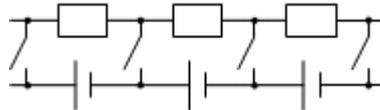
Fig. 8-2: Basic structure for shunting

For tractions batteries it is possible to be run in their optimal temperature range. For all modules the same operating behavior and hence the same temperature conditions shall be realized. It can be observed that the temperature inside the battery tray is higher than at the edge. Different temperatures yield to differently fast electrochemical reactions and thus different long term behavior. An exceedance of the admissible temperature range can lead to remaining damages. Hence the task of the battery management system is the interfering in charging and discharging, if the admissible temperature range is exceeded and there is no air-conditioning. For compensation of the temperature of each of the modules either water or air cooling can be used. The temperature difference between the hottest and the coldest point of the module can be kept to below $\Delta\vartheta = 5$ K in case of good cooling conditions. Due to this lower temperature difference temperature sensors become necessary in order to determine the hottest and coldest point of the battery. Another advantage is that under good cooling conditions the battery can be easier run in the admissible temperature range.

    a) Air cooling: For cooling with air a separated ventilation is required. Parallel air paths through the battery system have to be optimized due to different air gaps and flow cross sections.

    b) Water cooling: A water cooling is realized by water pockets resp. double-walled modules, which are connected to a water circuit by hoses. The water pump circulates the water at low power. The flow cross sections are significantly smaller than in a).

In order to estimate

    a) The remaining range of the battery powered electric vehicle

    b) The available power for acceleration and the possible intake of recuperative braking energy of a hybrid vehicle

The knowledge of operating data of the battery is necessary. The sum of those data is called „internal state". The temperature, age, number of cycles, internal resistance and state of charge is recorded.

The withdrawable capacity of a battery does not only depend on the discharging current, but also depend on this „internal state ". Due to the non-linear correlation of the single parameters the determination of the state of charge is very complicated (Fig. 8-3).

    a) Procedures for measuring the chemical active material on the electrodes for determination of state of charge (Fig. 8-3a) are currently only under big effort feasible for an automobile-appropriate serializing.

    b) That is why charge equilibration (one of the methods from Fig. 8-3b) is the classic method for determination of state of charge in the vehicle. The withdrawn charge during operation is measured by the line currents:

$$Q_{\text{out}} \int_{t=0}^{t_{\text{ab}}} i(t)\mathrm{d}t \qquad\qquad (8\text{-}1)$$

From this the state of charge is calculated (mostly given in % of the capacity C (= nominal amount of charge Q_N)).

$$SOC = 1 - \frac{Q_{\text{out}}}{Q_N} \qquad\qquad (8\text{-}2)$$

The drawback of this method is the over the application duration non-constant remaining value $C = Q_N$. The capacity C at full charge depends on temperature, discharging current, loading profile and aging behavior. For recalibration full charge is presumed. Hence for longer stand-still times the self-discharging is to be considered.

a)
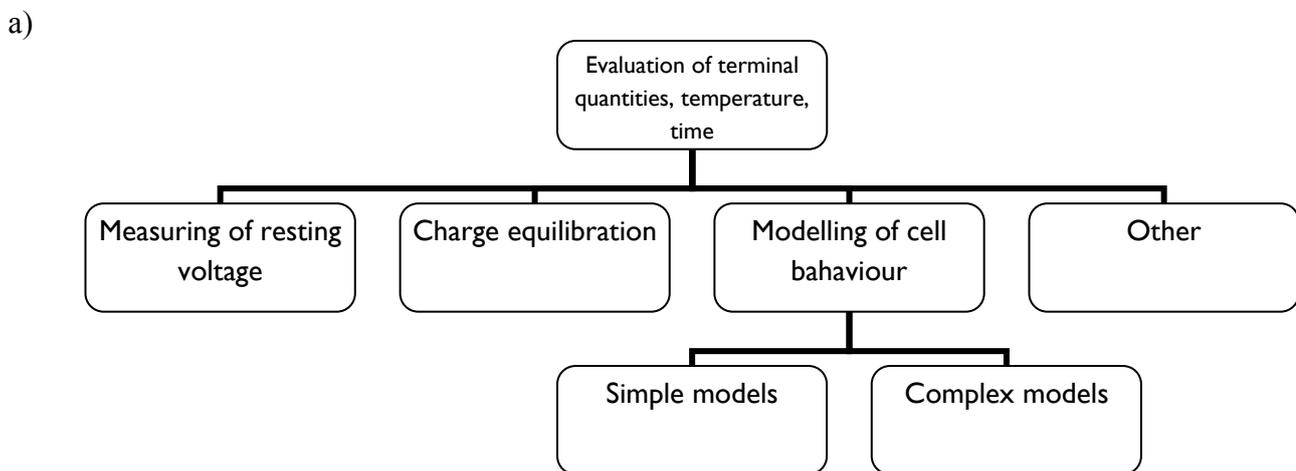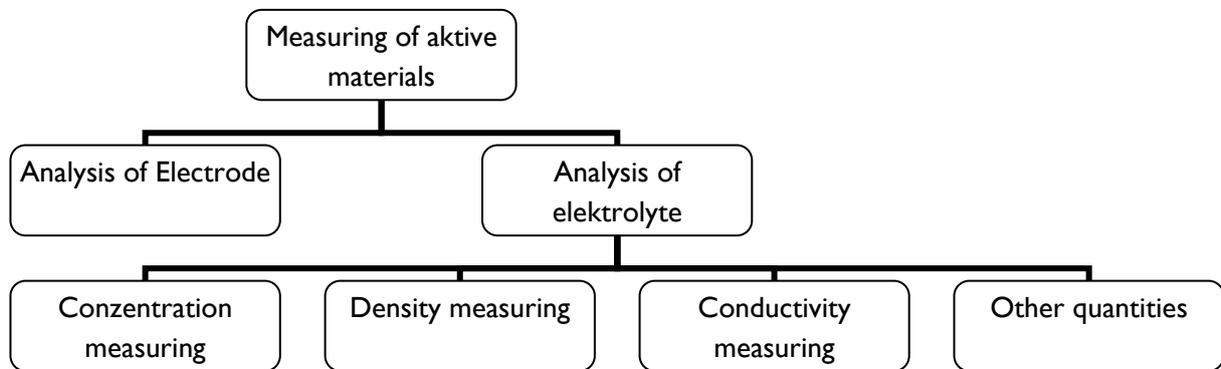
b)

Fig. 8-3: Two different methods a) and b) for determination of the state of charge of a battery

Methods, which describe physical models, are more effective. Simple models represent the battery according to equivalent circuits, more complex models us professional knowledge, which e. g. is represented by a fuzzy system.

Energy management system for battery and UltraCap:
UltraCaps are mainly used at peak power, that means when high power has to be stored in short time or has to be available, because batteries are less suitable for this operating state. In order to optimally use the withdrawable capacity of a battery, the battery should be discharged with constant current. Average loads should be withdrawn from the battery and peak loads from **power-assist power storage**, like for instance

an UltraCap. Those capacitors should be charged by a DC-DC-converter in phases of low current demand or by recuperation of braking energy.

The interaction of both energy storages is controlled by an **energy management system (EMS)**. If the EMS recognizes a collapse of the battery voltage, it is being assumed that it is being accelerated and the UltraCap is discharged by the boost-mode. But if the battery voltage significantly increases, it is a hint for recuperation of braking energy. By the buck-mode energy is stored in the UltraCap.
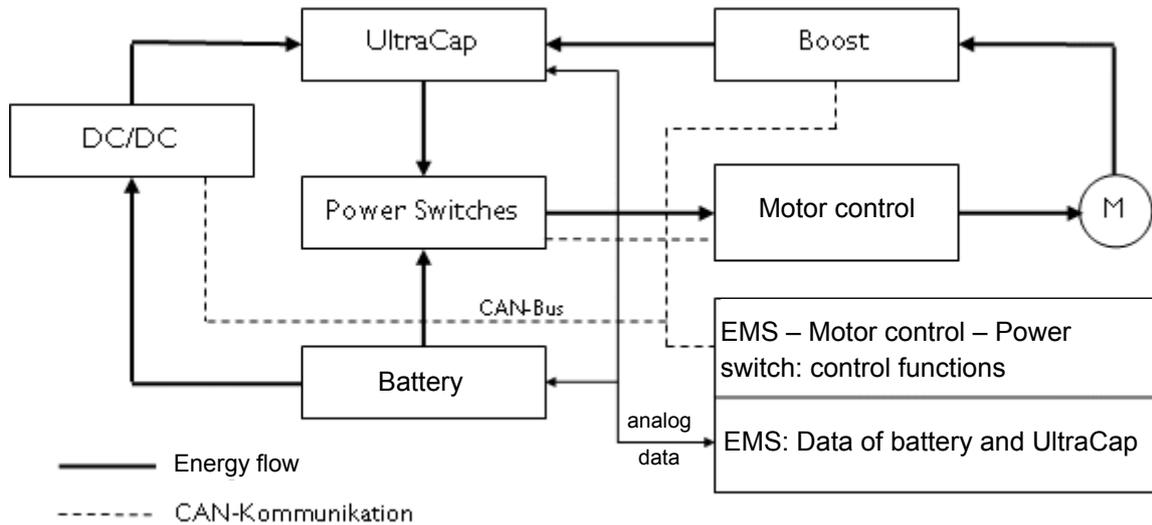
Fig. 8-4: Structure of the energy management system with switched battery- and power–assist-UltraCap-storage

The state of charge can also be controlled depending on the vehicle speed. At low speed the UltraCap should be recharged, because a soon acceleration of the vehicle is to be expected. Contrary at high speed a braking is to be expected and thus recuperation of braking energy. In order to capture this, the UltraCap should be discharged before.

In non-accelerating phases the energy should be delivered by the battery. As soon as the EMS releases the charge, the UltraCap is also being recharged by this charge. Accelerations are driven from the UltraCap. The EMS records data of the battery and the UltraCap and sends control signals to the power switch, the DC/DC-converter and the boost-converter.

9. Electric street vehicles

Nowadays the majority of companies, working in the automobile industry, introduce electric vehicles to the market. In the following a brief historical overview about electric vehicles of some manufacturers shall be given, as far as there is enough information published about their drives system. The presented models are of course not complete. The sequence of their presentation gives no ranking, but is arbitrarily.

9.1   *VW*

As the only big-series-manufacturer of electric vehicles on the *German* market until 2007 *VW* is to be mentioned. Since the 70s *VW* equipped several models of the *Golf* with an electric drive, in which different battery systems were used.

9.1.1   *Golf City-Stromer*

In 1994 the *VW Golf City-Stromer* on the basis *Golf III* went in series production. It was mainly offered to major customers and administrations and was sold 300 times *European*-wide. *Volkswagen* thus was the first manufacturer, which brought an electric vehicle to series maturity and sold it. The *Golf City-Stromer* was driven by a 6-pole-PM-synchronous-motor by the company *Siemens AG* and had a 5-stage switching gear.

Fig. 9.1.1-1: *Golf City-Stromer*

Table 9.1.1-1: *Golf City-Stromer* – Technical specification (Josefowitz, W., Köhle, S.: *Volkswagen* Elektro- u. Hybridfahrzeuge, Aktivitäten bei Hybrid-Antriebssystemen in Vergangenheit, Gegenwart und Zukunft und Beschreibung von Schlüsselkomponenten und deren Einfluss auf den Kraftstoffverbrauch, Braunschweiger Symposium, TU Braunschweig 2002)

Motor: PM-synchronous motor		
Power	18/25	kW
Battery: Lead-gel		
Voltage	96	V
Energy	11.4	kWh
Weight	480	kg
Driving performance		
v_{max}	100	km/h
Maximum slope	20	%
Acceleration from 0 to 50 km/h	13	s
Range	50 - 60	km

9.1.2 *Bora & Golf Electric*

Two more recent models, which *Volkswagen* equipped with an electric drive, are the *Golf* and the *Bora Electric*. Both can be equipped with drives of different power classes. Accelerations of 0-100 km/h in 12 seconds or maximum speeds of max. 140 km/h depending on the drive are possible. The needed energy is provided by Li-ion-batteries, which weight is 300 kg.

Fig. 9.1.2-1: *VW Bora Electric* & *VW Golf IV Electric* (http://www.elektroauto-tipp.de)

9.2 Daimler-Chrysler

9.2.1 *A-Class ZEBRA*

The *A-Class ZEBRA* is a purely electric vehicle, which is (name!) equipped with a *ZEBRA*-battery (NaNiCl – high-temperature-battery by *AEG Anglo Batteries*).

Fig. 9.2.1-1: *A-Class Zebra* (http://www.elektroauto-tipp.de)
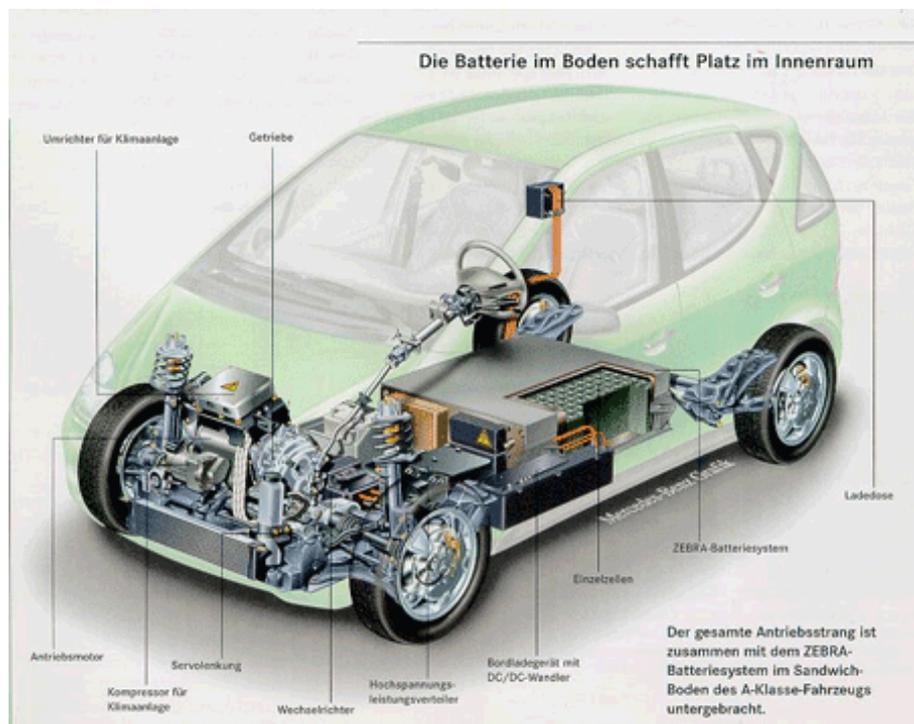
<u>Table 9.2.1-1:</u> Technical specification of the *Zebra-A-Class* (http://www.elektroauto-tipp.de)

Driving performance		
Acceleration from 0 to 100km/h	16.5	s
Max. speed (km/h)	130	km/h
Range (km)	200	Km
Battery: NaNiCl (Manufacturer: *AEG Anglo Batteries*)		
Amount	1	
Nominal capacity	104	Ah
Rated voltage	289	V
Voltage range	193-347	V
Power density	155	W/kg
Energy density	81	Wh/kg
Dimensions (L x B x H)	993x793x280	mm
Number of cells	448	
Max. output power (80% DOD, 2/3 OCV, 30s, 335°C)	56	kW
Max. output current < 1 min	260	A
Coolant	oil/water	
Admissible ambient temperature Battery	-40 to +70	°C
Weight		
Empty weight with battery	1380	kg
Weight – battery	370	kg
Admissible total weight	1730	kg
Charging device		
Voltage single phase	230	V
Charging duration with board charger	7	h
Charging duration with external charger	1	h
Dimensions		
Length	3575	mm
Breadth	1719	mm
Height	1601	mm
Motor: Squirrel cage induction machine		
Continuous power	30	kW
Peak power	50	kW
Max. speed	9700	min^{-1}
Max. torque	180	Nm

DOD: Depth of Discharge, OCV: Open Circuit Voltage

However, the further development of the *A-Class* with an alternative drive concept the concern increasingly concentrated on the *NECAR 3, 4* and *5*, which were equipped with a fuel cell drive.

9.2.2 *Epic* Minivan

1998 *Chrysler* introduced *Epic Minivan*, which was planned for fleet cars. *EPIC* stands for „**E**lectric **P**owered **I**nterurban **C**ommuter". The *Epic* was created on the basis of two other vehicles by *Chrysler* - on the one hand on the *Dodge Caravan* and on the *Plymouth Voyager* on the other.

Table 9.2.2-1: Technical specifications of the *Chrysler Epic Minivan* (http://www.elektroauto-tipp.de)

Motor: Induction motor (Manufacturer: *Siemens AG*)		
Continuous power	55	kW
Peak power	73	kW
Battery: NiMH (Manufacturer: *SAFT*)		
Voltage	336 (28x12)	V
Driving performance		
v_{max}	135	km/h
Acceleration from 0 to 100 km/h	17	s
Range	135 - 150	km

Fig. 9.2.2-1: *Chrysler Epic Minivan* (http://www.elektroauto-tipp.de)

9.3 BMW

Before *BMW* concentrated on the development of fuel cell vehicles, the enterprise gathered already in the 80s experience in the domain of high power batteries, especially on the basis of the sodium-sulfur-battery. In the course of this development work the first experimental vehicle with an electric drive was presented in 1991 by *BMW* - the *BMW E1*.

Fig. 9.3-1: *BMW E1* (http://www.elektroauto-tipp.de)

Table 9.3-1: Technical specification of the *BMW E1* (http://www.elektroauto-tipp.de)

Motor		
Power	32	kW
Torque	150	Nm
Battery: Sodium-sulfur		
Voltage	120	V
Capacity		
Energy content	19	kWh
Driving performance		
v_{max}	120	km/h
Acceleration from 0 to 50 km/h	6	s
Range	250	km

9.4 *Opel*

In the 90s *Opel* equipped vehicles with electric drives. The *Opel Astra Impuls 2* and *3* served as modeling platform. Newer development efforts made by *Opel* concentrated, like other *German* manufacturer, on fuel cell and hybrid vehicles.

Fig. 9.4-1: *Opel Astra* platform (http://www.elektroauto-tipp.de)

Table 9.4-1: Technical specifications of the *Opel*-electro-models (http://www.elektroauto-tipp.de)

Model		*Opel GT*	*Opel Kadett Impuls*	*Opel Astra Impuls 2*	*Opel Astra Impuls 3*
Year		1970	1990	1991	1993
Battery		Ni-Cd	Ni-Cd	Lead-acid	Ni-Cd or NaNiCl$_2$
Range	km	44	80	70	160
Power	kW	100	20	85	45
v_{max}	km/h	100	100	120	120

9.5 *Ford*

9.5.1 *e-KA*

In cooperation with the French enterprise *SAFT* the *Aachener Ford-Forschungszentrum* developed the lithium-ion-battery system, which is characterized by its high energy density and storability. This technology was realized for a pure electric car by *Ford* for the *e-KA* and presented to the audience in May 2001.

Fig. 9.5.1-1: *Ford e-KA* (http://www.elektroauto-tipp.de)

Table 9.5.1-1: Technical specification of the *Ford e-KA* (http://www.tuningford.de/sonder_ka_elektroantrieb.htm)

Motor: Squirrel cage induction motor		
Power	65	kW
Torque	190	Nm
Battery: Lithium-ion		
Voltage	120	V
Energy content	28	kWh
Weight	280	kg
Driving performance		
v_{max}	130	km/h
Acceleration 0-50 km/h	3.9	s
Acceleration 0-100 km/h	12.7	s
Range	>150	km
Range at v = 80 km/h	200	km

9.5.2 *Ranger*

The *Ford Ranger* is produced in series since its market introduction in 1998 in the *USA* and is still one of the few purely electric vehicles available on the market. It also has the possibility to feed energy back to the batteries during driving. It is equipped with a four-pole induction machine in transaxle design with a water jacket cooling by the company *Siemens AG*.

Fig. 9.5.2-1: *Ford Ranger* (http://www.elektroauto-tipp.de)

9.5.3   *Th!nk*

In 1998 *Ford* started the production electric vehicles by buying producer of the *Norway* „*Pivko*" and starting their own production. Out of this the **Th!nk** came into being. But the marketability of this model suffered like the ones of many other models under the limited battery capacity, so that *Ford* eventually ended the production in 2002.

Fig. 9.5.3-1: *Ford Th!nk* (http://www.elektroauto-tipp.de)

Table 9.5.3-1: Technical specification *Ford Th!nk* (http://www.elektroauto-tipp.de)

Motor: Induction motor		
Battery: Nickel-cadmium (manufacturer: *SAFT*)		
Energy content	11.5	kWh
Driving performance		
v_{max}	90	km/h
Range	85	km

9.5.4 *Ford Transit Connect Electric*

The *Ford Transit Connect Electric* is a compact van, which is especially suitable for delivering and distribution traffic in limited regions. The car is based on a conventional *Ford Transit*, which was nominated as the "truck of the year" in *North America* in 2010. The electric version is produced by *Ford* and the *American Azure Dynamics Corporation*, which is responsible for the patented „*Force Drive*". The *Azure Dynamics Corporation* belongs world-wide to the technology-leaders of electro-hybrid-drives, electric components and drive systems.

Fig. 9.5.4-1: *Ford Transit Connect Electric* (http://media.ford.com)

Table 9.5.1-1: Technical specifications of the *Ford Transit Connect Electric* (http://media.ford.com/)

	Specification		
	Length	4587	mm
Dimensions	Breadth	1795	mm
	Height	2014	mm
	Wheelbase	2910	mm
	Trunk volume	3822	l
	Empty weight	1790	kg
Loading	Admissible weight	2244	kg
	Load capacity	454	kg
	Seats	2	
	Energy consumption	218	Wh/km
Driving performance	Range	128	km
	v_{max}	120	km/h
	Nominal voltage	672	V
	Electric charge	41	Ah
Battery	Energy	27522	Wh
	Weight		
	Energy density		
	Type	Induction machine	
Motor data	Rated power		
	Max. torque	235	Nm

9.6 *Renault*

9.6.1 *Renault Clio électrique*

Apart from a DC-machine by the company *ABB* also an induction machine by the company *Siemens AG* was tested as a drive.
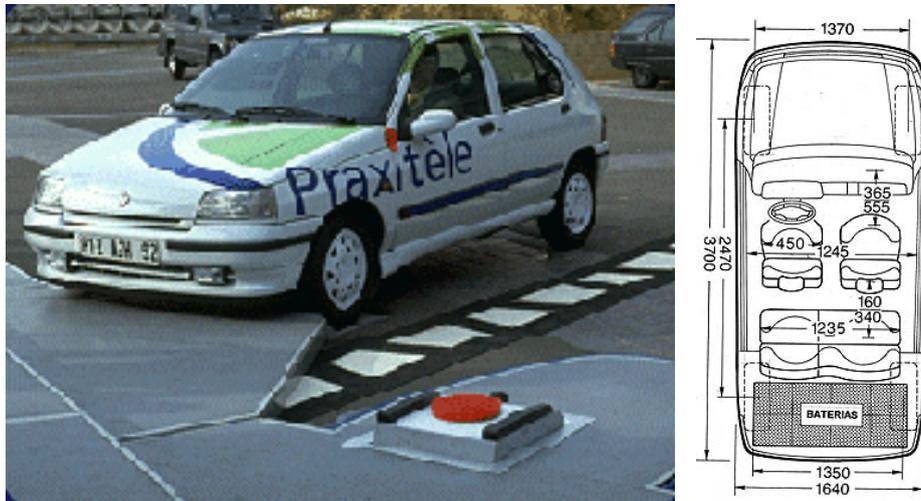
Fig. 9.6.1-1: *Renault Clio électrique* (http://www.elektroauto-tipp.de)

Table 9.6.1-1: Technical specifications of the *Renault Clio électrique* (http://www.elektroauto-tipp.de)

Motor: DC-motor (manufacturer: *ABB*)		
Rated power	16.3	kW
Max. power	21.7	kW
Max. torque	135	Nm
Battery: NiCd		
Amount	19	
Voltage	114	V
Capacity	100	Ah
Energy consumption	0,22	kWh/km
Driving performance		
v_{max}	95	km/h
Acceleration from 0 to 50 km/h	8.5	s
Range	80	km
Weight	1150	kg

9.6.2 Renault Kangoo électrique

There are versions of the *Renault Kangoo électrique* with NiCd-batteries as well as with Li-ion-batteries by the manufacturer *SAFT*. The energy content is 28 kWh.

9.6.3 Kangoo Rapid Z.E.

On the *IAA* (*Internationale Automobil-Ausstellung*) in September 2010 in *Frankfurt/Main* the *Renault Kangoo Rapid Zero Emission* was publicly presented for the first time. The line produced delivery van will be available for 24.000 € on the *German* market. However the batteries are not included in the price. Those have to be leased from *Renault* for a term of 48 months for mileage of 15.000 km/year. The leasing costs are 85.68 € per month. The advantage for the customer is that the single costs are lower and after four years it can be switched to a new battery technology, without having to dispose the old batteries resp. to store them. Nevertheless a drawback is the bond to *Renault* for four years. The electric delivery van as

well as the *Ford Transit Connect Electric* are interesting alternatives for delivery services or craft enterprises.

Fig. 9.6.3-1: *Kangoo Rapid Z.E.* (http://www.renault-ze.com)

Table 9.6.3-1: Technical specifications of the *Kangoo Rapid Z.E.* (http://www.renault-ze.com)

	Specification		
	Length	4213	mm
Dimensions	Breadth	2133	mm
	Height	1818	mm
	Wheelbase	2697	mm
	Trunk volume	3500	l
	Empty weight	1410	kg
Loading	Admissible weight	2060	kg
	Load capacity	650	kg
	Seats	2	
	Energy consumption	137.5	Wh/km
Driving performance	Range	160[1]	km
	v_{max}	130	km/h
	Nominal voltage	360	V
	Electric charge	66	Ah
Battery	Energy	23760	Wh
	Weight	182	kg
	Energy density	130	Wh/kg
	Type	PM-synchronous motor	
Motor data	Rated power	44	kW
	Max. torque	226	Nm

[1] according to EU-standard RL 93/116/EWG

9.7 *Peugeot*

9.7.1 *Peugeot Partner électrique*

Table 9.7.1-1: Technical specifications of the *Peugeot Partner électrique* (http://www.dges.de)

Motor: DC-motor		
Cooling	Air blasts	
Max. power	28	kW
Max. speed	6500	min^{-1}
Battery NiCd (manufacturer: *SAFT*)		
Voltage	162	V
Capacity	100	Ah
Energy consumption	28	kWh/100 km
Weight	355	kg
Driving performance		
v_{max}	95	km/h
Range	80-100	km

9.7.2 *Peugeot 106 électrique*

Fig. 9.7.1-1: *Peugeot 106 électrique* (http://www.elektroauto-tipp.de)

9.8 *Citroen*

The models by *Citroen* were mainly available on the *European* market, especially on the ones of *France*, *Germany* and *Switzerland*.

9.8.1 *Citroen Saxo électrique*

1 Fahrzeug-Anschlußstecker
2 Fahrbatterien
3 Elektronisches Steuergerät
4 Antriebseinheit (Motor)
5 Hilfsbatterie
6 Batteriekühlung
7 Motorkühlung
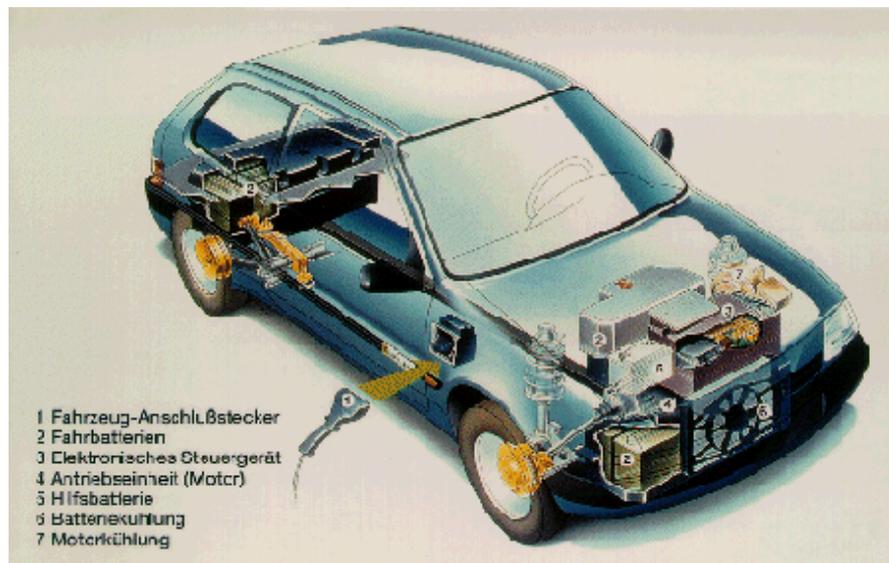
Fig. 9.8.1-1: *Citroen Saxo électrique* (http://www.elektroauto-tipp.de)

Table 9.8.1-1: Technical specifications of the *Citroen Saxo électrique* (http://www.elektroauto-tipp.de)

Motor: DC-motor		
Rated power	20	kW
Battery: NiCd		
Voltage	120	V
Energy consumption	18	kW/100km
Driving performance		
v_{max}	91	km/h
Acceleration from 0 to 50km/h	in 8.4	s
Range	75	km

9.8.2 *Citroen Berlingo*

Fig. 9.8.2-1: *Citroen Berlingo* (**http://www.dges.de**)

Table 9.8.2-1: Technical specifications of the *Citroen Berlingo* (http://www.e-mobile.ch)

Motor: DC-motor		
Cooling	Air blasts	
Rated power	15,5	kW
Max. Power	28	kW
at speed	1500-5500	min^{-1}
Max Torque	180	Nm
at speed	0-1500	min^{-1}
Battery: NiCd		
Voltage	162	V
Driving performance		
v_{max}	95	km/h
Acceleration (0-50km/h)	8,4	s
Range	95	km

9.9 *Honda*

9.9.1 *Honda EV*

Fig. 9.9.1-1: *Honda EV* (http://www.elektroauto-tipp.de)

The *Honda EV* could be leased since March 1997 in the *USA*, but it could not be bought. However the production was stopped already in 1999 after less than 400 vehicles, because the enterprise did not calculate any marketability for that E-car due to the high weight and the limited range. Also *Honda* developed itself in the meantime the domain of fuel cell and the hybrid drive (*Honda Civic*).

Table 9.9.1-1: Technical specifications of the *Honda EV* (http://www.e-mobile.ch)

Motor: PM-synchronous motor		
Position	Front motor	
Power at speed	49 1700 – 8750	kW min⁻¹
Torque at speed	275 0-1700	Nm min⁻¹
Battery: Nickel-metal-hydride		
Position	Under floor	
Amount	24	
Voltage	288	V
Capacity	95	Ah
Charging power	110V/1,1 kW od. 220 V/4,2kW	
Charging duration	8	h
Force transmission	Front wheel drive	
Gear	Single-stage	
Transmission ratio	7.446	
Driving performance		
v_{max}	130	km/h
Acceleration from 0 to 100km/h	18.7	s
Range	160	km

9.10   *Toyota*

Toyota, for several years the market leader on the field of hybrid drives, has also developed models for the purely electric vehicle market.

9.10.1 *Toyota RAV 4 EV*

The *Toyota RAV 4 EV* came on the *California* market in autumn 1997. It was the first model with a purely electric drive by *Toyota*. One year before the *RAV 4 EV* was already available on the *Japanese* market for 35.000 €. In the *Toyota RAV 4 EV* nickel-metal-hydride-batteries were used for the first time in series. The development and production of the battery system were not done by *Toyota* alone. This was a joint venture with *Matsushita Electric Industrial*, in which *Toyota* participated with 40%.

Fig. 9.10.1-1: *Toyota RAV 4 EV* (http://www.elektroauto-tipp.de)

Table 9.10.1-1: Technical specifications of the *Toyota RAV 4 EV* (http://www.elektroauto-tipp.de)

Motor: PM-synchronous motor		
Max. power	45	kW
at speed	2600-8600	min⁻¹
Max. torque	165	Nm
at speed	0-2600	min⁻¹
Battery: Nickel-metal-hydride (gas proof)		
Amount (cells)	24	
Voltage	12	V/cell
Capacity	95	Ah
Driving performance		
v_{max}	125	km/h
Range	215	km
Dimensions		
Length	3565	mm
Breadth	1695	mm
Height	1620	mm
Weight	1460	kg

9.10.2 *Toyota e-com*

The *Toyota e-com* is a small two-seated vehicle, which was designed for commuting traffic in 1997. Since 1999 50 *Toyota*-staff members have been testing the *Toyota e-com* for exactly this application, because also the market introduction in the *USA* was already planned at that time.

Fig. 9.10.2-1: *Toyota e-com* (http://www.elektroauto-tipp.de)

Table 9.10.2-1: Technical specifications of the *Toyota e-com* (http://www.elektroauto-tipp.de)

Motor: Squirrel cage induction motor		
Max. power	18,5	kW
at speed	2300-4500	min⁻¹
Battery: Nickel-Metal-hydride (gas proof)		
Amount (cells)	24	
Voltage	24x12=288	V
Driving performance		
v_{max}	100	km/h
Range	100	km

9.11 *Nissan*

9.11.1 *Nissan Altra*

The *Nissan Altra* is a compact van, equipped with a lithium-battery by *Sony*, with which vast fleet tests were done in 1998 to 2000, before it was offered for sale in 2000.

Fig. 9.11.1-1: *Nissan Altra* (http://www.elektroauto-tipp.de)

Table 9.11.1-1: Technical specifications of the *Nissan Altra* (http://www.elektroauto-tipp.de)

Motor: PM-synchronous motor (NdFeB)		
Power	62	kW
Speed	13000	min^{-1}
Battery: Lithium-ion (manufacturer: *Sony*)		
Capacity	282	Ah
Voltage	345	V
Modules per battery pack	12	
Driving performance		
v_{max}	120	km/h
Range	190	km
Energy consumption (highway/city)	190/213	Wh/km
Dimensions		
Length	4850	mm
Breadth	1760	mm
Height	1690	mm
Weight	1700	kg

9.11.2 *HyperMini*

The special property of the compact electric vehicle, which was presented in 1999 in *Tokio* for the first time, is its chassis made of recycled polymer.

Fig. 9.11.2-1: *Nissan Hyper Mini* (http://www.elektroauto-tipp.de)

Table 9.11.2-1: Technical Specifications of the *Nissan Hyper Mini* (http://www.elektroauto-tipp.de)

Motor: PM-synchronous motor (NeFeB)		
Power	20	kW
Speed	15000	min^{-1}
Battery: Lithium-ion		
Capacity	270	Ah
Voltage	120	V
Modules per battery pack	4	
Driving performance		
v_{max}	100	km/h
Range	130	km

9.11.3 *Nissan LEAF*

The *Nissan LEAF* was presented to the audience for the first time in August 2009 in *Japan*. The abbreviation *LEAF* stands for "*Leading, Environmentally Friendly, Affordable, Family Car*". As a five-door the vehicle belongs to the compact class. End of 2011 the *LEAF* is supposed to be available in *Germany* for approx. 35.000 €.

Fig. 9.11.3-1: *Nissan LEAF* (www.spiegel.de)

Table 9.11.3-1: Technical specifications of the *Nissan LEAF* (http://www.nissan-zeroemission.com)

	Specification		
Dimensions	Length	4445	mm
	Breadth	1770	mm
	Height	1545	mm
	Wheelbase	2700	mm
Loading	Trunk volume	330	l
	Empty weight	1595	kg
	Admissible weight	2035	kg
	Load capacity	440	kg
	Seats	5	
Driving performance	Energy consumption	149	Wh/km
	Range	160[1]	km
	v_{max}	144	km/h
Battery	Nominal voltage	360	V
	Electric charge	66	Ah
	Energy	23760	Wh
	Weight	182	kg
	Energy density	130	Wh/kg
Motor data	Type	PM-synchronous motor	
	Rated power	80	kW
	Max. torque	280	Nm

[1] determined with the US EPA LA4 driving cycle

9.12   *General Motors*

9.12.1 *GM EV 1 GEN II*

The electric vehicle *EV 1* by *GM* is probably one of the most popular electric vehicles from the *USA*. The prototype of the *EV 1 GEN II* established a speed record for electric vehicles, which was at almost 300 km/h (183 mph). The sportcoupé is being sold in *South California* and *Arizona* since December 1996. According to company reports it was supposed to be the first electric vehicle which could compare to a common vehicle concerning driving performance.

Fig. 9.12.1-1: *GM EV 1 GEN II* (http://www.elektroauto-tipp.de)
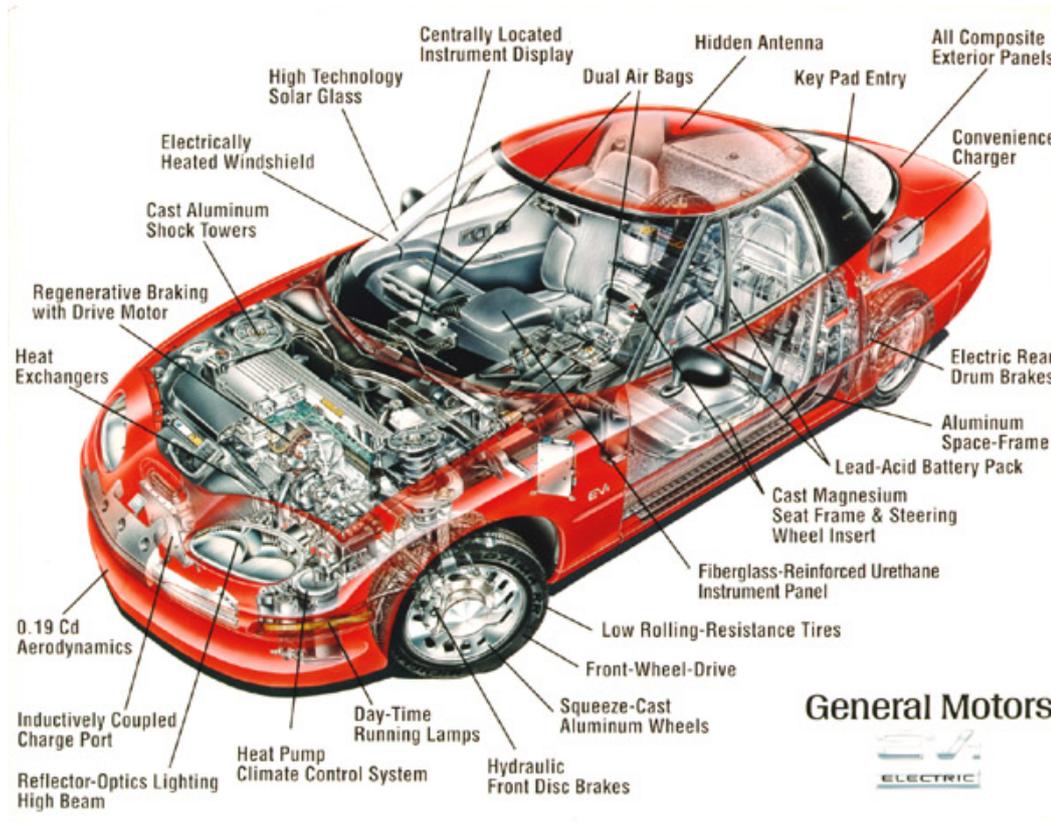
Table 9.12.1-1: Technical specifications of the *GM EV I GEN II* (http://www.gm.com)

Motor: Squirrel cage induction motor		
Power	102	kW
Motor torque	110	Nm
at speed	7000	min^{-1}
Axle torque	1209	Nm
at speed	636	min^{-1}
Battery: Lead-acid		
Voltage	12	V
Modules per battery pack	26	
Driving performance		
Acceleration from 0 to 100 km/h	9	s
Acceleration from 0 to 50 km/h	3	s
v_{max}	130	km/h
Range	80-150	km

9.12.2 *Chevrolet S-10 EV*

Fig. 9.12.2-1: *Chevrolet S-10 EV* (http://www.elektroauto-tipp.de)

Table 9.12.2-1: Technical specifications of the *Chevrolet S-10 EV* (http://www.gm.com)

Motor: Squirrel cage induction motor		
Power	85	kW
Speed	15000	min^{-1}
Battery: Lead-acid (*Panasonic*)		
Capacity	60	Ah
Voltage	312	V
Modules per battery pack	26	
Driving performance		
v_{max}	115	km/h
Range	65-74	km
Dimensions		
Length	4780	mm
Breadth	1724	mm
Height	1620	mm

9.13   *Mitsubishi*

9.13.1 *i-Miev*

The *Mitsubishi i-MiEV* by the Japanese automobile manufacturer *Mitsubishi Motors* is based on the *Mitsubishi I*, which was introduced in 2006. The abbreviation *MiEV* stands for „*Mitsubishi innovative Electric Vehicle*". On the June 5th 2009 the series production started in Japan and in the end of the same year first tests with right-hand drive vehicles were done in *Germany*. The sales start in *Germany* of the *European* version was end of December 2010. For the *European* version the car had to be adjusted to the *EU*-specifications. In order to do that not only the design as a left-hand drive is necessary, but also other different adjustments to local regularities such as bigger exterior mirrors, engine immobilizer, side and head airbags, seatbelt control lamp, bigger headrests and rear fog-light. According to *Mitsubishi* the price was in 20110 34.390 €.

Fig. 9.13.1-1: *Mitsubishi i-MiEV* (http://presse.mitsubishi-motors.de)

Table 9.13.1-1: Technical specifications *Mitsubishi i-MiEV* (http : //www.imiev.de)

	Specification		
Dimensions	Length	3475	mm
	Breadth	1475	mm
	Height	1610	mm
	Wheelbase	2550	mm
Loading	Trunk volume	227/860	l
	Empty weight	1110	kg
	Admissible weight	1450	kg
	Load capacity	340	kg
	Seats	4	
Driving performance	Energy consumption	135	Wh/km
	Range	150[1]	km
	v_{max}	130	km/h
Battery	Nominal voltage	330	V
	Electric charge	50	Ah
	Energy	16500	Wh
	Weight	165	kg
	Energy density	100	Wh/kg
Motor data	Type	PM-synchronous motor	
	Rated power	35	kW
	Max. torque	180	Nm

[1] determined by NEDC

9.14 *Some electric vehicles of the year 2016*

ELEKTROAUTOS

UNTER 30 000 EURO

1a | Kia Soul EV

Motorleistung:	81 kW/110 PS
Batteriekapazität:	27 kWh
Ladezeit:	14 h (230 V)
Reichweite:	212 km
Verbrauch:	14,7 kWh/100 km
Leergewicht:	1565 kg
Höchstgeschwindigkeit:	145 km/h
Basispreis:	28 890 €

1b | Nissan Leaf 24

Motorleistung:	80 kW/109 PS
Batteriekapazität:	24 kWh
Ladezeit:	10 h (230 V)
Reichweite:	250 km
Verbrauch:	15,0 kWh/100 km
Leergewicht:	1475 kg
Höchstgeschwindigkeit:	144 km/h
Basispreis:	29 265 €

1c | Renault ZOE

Motorleistung:	65 kW/88 PS
Batteriekapazität:	22,0 kWh
Ladezeit:	6–9 h (230 V)
Reichweite:	240 km
Verbrauch:	14,6 kWh/100 km
Leergewicht:	1503 kg
Höchstgeschwindigkeit:	135 km/h
Basispreis:	21 500 €

1d | Mitsubishi i-MIEV

Motorleistung:	49 kW/67 PS
Batteriekapazität:	16,0 kWh
Ladezeit:	8 h (230 V)
Reichweite:	160 km
Verbrauch:	12,5 kWh/100 km
Leergewicht:	1185 kg
Höchstgeschwindigkeit:	130 km/h
Basispreis:	23 790 €

ÜBER 30 000 EURO

2a | VW e-Golf

Motorleistung:	85 kW/115 PS
Batteriekapazität:	24,2 kWh
Ladezeit:	8 h (230 V)
Reichweite:	190 km
Verbrauch:	12,7 kWh/100 km
Leergewicht:	1585 kg
Höchstgeschwindigkeit:	140 km/h
Basispreis:	34 900 €

2b | Ford Focus electric

Motorleistung:	107 kW/145 PS
Batteriekapazität:	23,0 kWh
Ladezeit:	10–11h (230 V)
Reichweite:	162 km
Verbrauch:	15,4 kWh/100 km
Leergewicht:	1700 kg
Höchstgeschwindigkeit:	137 km/h
Basispreis:	34 900 €

2c | BMW i3

Motorleistung:	125 kW/170 PS
Batteriekapazität:	21,6 kWh
Ladezeit:	8 h (230 V)
Reichweite:	190 km
Verbrauch:	12,9 kWh/100 km
Leergewicht:	1195/1270 kg
Höchstgeschwindigkeit:	150 km/h
Basispreis:	34 950 €

2d | Mercedes B 250 e Sports Tourer

Motorleistung:	132 kW/179 PS
Batteriekapazität:	28,0 kWh
Ladezeit:	2,4 h (400 V)
Reichweite:	200 km
Energie:	ab 16,6 kWh/100 km
Leergewicht:	1725 kg
Höchstgeschwindigkeit:	160 km/h
Basispreis:	39 151 €

Quelle: T. Westermann, Elektromobile für „Windhunde", in: e-vision, Beilage zu „Die Zeit", Juni 2016, p. 12 [40]

10. Hybrid vehicles

Nowadays the majority of companies, working in the automobile industry, introduce hybrid electric vehicles to the market. In the following a brief historical overview about current hybrid vehicles of some manufacturers shall be given, as far as there is enough information published about their drives system. The presented models are of course not complete. The sequence of their presentation gives no ranking, but is arbitrarily.

Table 10-1: Classification of different hybrid vehicles in hybridization classes and hybrid topologies

	Mild hybrid	**Full hybrid**
Series hybrid	(does not make sense)	*Audi*: • *A1 e-tron (Plug-In) (2013)* *BMW*: • *Megacity Vehicle (Plug-In)(2013)*
Parallel hybrid: torque addition	*Honda ("IMA")*: • *Jazz* • Insight • CR-Z *BMW*: • **ActiveHybrid 7** *Mercedes-Benz*: • **S400 BlueHYBRID**	*Audi*: • **Q5 Hybrid (2011)** • **A8 Hybrid (2011)** *VW*: • **Touareg Hybrid (2011)** *Porsche*: • **Cayenne S Hybrid**
Parallel hybrid: traction force addition	(unknown)	*Peugeot ("Hybrid4")*: • 3008 (2011) *Audi*: • *e-tron Spyder (study form 2010)*
Mixed hybrid: combined	(does not make sense)	*Opel*: • Ampera (2011) *Chevrolet*: • Volt (2011)
Mixed hybrid: power-split (one-mode)	(does not make sense)	*Toyota ("HSD")*: • Prius 3 • *Auris HSD* *Lexus ("HSD")*: • **CT 200h** • *HS 240h* • *GS 450h* • **LS 600h** • **RX 450h**
Mixed hybrid: power-split (two-mode)	(does not make sense)	*BMW*: • **X6 ActiveHybrid** *Mercedes*: • **ML 450 Hybrid**

Approximate classification in vehicle classes:

Compact class   middle class   *upper middle class*   **upper class**   *sports car*   **SUV/Jeep**

10.1 *Audi*

10.1.1 *Audi Q5 Hybrid Quattro 2010*

Table10.1.1-1: Technical specifications of the *Audi Q5 Hybrid Quattro 2010* (http://www.hybrid-autos.info)

Internal combustion engine	
Fuel	Gasoline
Engine displacement	1984 ccm
Rated power	155 kW / 211 PS
Maximum torque	350 Nm
E-machine	
Type	PM-synchronous machine
Maximum power (10 s)	33 kW / 45 PS
Maximum torque	211 Nm
Energy storage	
Type	Lithium-ion
Energy content	1.3 kWh
Weight	38 kg
Total vehicle	
Total system power	180 kW / 245 PS
Total torque	480 Nm
Average fuel consumption	< 7.0 l / 100 km
Total vehicle weight	2000 kg

Fig. 10.1.1-1: *Audi Q5 Hybrid Quattro 2010*

(http://www.hybrid-autos.info)

Due to the technical specifications it is to assume, that this SUV is a full hybrid. According to *Audi* purely electric driving as well as pure driving with the internal combustion engine was possible. Thus it can be presumed that this is a parallel hybrid, in which it is possible to separate the ICE from the drive train by a clutch.

10.1.2 *Audi A8 Hybrid 2010*

Table 10.1.2-1: Technical specifications of the *Audi A8 Hybrid 2010* (http://www.hybrid-autos.info)

Internal combustion engine	
Fuel	Gasoline
Engine displacement	1984 ccm
Rated power	155 kW / 211 PS
Maximum torque	350 Nm
E-machine	
Type	PM-synchronous machine
Maximum power (10 s)	33 kW / 45 PS
Maximum torque	211 Nm
Energy storage	
Type	Lithium-ion
Energy content	1.3 kWh
Weight	38 kg
Total vehicle	
Average fuel consumption	6.2 l / 100 km
Total vehicle weight	1885 kg

Fig. 10.1.2-1: *Audi A8 Hybrid 2010*

(http://www.hybrid-autos.info)

Like previously for the model *Audi Q5 Hybrid Quattro*, which has the same drive train, it is to assume that this limousine is a full hybrid with a parallel hybrid topology.

10.1.3 *Audi e-tron Spyder 2010*

Table 10.1.3-1: Technical specifications of the *Audi e-tron Spyder 2010* (http://www.hybrid-autos.info)

Internal combustion engine	
Fuel	Diesel
Engine displacement	3000 ccm
Rated power	221 kW / 300 PS
Maximum torque	650 Nm
E-machines	
Type	2 x induction machines
Maximum power (10 s)	2 x 32 kW / 2 x 44 PS
Maximum torque	352 Nm
Energy storage	
Type	Lithium-ion
Energy content	9.1 kWh
Weight	(unknown)
Total vehicle	
Average fuel consumption	2.2 l / 100 km
Total vehicle weight	1450 kg

Fig. 10.1.3-1: *Audi e-tron Spyder 2010*

(http://www.hybrid-autos.info)

This sports car study is designed as a full hybrid and has a parallel „*through-the-road*"-architecture, in which the E-machines drive the rear axles and the internal combustion engine drives the front axle.

10.1.4 *Audi A1 e-tron 2010*

Table 10.1.4-1: Technical specifications of *the Audi A1 e-tron 2010* (http://www.hybrid-autos.info)

Internal combustion engine	
Fuel	Gasoline
Engine displacement	254 ccm
Rated power	(unknown, supplied by a 15 kW / 20 PS Generator)
E-machine	
Type	Synchronous machine
Power	61 kW / 83 PS (max. 75 kW / 103 PS)
Torque	150 Nm (max. 240 Nm)
Energy storage	
Type	Lithium-ion
Energy content	12 kWh
Weight	(unknown)
Total vehicle	
Average fuel consumption	1,9 l / 100 km
Total vehicle weight	1200 kg

Fig. 10.1.4-1: *Audi A1 e-tron 2010*

(http://www.hybrid-autos.info)

This compact car is designed as a series plug-in hybrid with a maximum range of 50 km. The function of the „range-extenders" is conducted in this structure by a *Wankel* engine.

10.2 *BMW*

After the studies „*Concept X6*" in 2007 and „*Concept 7*" in 2008, *BMW* offered the two models *ActiveHybrid 7* and *ActiveHybrid X6* since 2009/2010.

10.2.1 *BMW ActiveHybrid 7 2009*

Table 10.2.1-1: Technical specifications of the *BMW*

ActiveHybrid 7 2009 (http://www.hybrid-autos.info)

Internal combustion engine	
Fuel	Gasoline
Engine displacement	4395 ccm
Rated power	330 kW / 449 PS
Maximum torque	700 Nm
E-machine	
Type	PM-synchronous machine
Rated power	15 kW / 20 PS
Maximum torque	210 Nm
Energy storage	
Type	Lithium-ion
Energy content	0.4 kWh
Weight	27 kg
Total vehicle	
Average fuel consumption	9.4 l / 100 km
Total vehicle weight	2045 kg

Fig. 10.2.1-1: *BMW ActiveHybrid 7 2009*

(http://www.hybrid-autos.info)

This limousine is a mild-hybrid, in which the E-machine is placed between internal combustion engine and the converter of the automatic gear. The E-machine is not supposed to provide purely electric driving, which can be seen from its dimension compared to the total vehicle, but it shall support the internal combustion engine.

10.2.2 *BMW ActiveHybrid X6 2009*

Table10.2.2-1: Technical specifications of the *BMW ActiveHybrid X6 2009* (http://www.hybrid-autos.info)

Internal combustion engine	
Fuel	Gasoline
Engine displacement	5.0 l
Rated power	300 kW / 407 PS
Maximum torque	600 Nm
E-machines	
Type	2 x PM-synchronous machines
Rated power	67 kW / 91 PS resp. 63 kW / 86 PS
Maximum torque	280 Nm resp. 260 Nm
Energy storage	
Type	Nickel-metal-hydride
Energy content	2.4 kWh
Weight	(unknown)
Total vehicle	
Average fuel consumption	9.9 l / 100 km
Total vehicle weight	(unknown)

Fig. 10.2.2-1: *BMW ActiveHybrid X6 2009*

(http://www.hybrid-autos.info)

This as „*Sport Activity Vehicle*" (SAC) praised vehicle, which is being sold since August 2010, is a full hybrid. It uses the two-mode gear and is thus a power-split hybrid.

10.3 *Citroën*

Citroen and the sister company *Peugeot* put their focus on the development of diesel hybrids. Already in 2006 prototype was presented:

10.3.1 *Citroën C4 Hdi Hybrid 2006 (Prototype)*

Table 10.3.1-1: Technical specifications of the *Citroën C4 Hdi Hybrid 2006* (http://www.hybrid-autos.info)

Internal combustion engine	
Fuel	Diesel
Engine displacement	1.6 l
Rated power	66 kW / 92 PS
Maximum torque	(unknown)
E-machine	
Type	PM-synchronous machine
Rated power	16 kW / 21 PS
Maximum torque	(unknown)
Energy storage	
Type	Nickel-metal-hydride
Energy content	6.5 kWh
Weight	(unknown)
Total vehicle	
Fuel consumption in city traffic	3.0 l / 100 km
Total vehicle weight	(unknown)

Fig. 10.3.1-1: *Citroën C4 Hdi Hybrid 2006*

(http://www.hybrid-autos.info)

This model is technically identical with the *Peugeot 307 Hdi Hybrid* and shall provide as a single-shaft-hybrid purely electric driving for 5 km. In the meantime there is an available version, which is named as a mild-hybrid.

10.4 *Mercedes-Benz*

Beside the *ML 450 HybridM,* which is available in the *USA*, *Mercedes Benz* published in the past different research vehicles and prototypes, e. g. the *S-Class*, which belongs to the upper class.

10.4.1 *Mercedes-Benz ML 450 Hybrid*

Table 10.4.1-1: Technical specifications of the *Mercedes-Benz ML 450 Hybrid* (http://www.hybrid-autos.info)

Internal combustion engine	
Fuel	Gasoline
Engine displacement	3498 ccm
Maximum power	205 kW / 279 PS
Maximum torque	350 Nm
E-machines	
Type	2 x PM-synchronous machines
Rated power	62 kW / 84 PS resp. 60 kW / 82 PS
Maximum torque	235 Nm resp. 260 Nm
Energy storage	
Type	Nickel-metal-hydride
Energy content	2.4 kWh
Weight	83 kg
Total vehicle	
Total system power	250 kW / 340 PS
Maximum torque	517 Nm
Fuel consumption in city traffic	(unknown)
Total vehicle weight	(unknown)

Fig. 10.4.1-1: *Mercedes-Benz ML 450 Hybrid*

(http://www.hybrid-autos.info)

This SUV has two-mode gear and hence belongs to the category power-split hybrid.

10.4.2 *Mercedes-Benz S 500 Plug-In Hybrid (Prototype)*

Table 10.4.2-1: Technical specifications of the *Mercedes-Benz S 500 Hybrid Plug-In 2009* (http://www.hybrid-autos.info)

Internal combustion engine	
Fuel	Gasoline
Engine displacement	3500 ccm
Maximum power	(unknown)
Maximum torque	(unknown)
E-machines	
Type	PM-synchronous machine
Rated power	44 kW / 60 PS
Maximum torque	250 Nm
Energy storage	
Type	Lithium-ion
Energy content	10 kWh
Weight	130 kg
Total vehicle	
Average fuel consumption	3.2 l / 100 km
Total vehicle weight	(unknown)

Fig. 10.4.2-1: *Mercedes-Benz S 500 Hybrid Plug-In 2009* (http://www.hybrid-autos.info)

In this limousine prototype the hybrid module is located in the gear housing, which means that this is a parallel hybrid with torque addition.

10.5 *Toyota*

Toyota represents a manufacturer with a great experience in building hybrid vehicles. Here the *Toyota Prius* is considered representatively for the different hybridized models.

10.5.1 *Toyota Prius 3*

Table 10.5.1-1: Technical specifications of the *Toyota Prius 3*

(http://www.hybrid-autos.info)

Internal combustion engine	
Fuel	Gasoline
Engine displacement	1.8 l
Maximum power	72 kW / 98 PS
Maximum torque	350 Nm
E-machines	
Type	2 x PM-synchronous machines
Energy storage	
Type	Nickel-metal hydride
Total vehicle	
Fuel consumption in city traffic	3.9 l / 100 km
Total vehicle weight	1445 kg

Fig. 10.5.1-1: *Toyota Prius 3*

(http://www.hybrid-autos.info)

The *Toyota Prius* has the known architecture of the power-split hybrid with planetary gear.

10.6 *Some hybrid electric vehicles of the year 2016*

PLUG-IN-HYBRIDE

UNTER 40 000 EURO

3a | VW Golf GTE

Systemleistung:	150 kW/204 PS
Batteriekapazität:	8,7 kWh
Ladezeit:	3 h
Reichweite elektrisch:	50 km
Verbrauch:	1,7 l B/100 km (NEFZ)
Leergewicht:	1599 kg
Höchstgeschwindigkeit:	222 km/h
Basispreis:	36 900 €

3b | BMW 225xe Active Tourer

Systemleistung:	165 kW/224 PS
Batteriekapazität:	7,6 kWh
Ladezeit:	3 h
Reichweite elektrisch:	41 km
Verbrauch:	2,0 l B/100 km (NEFZ)
Leergewicht:	1575 kg
Höchstgeschwindigkeit:	202 km/h
Basispreis:	38 700 €

3c | Audi A3 e-tron

Systemleistung:	150 kW/204 PS
Batteriekapazität:	8,8 kWh
Ladezeit:	3 h
Reichweite elektrisch:	50 km
Verbrauch:	1,5 l B/100 km (NEFZ)
Leergewicht:	1655 kg
Höchstgeschwindigkeit:	222 km/h
Basispreis:	38 400 €

3d | Toyota Prius Plug-in

Systemleistung:	100 kW/136 PS
Batteriekapazität:	5,2 kWh
Ladezeit:	1,5 h
Reichweite elektrisch:	25 km
Verbrauch:	2,1 l B/100 km (NEFZ)
Leergewicht:	1525 kg
Höchstgeschwindigkeit:	180 km/h
Basispreis:	36 600 €

ÜBER 40 000 EURO

4a | VW Passat GTE

Systemleistung:	160 kW/218 PS
Batteriekapazität:	9,9 kWh
Ladezeit:	4,5 h
Reichweite elektrisch:	50 km
Verbrauch:	1,6 l B/100 km (NEFZ)
Leergewicht:	1772 kg
Höchstgeschwindigkeit:	225 km/h
Basispreis:	44 250 €

4b | Mitsubishi Outlander PHEV Plus

Systemleistung:	209 kW/285 PS
Batteriekapazität:	12 kWh
Ladezeit:	5 h
Reichweite elektrisch:	52 km
Verbrauch :	1,8 l/100 km (NEFZ)
Leergewicht:	1910 kg
Höchstgeschwindigkeit:	170 km/h
Basispreis:	45 990 €

4c | Mercedes C 350 e Limousine

Systemleistung:	205 kW/279 PS
Batteriekapazität:	6,4 kWh
Ladezeit:	2 h
Reichweite elektrisch:	31 km
Verbrauch:	2,1 l/100 km
Leergewicht:	1780 kg
Höchstgeschwindigkeit:	250 km/h
Basispreis:	51 051 €

4d | Volvo V60 D6 Twin engine AWD

Systemleistung:	212 kW/288 PS
Batteriekapazität:	11,2 kWh
Ladezeit:	3,5 h
Reichweite elektrisch:	50 km
Verbrauch:	1,8 D/100 km
Leergewicht:	2048 kg
Höchstgeschwindigkeit:	230 km/h
Basispreis:	56 900 €

Fotos: Getty Images, Presse Hersteller (7)

Source: T. Westermann, Elektromobile für „Windhunde", in: e-vision, Beilage zu „Die Zeit", Juni 2016, p. 13 [40]

11 Bibliography

[1] Binder, A.: Skriptum „Electrical machines and drives ", TU Darmstadt, 2010

[2] Binder, A.: Skriptum „Motor development for electrical drive systems", TU Darmstadt, 2010

[3] Binder, A.: Skriptum „Neue Technologien elektrischer Energiewandler", TU Darmstadt, 2004

[4] Neudorfer, H.: Skriptum „Aktuelle Konzepte für Elektro- und Hybridfahrzeuge", TU Darmstadt 2010

[5] Josefowitz, W., Köhle, S.: Volkswagen Elektro – Hybridfahrzeuge Aktivitäten bei Hybrid Antriebssystemen in Vergangenheit, Gegenwart und Zukunft und Beschreibung von Schlüsselkomponenten und deren Einfluss auf den Kraftstoffverbrauch, Beitrag zum Braunschweiger Symposium, TU Braunschweig 2002

[6] Köhle, S.: Der Volkswagen Bora Hybrid, Entwicklungsziele, Fahrzeugbeschreibung und erste Messergebnisse of the VW Bora mit Hybridantrieb, 2003

[7] Honda Insight – Technik und Spezifikationen, Honda Motor Europe GmbH, 5/2000

[8] Honda Presse Information „Civic Hybrid mit neuem IMA-System", Honda Motor Europe GmbH

[9] Toyota Hybrid System THS II, Presseinformation, www.toyota.co.jp, 2003

[10] Naunin, D.: Hybrid-, Batterrie- und Brennstoffzellenfahrzeuge: Technik, Strukturen und Entwicklungen, Renningen: Expert Verlag, 2004

[11] Hybridfahrzeuge und Energiemanagement: Beiträge zum gleichnamigen 1. Braunschweiger Symposium, TU Braunschweig, 2002

[12] Köhler, U.: Batterien für Elektro- und Hybridfahrzeuge, from [10], pages 34 – 48

[13] Heinemann, D.: Batteriemanagement mit Batterien und Super Caps, from [10], pages 49 – 64

[14] Biemann, J.: Der Elektro-Hybrid – eine Übersicht zu einem Erfolg versprechendem, alternativen Fahrzeugantrieb, from [10], pages 65 – 76

[15] Noreikat, K.E., Neiß, K.: Hybride Fahrzeugantriebe – Marktfähig nur mit Mehrwert?, from [10], pages 78 – 88

[16] Kok, D., Ploumen, S., Spijker, E., Karden, E.: Strategien zum Energiemanagement in Hybridfahrzeugen, from [10], pages 89 – 101

[17] Wandt, H.-P., Brachmann, T.: Das Marktangebot von Hybrid-Elektrofahrzeugen, from [10], pages 104 – 113

[18] Gerl, B.: Innovative Automobilantriebe: Konzepte auf der Basis von Brennstoffzellen, Traktionsbatterien und alternativen Kraftstoffen, Landsberg/Lech: Verlag Moderne Industrie, 2002

[19] Krasser, B., Blome, F., Kozlowski, F.: Continental Mild-Hybrid: Kraftstoffeinsparung durch modular aufgebauten, universell einsetzbaren elektrischen Antrieb im KFZ, Continental Temic, 2003

[20] Neudorfer, H., Binder, A., Ade, M.: Energieeinsparungspotential bei Hybridfahrzeugen durch den Einsatz von innovativen elektrischen Antriebssystemen, VDE Kongress, 18.-20.10.2004 Berlin, Fachtagungsberichte Band 1, pages 459-465

[21] DGES, Elektrofahrzeuge: Entwicklungen und Perspektiven, Fachtagung Karlsruhe, 1999

[22] DGES, Elektrofahrzeuge – Hybridtechnik im Aufschwung, Fachtagung Aachen, 2003

[23] Auto Fig., Ausgabe Nr. 7, März 2004, pages 54-58

[24] Auto Fig., Ausgabe Nr.11, März 2004, pages 13

[25] Auto Fig., Ausgabe Nr.22, Mai 2004, pages 22

[26] Auto Fig., Ausgabe Nr.31, Juli 2004, pages 11-14

[27] Auto Fig., Ausgabe Nr.32, August 2004, pages 28

[28] Lexus 2006 RX 400h product information

[29] Poslednik, E.: Marktstudie über Einsatz und Akzeptanz von Elektro- und Hybridfahrzeugen aus technischer, wirtschaftlicher und ökologischer Sicht; Diplomarbeit TU Darmstadt, 2003

[30] Schlenter, D.: Chancen und Risiken innovativer Elektro- und Hybridfahrzeuge in Abhängigkeit von ökologischen und ökonomischen Rahmenbedingungen, Diplomarbeit TU Darmstadt 2004

[31] Klementz, C.: Erstellung einer Marktanalyse von Brennstoffzellen für den Einsatz in Kraftfahrzeugen, Studienarbeit TU Darmstadt, 2004

[32] Voelcker, J.: Lithium batteries take to the road, IEEE Spectrum, Sept. 2007, pages 18-23

[33] Thounthong, P.; Davat, B.; Rael, S.: Drive friendly – Fuell Cell/Supercapacitor Hybrid power sources for future automotive power generation, IEEE power & energy magazine, Jan./Feb. 2008, pages 69-76

[34] Kukuck, H.-A. (Hrsg.): Die Zukunft des Elektroautos, Reihe „Stromdiskussion", Informationszentrale der Elektrizitätswirtschaft IZE, Frankfurt/Main, 1996 (250 pages)

[35] Zweibel, K.; Mason, J.; Fthenakis, V.: Amerikas Weg ins solare Zeitalter, Spektrum der Wissenschaften, März 2008, pages 61-70

[36] Kusko, A.; Dedad, J.: Stored energy – short-term and long-term storage methods for standby electric power systems, IEEE Ind. Appl. Magazine, July/Aug. 2007, pages 66-72 (detailed bibliography)

[37] Benger, R.; Ropeter, C.; Wenzl, H.; Beck, H.-P.: Auswirkungen steiler Stromänderungen auf elektrochemische Systeme, etz Zeitschrift, H.3/2008, pages 54-61

[38] Brüggemann, M.; Hybride Antriebe für Straßenfahrzeuge - Topologien, Möglichkeiten und Stand der Technik; Studienarbeit TU Darmstadt, 2011

[39] Schuck, M.; Evaluation of Different Accumulator Chemistries for Usage in Electric Bicycle; Seminararbeit TU Darmstadt, 2011

[40] Westermann, T.: Elektromobile für „Windhunde", in: e-vision, Beilage zu „Die Zeit", Juni 2016, p. 12-13

Internet-Quellenverzeichnis

Quelle	Adresse
[1.01]	http://de.lexus-hybrid.com/how/index.html
[1.02]	http://de.varta.com/index.html
[1.03]	http://planetis.quotidienauto.com/mag/030324/electroad/default.asp
[1.04]	http://www.adac.de
[1.05]	http://www.autoFig..de
[1.06]	http://www.automobiles.honda.com
[1.07]	http://www.auto-motor-und-sport.de
[1.08]	http://www.bmw.de
[1.09]	http://www.bmwworld.com/software1.htm
[1.10]	http://www.chrysler.com/home_flash.html
[1.11]	http://www.city-el.de
[1.12]	http://www.conti-online.com/generator/www/com/de/continentalisad/continentalisad/themen/isad/folder_de.html
[1.13]	http://www.daimlerchrysler.com/dccom
[1.14]	http://www.dges.de
[1.15]	http://www.elektroauto-tipp.de
[1.16]	http://www.el-mundo.es/motor/Mvnumeros/97/MV009/MV009renaultficha.html#ficha
[1.17]	http://www.e-mobile.ch
[1.18]	http://www.energie.ch/at/sonder
[1.19]	http://www.ford.com
[1.20]	http://www.gm.com
[1.21]	http://www.honda.com
[1.22]	http://www.honda.de
[1.23]	http://www.honda.fr/html/fr1/corporate/recherche04.shtml
[1.24]	http://www.hybridford.com/index.asp
[1.25]	http://www.ict.fhg.de/deutsch/scope/ae/Libattery.gif
[1.26]	http://www.innovations-report.de/html/berichte/verkehr_logistik/bericht-6093.html
[1.27]	http://www.nissan.de
[1.28]	http://www.opel.de
[1.29]	http://www.peugeot.fr
[1.30]	http://www.psa-peugeot-citroen.com/fr/nuit.php
[1.31]	http://www.renault.fr/index_fr.html
[1.32]	http://www.rwth-aachen.de
[1.33]	http://www.toyota.com
[1.34]	http://www.toyota.de
[1.35]	http://www.tu-braunschweig.de
[1.36]	http://www.tuning-ford.de/sonder_ka_elektroantrieb.htm
[1.37]	http://www.twike.de
[1.38]	http://www.volkswagen.de